Mesh-free Particle Method for Numerical Investigations of Moving Crowd - Applications to Interaction with Moving Obstacles and Disease Contagion

Parveena Shamim Abdul Salam

Vom Fachbereich Mathematik der
Rheinland-Pfälzischen Technischen Universität Kaiserslautern-Landau
zur Verleihung des akademischen Grades
Doktor der Naturwissenschaften (Doctor rerum naturalium, Dr. rer. nat.)
genehmigte Dissertation

Gutachter:
Prof. Dr. Axel Klar, RPTU Kaiserslautern-Landau
Prof. Dr. Subbiah Sundar, IIT Madras
Prof. Dr. Simone Göttlich, Universität Mannheim

Datum der Disputation: 10. Juli 2023

DE-386

Dedication

To my forebears, by blood and by math, without whom this brook (me) has no source . . .

Declaration

I hereby declare that except where specific reference is made to the work of others, the contents of this dissertation are original and has been submitted by me to the Rheinland-Pfälzische Technische Universität Kaiserslautern-Landau, Germany and the Indian Institute of Technology Madras, Chennai, India for the award of the double doctoral degree. This dissertation has not been submitted in whole or in part for consideration for any other degree or qualification in this, or any other university. This dissertation is my own work and contains nothing which is the outcome of work done in collaboration with others, except as specified in the text and Acknowledgements. Parts of this work have been submitted to and published in peer-reviewed journals, appropriately noted in the corresponding chapters. A detailed list of these publications can be found on the next page.

Parveena Shamim Abdul Salam

Datum der Disputation: 10. Juli 2023

Journal articles

The following articles, which were published in peer-reviewed journals or as proceedings of a conference, were used in this thesis:

[2] P. S. ABDUL SALAM, W. BOCK, A. KLAR, **and** S. TIWARI. *Disease contagion models coupled to crowd motion and mesh-free simulation*. *Mathematical Models and Methods in Applied Sciences*, 31: 1277–1295, 2021. DOI: 10.1142/S0218202521400066

[3] P. S. ABDUL SALAM, S. TIWARI, **and** A. KLAR. *Modeling and Simulation of Pedestrian Interaction with Moving Obstacles Using Particle Method*. **in***Progress in Industrial Mathematics at ECMI 2021*. **byeditor**M. EHRHARDT **and** M. GÜNTHER Cham: Springer International Publishing, 2022. 337–342 DOI: 10.1007/978-3-031-11818-0_44

[4] P. S. ABDUL SALAM, S. TIWARI, A. KLAR, **and** S. SUNDAR. *A numerical investigation of pedestrian dynamics based on rational behaviour in different density scenarios*. *Physica A: Statistical Mechanics and its Applications*, 624: 128933, 2023. DOI: 10.1016/j.physa.2023.128933

Furthermore, the following preprints have been submitted:

[1] P. S. ABDUL SALAM, W. BOCK, A. KLAR, **and** S. TIWARI *Coupling pedestrian flow and disease contagion models* **in** In Crowd Dynamics (Vol. 4), Springer.

[5] P. S. ABDUL SALAM, S. TIWARI, A. KLAR, **and** S. SUNDAR *Particle Method for Macroscopic Model of Coupled Pedestrian and Vehicular Traffic Flow* **in** Traffic and Granular Flow 2022 : Springer Conference Proceedings.

Acknowledgements

Firstly, I thank my supervisors, Prof. S. Sundar and Prof. A. Klar, without whom I would not have had the opportunity to embark on this journey of obtaining a doctoral degree. I express my gratitude to Prof. Sundar, who strongly believed in my potential to carry out the PhD work from the day I decided to pursue the degree under his supervision and supported me throughout my tenure to face all adversities academically and non-academically. I express my gratitude to Prof. Klar and Dr Tiwari, who cared profoundly about my work and provided the right direction for my research through regular discussions. I deeply appreciate Dr Tiwari, who was not just a mentor academically but has also been a mentor otherwise during my life in Germany. I also thank Dr Wolfgang Bock, my collaborator and the friendliest colleague who was an integral part of my time at the Department of Mathematics at TUKL.

I thank Prof. Sitabhra Sinha and Dr Shakti N Menon, who continue to be my collaborators and valuable mentors ever since I began my research journey as a Project Assistant at IMSc. I thank my Doctoral Committee members, Prof. YVSS Sanyasiraju, Dr Sruthi Dubey and Dr Arul Prakash, for their continuous efforts in the evaluation of my research activities and for providing support and valuable suggestions. Additionally, I extend special gratitude to Prof. Ch. Srinivas Rao and Prof. Manam Rao for their well-wishing attitude and encouragement since my M.Sc. days at IIT Madras.

I thank my colleagues and friends, Divya Murali, Fredy Joy, Mohamed Atif, Pratiksha Singavekar, Rohini Satish, Satyam Kumar and Vivek Singh, whose companionship has made life inside campus more memorable. Special thanks to colleague Somnath Maity for all the discussions including qualms in research and life at any time of the day. I would also like to thank my friends Aswathy M.S. and Vishnu Ravindran, who have been an integral part of my life at IITM.

I thank my colleagues and friends at TUKL whose presence made the days in Germany more vibrant. I express my gratitude to my friends Bavithra G and Sheena Melwani, who have been of great emotional support while in Germany and continue to be. I thank Arsha Sherly, Sreejani Barua, Deepthy Maria, Remilou Liguarda, Aiswarya M, Sravani Kalluri and Nazrul Arif, who are amongst the finite number of people who made life away from India special, helping me make cherishable memories. I thank my colleague Corinna Zurloh for introducing me to authentic parts of German life, including baking.

I express my gratitude to my family, who have been my biggest support system throughout - my brother Omer Sherif, one who believed in my dreams and stood by me right from my high school years, my Mom Farida and Dad Abdul Salam, who provided me with the wings to fly high. I also thank some special family members, my cousins, Thanish, Jawahar and Rinshy and aunts Shama and Vanitha, for their continuous love and support. I thank my sister-in-law Ananya Sen who has

been an inspiration personally and professionally, and my little niece Samaira who has adorably provided me encouragement. Friends are the family we choose, and I am grateful for the constants in my life, Sumesh, Pratik, Prashant and Fayaz, who never left a chance to adore me and be there for me, always just a call away.

I would like to thank the department colleagues at both IITM and TUKL for their support. I also thank the DAAD for the research grant for Bi-nationally supervised doctoral degree programme.

Last but not least, I thank my alma mater IIT Madras and the wonderful and serene campus for its beautiful existence and for being a witness to the decade-long journey of my 20s transforming me from a girl to a woman.

Abstract

Understanding human crowd behaviour has been an intriguing topic of interdisciplinary research in recent decades. Modelling of crowd dynamics using differential equations is an indispensable approach to unraveling the various complex dynamics involved in such interacting particle systems. Numerical simulation of pedestrian crowd via these mathematical models allows us to study different realistic scenarios beyond the limitations of studies via controlled experiments.

In this thesis, the main objective is to understand and analyse the dynamics in a domain shared by both pedestrians and moving obstacles. We model pedestrian motion by combining the social force concept with the idea of optimal path computation. This leads to a system of ordinary differential equations governing the dynamics of individual pedestrians via the interaction forces (social forces) between them. Additionally, a non-local force term involving the optimal path and desired velocity governs the pedestrian trajectory. The optimal path computation involves solving a time-independent Eikonal equation, which is coupled to the system of ODEs. A hydrodynamic model is developed from this microscopic model via the mean-field limit.

To consider the interaction with moving obstacles in the domain, we model a set of kinematic equations for the obstacle motion. Two kinds of obstacles are considered - "passive", which move in their predefined trajectories and have only a one-way interaction with pedestrians, and "dynamic", which have a feedback interaction with pedestrians and have their trajectories changing dynamically. The coupled model of pedestrians and obstacles is used to discern pedestrian collision avoidance behaviour in different computational scenarios in a long rectangular domain. We observe that pedestrians avoid collisions through route choice strategies that involve changes in speed and path. We extend this model to consider the interaction between pedestrians and vehicular traffic. We appropriately model the interactions of vehicles, following lane traffic, based on the car-following approach. We observe how the deceleration and braking mechanism of vehicles is executed at pedestrian crossings depending on the right of way on the roads.

As a second objective, we study the disease contagion in moving crowds. We consider the influence of the crowd motion in a complex dynamical environment on the course of infection of pedestrians. A hydrodynamic model for multi-group pedestrian flow is derived from the kinetic equations based on a social force model. It is coupled along with an Eikonal equation to a non-local SEIS contagion model for disease spread. Here, apart from the description of local contacts, the influence of contact times has also been modelled. We observe that the nature of the flow and the geometry of the domain lead to changes in density which affect the contact time and, consequently, the rate of spread of infection.

Finally, the social force model is compared to a variable speed based rational behaviour pedestrian model. We derive a hierarchy of the heuristics-based model from microscopic to macroscopic

scales and numerically investigate these models in different density scenarios. Various numerical test cases are considered, including uni- and bi-directional flows and scenarios with and without obstacles. We observe that in low-density scenarios, collision avoidance forces arising from the behavioural heuristics give valid results. Whereas in high-density scenarios, repulsive force terms are essential.

The numerical simulations of all the models are carried out using a mesh-free particle method based on least square approximations. The meshfree numerical framework provides an efficient and elegant way to handle complex geometric situations involving boundaries and stationary or moving obstacles.

Abstrakt

Das Verhalten von Menschenmengen zu verstehen, war in den letzten Jahrzehnten ein wichtiges Thema der interdisziplinären Forschung. Die Modellierung der Dynamik von Menschenmengen mit Hilfe von Differentialgleichungen ist ein wesentlicher Ansatz, um die verschiedenen komplexen Dynamiken zu entschlüsseln, die an solchen interagierenden Teilchensystemen beteiligt sind. Die numerische Simulation von Fußgängerströmen mit Hilfe dieser mathematischen Modelle ermöglicht es uns, verschiedene realistische Szenarien zu untersuchen, die über die Grenzen von Studien mit kontrollierten Experimenten hinausgehen.

In dieser Arbeit geht es in erster Linie darum, die Dynamik in einem Gebiet zu verstehen und zu analysieren, das sowohl von Fußgängern als auch von sich bewegenden Hindernissen genutzt wird. Wir modellieren die Bewegung von Fußgängern, indem wir das Konzept der sozialen Kräfte mit der Idee der optimalen Pfadberechnung kombinieren. Dies führt zu einem System gewöhnlicher Differentialgleichungen, das die Dynamik der einzelnen Fußgänger über die Interaktionskräfte (soziale Kräfte) zwischen ihnen steuert. Zusätzlich regelt ein nichtlokaler Kraftterm, der den optimalen Pfad und die gewünschte Geschwindigkeit einbezieht, die Trajektorie des Fußgängers. Die Berechnung des optimalen Pfades beinhaltet die Lösung einer zeitunabhängigen Eikonal-Gleichung, die mit dem System der gewöhnlichen Differentialgleichungen gekoppelt ist. Aus diesem mikroskopischen Modell wird über das Mean-Field-Limit ein hydrodynamisches Modell entwickelt.

Um die Interaktion mit beweglichen Hindernissen im Gebiet zu berücksichtigen, modellieren wir die Bewegung der Hindernisse mit einer Reihe kinematischer Gleichungen. Es werden zwei Arten von Hindernissen betrachtet: „passive“, die sich auf ihren vordefinierten Bahnen bewegen und nur in eine Richtung mit den Fußgängern interagieren, und „dynamische“, die eine Rückkopplung mit den Fußgängern haben und deren Bahnen sich dynamisch ändern. Das gekoppelte Modell von Fußgängern und Hindernissen wird verwendet, um das Kollisionsvermeidungsverhalten von Fußgängern in verschiedenen Berechnungsszenarien in einem langen rechteckigen Gebiet zu untersuchen. Wir beobachten, dass Fußgänger Kollisionen durch Routenwahlstrategien vermeiden, indem sie die Geschwindigkeit und den Weg ändern. Wir erweitern dieses Modell, um die Interaktion zwischen Fußgängern und Fahrzeugverkehr zu berücksichtigen. Wir modellieren die Interaktionen von Fahrzeugen, die dem Verkehr auf der Fahrbahn folgen, auf der Grundlage des Car-Following-Ansatzes. Wir beobachten, wie die Verzögerungs- und Bremsmechanismen der Fahrzeuge an Fußgängerüberwegen je nach Vorfahrtsregelung auf den Straßen ausgeführt werden. Als zweite Anwendung untersuchen wir die Ansteckung von Krankheiten in sich bewegenden Menschenmengen. Wir untersuchen den Einfluss der Bewegung der Menschenmenge in einer komplexen dynamischen Umgebung auf den Verlauf der Ansteckung von Fußgängern. Aus den

kinetischen Gleichungen, die auf einem sozialen Kraftmodell basieren, wird ein hydrodynamisches Modell für den Fluss von Fußgängern in mehreren Gruppen abgeleitet. Es wird zusammen mit einer Eikonal-Gleichung an ein nicht-lokales SEIS-Ansteckungsmodell für die Krankheitsausbreitung gekoppelt. Hier wurde neben der Beschreibung lokaler Kontakte auch der Einfluss von Kontaktzeiten modelliert. Wir stellen fest, dass die Art der Strömung und die Geometrie des Gebiets zu einer Änderung der Dichte führen, die sich auf die Kontaktzeit und folglich auf die Ausbreitungsrate der Infektion auswirkt.

Abschließend wird das Modell der sozialen Kräfte mit einem auf variabler Geschwindigkeit basierenden Modell für rationales Verhalten von Fußgängern verglichen. Wir leiten eine Hierarchie des auf Heuristiken basierenden Modells von mikroskopischen zu makroskopischen Skalen ab und untersuchen diese Modelle numerisch in verschiedenen Dichteszenarien. Es werden verschiedene numerische Testfälle betrachtet, darunter uni- und bidirektionale Strömungen sowie Szenarien mit und ohne Hindernissen. Wir stellen fest, dass in Szenarien mit geringer Dichte die aus den Verhaltensheuristiken resultierenden Kollisionsvermeidungskräfte sinnvolle Ergebnisse liefern. In Szenarien mit hoher Dichte sind abstoßende Kräfte jedoch unerlässlich.

Die numerischen Simulationen aller Modelle werden mit einer gitterfreien Partikelmethode auf der Grundlage von Kleinste-Quadrate-Näherungen durchgeführt. Der gitterfreie numerische Rahmen bietet eine effiziente und elegante Möglichkeit, komplexe geometrische Situationen mit Begrenzungen und stationären oder beweglichen Hindernissen zu behandeln.

Contents

Introduction

1 Introduction

1.1 Background and Motivation

Human behaviour is an extremely complex phenomenon governed by a myriad of factors, both from the external environment and from the internal mental landscape of individuals. Social and behavioural scientists have spent decades researching various individual or crowd behavioural tendencies in diverse contexts. Each individual's physiological behaviour is influenced by their perception of the environment and their physiological and safety needs. Research shows that decisions or actions are taken by individuals based on these factors and are not entirely unpredictable. A thorough understanding of the basic rules of human behaviour is a necessary ingredient for modelling at all scales.

The modelling of such systems involving many interacting particles, here humans/pedestrians, has been a widely active area of research amongst mathematicians, physicists and engineers alike. The modelling problem of such complex living systems is quite challenging and has hence intrigued researchers over the last few decades. These systems involve entities which not only have individual strategies but also interact with other entities and evolve cooperative strategies to regulate their overall dynamics. The particles may be influenced by physical forces such as gravity, electrostatics, or friction, or they may interact through more complex mechanisms such as diffusion, chemical reactions, or social interactions. The emergence of spontaneous self-organised patterns in space and phase transitions arising out of such interactions is a typical feature of such systems. Pedestrian groups exhibit patterns like lane formation in bi-directional flow, stripe formation in intersecting flows and oscillations at bottlenecks. It is crucial to study these phenomena and gain an understanding of the underlying mechanisms to predict the behaviour of the system under various scenarios.

An important aspect of the human crowd is a sense of social identity which induces collective behaviours. These herd behavioural inclinations can, many a time, overpower individual judgement and lead to destructive behaviour. For example, during a panic situation, people may rush to avoid danger but, in turn, may fall and trample upon each other, causing a stampede, or they might get disoriented and run in the wrong direction as a group and hence not find the way to safety. Throughout history, we see that such crowd behaviours have led to large disasters around the world, like the Love Parade Disaster in 2010 (Fig. 1.1) or the recent Halloween stampede in Seoul in 2022; see [96] for a review of crowd stampedes in India. Hence, crowd behaviour in any mass event has been of particular research interest, considering the information we need to obtain to prevent such crowd disasters. An understanding of crowd behaviour in normal as well as panic situations is essential to devise safety measures and evacuation planning in large public spaces like stadiums or

Figure 1.1 – Crowd Disasters - Love Parade Disaster in 2010 [1] ([131])

Figure 1.2 – Religious Gatherings - Hajj Pilgrimage [2] (left: [112]) , Kumbh Mela[3] (right: [78])

arenas, airports, railway platforms and buildings consisting of office spaces or schools or hospitals. Collision avoidance in pedestrian flow is an indispensable problem in urban planning, crowd management and transportation engineering. Pedestrians follow different strategies for collision avoidance with other pedestrians and obstacles in the environment. Some involve reactive strategies, like separation and stop-and-go waves, where individuals react to the cues from immediate surroundings. On the other hand, proactive strategies include signs and signals to guide pedestrians or infrastructure like columns to demarcate opposing walking directions. Apart from this, obstacles can be used to regulate the flow and improve evacuation efficiency too [59, 79]; for example, cylindrical obstacles near a narrow exit improve evacuation efficiency [176]. Hence, it is essential to formulate pedestrian models that investigate pedestrian-obstacle interactions for both stationary and moving obstacles.

Information regarding possible congestion, jams or high-density areas in a public area is essential for evacuation planning and crowd control during any public event, for instance, during religious

[1] Photograph "Entry and exit ramp of the Loveparade 2010" © Arne Müseler under a CC BY-SA 3.0 license via Wikimedia Commons.

[2] Photograph "Mecca Saudi Arabia" © Konevi under a CC0 license.

[3] Photograph "Kumbh Mela in Allahabad (Indien)" © Lars Hanf under a CC BY-NC-SA 3.0 license.

Figure 1.3 – Woonerf Principle - Living Streets or Shared Spaces (left[4]: [58], right[5]: [53])

gatherings, as shown in Fig. 1.2, like Kumbh Mela or Hajj [69] or festive celebrations like New Year's Eve. Such information is also essential to manage smaller public spaces like shopping areas in malls, outside schools or peak office hours in a metro. Lately, there has been the intervention of technology, say, the use of sensors and cameras, which provide real-time data to identify collision risks. In this regard, robots are also used to navigate and regulate the flow in evacuation environments.

The concept of *'shared spaces'* has taken over urban planning in recent years. The philosophy of space sharing originated with ideas in the West [97, 120] which were developed and implemented, for example, via the woonerf concept in Europe (see Fig. 1.3 (left)), which started in the Netherlands [76]. Shared spaces (see Fig. 1.3 (right)) are gaining popularity in every major city - with more and more streets in the city centres becoming pedestrian friendly. The concept of "streets for people" in place of "streets for traffic" has been a major shift of focus in urban mobility. In such areas, both the vehicles and the pedestrians are given equal priority, contrary to the usual roads. Also, the traffic responsibility falls directly on the road users rather than through any interventions like signals or signs. This concept is another prominent reason to study pedestrian-moving obstacle interactions, where we consider the moving obstacles as entities which have decision-making capabilities like those of pedestrians. Such a framework indeed can be extended for direct applications in autonomous vehicle as well as robot navigation.

Apart from the inconveniences and challenges caused by dense crowds, either in the form of incidence of injuries and fatalities during mass events or the congestion caused in smaller domains, say in public transport or malls, the transmission of diseases which can spread through physical contact is another concern. During the recent pandemic, controlling the spread of COVID-19 infection involved measures like social distancing and restrictions on mass gatherings. These circumstances promptly led to a need to study the dynamics of virus spread in crowds, focused chiefly on the movement of people in indoor public spaces, that is, closed domains. Though there have been several attempts to understand various aspects of disease spread in crowds [173], there is a lack of niche mathematical models versatile enough to capture the information in dense moving

[4]Photograph "Nederlands Woonerf (Dan Burden)" © Erauch under a CC BY-SA 3.0 license via Wikimedia Commons.

[5]Photograph "Fishergate Shared Space, Preston, Lancashire, England" © David Dixon under a CC BY-SA 2.0 license.

crowds. Moreover, the effect of obstacles in the domain has only been explored in the context of designing of spaces as preventive responses. However, specific dynamics and flow patterns which affect disease transmission under the influence of obstacles are seldom studied and hence our goal.

1.2 Overview

Pedestrians' actions are, most often than not, patterns of motion based on learnt behaviour and individuals illicit rather automatic responses in most standard situations. The deterministic modelling of pedestrians follows this notion. *Microscopic models* using force terms reflecting the different social factors, internal and external, were developed initially in [82] and later extended and studied further. The primary assumption in such *'social force'* based models is the superposition of the different forces, which leads to an easy formulation of differential equations governing the system. Social or behavioural force based models have been revolutionary amongst agent-based models, not only because of their ease of formulation and solution through existing numerical methods but also due to the fact that they are able to illustrate several spatiotemporal patterns of self-organisation phenomenon. But these physics based models do have their limitations - first, in the flawed homogeneous assumption; second, in the difficulty involved in the calibration of the numerous parameters; and third, the criticised superposition principle of non-Newtonian, non-linear forces. Meanwhile, agent-based models based on simple heuristics (simple and fast cognitive decisions) derived from the rational behaviour of pedestrians also provide a route to describe pedestrian motion. Such cognitive heuristics based on vision was described in [129]. This idea was further developed to make a model, in [15], involving a heuristics-based perception phase followed by a decision phase modelled as a dynamically varying cost potential reflecting the behavioural outcomes from their interactions. We observe in our work that the latter model, though is able to reproduce self-organising patterns, only works well in low-density scenarios, while the social force type models are better when we are dealing with larger densities. More often, larger densities are not handled efficiently by microscopic models. They involve a large number of equations and hence are computationally expensive. To deal with high-density crowds, we need models at the kinetic or macroscopic level.

Deriving macroscopic physics from the microscopic dynamics of the elementary entities is the foundation of statistical mechanics, and it involves the kinetic theory of gases for mathematical formulation. Pedestrians are self-propelled *'active' particles* whose actions are governed by different social strategies, in contrast to inert matter. In continuum mechanics, a point particle in the continuum is part of the system, negligible with respect to its size, but quite large compared to the molecular length. We note that meso or macro scale approaches involve a continuum hypothesis which is valid only when the density is high such that the distances between the pedestrians are quite small. This translates directly to how we view packing capacity and mean free path in gases; that is, how low the *Knudsen number* is. Also, in dilute gases where kinetic theory is applied, particle collisions are one-to-one, and particles spend very little time on collision. But in fluids/dense gases, this is not the same [114]. For such systems, gas kinetic theory can be used to model the dynamics

using probability distribution functions while the interactions are still modelled at a particle level. The structure depends on how the interactions are modelled; long-range leads to Vlasov type equations and localized leads to Boltzmann type equations. The *kinetic models* act as a bridge between the microscopic and macroscopic scale of models. These models assume a homogeneous crowd and consider the average behaviour. This assumption, as well as the continuum assumption, has been widely criticized, but still, the models work well and provide an array of qualitative and quantitative information along with a huge advantage in computational efficiency.

Macroscopic models are more focused on aggregate behaviour rather than individual behaviour of the pedestrians. A large crowd displays attributes of a fluid, and hence a fluid-dynamic approach can be used for modelling the pedestrians at this scale. Such a formulation enables analytical analyses of macro variables as well as parameters in the model, allowing a better understanding of the flow dynamics, for example, through flow-density diagrams. This information at the global level and macroscopic scale is essential because it is not the individual dynamics but the overall dynamics which can be seen and interpreted easily from empirical studies. Both first and second-order macroscopic models can be defined independently by direct formulation of fluid equations of continuity and momentum and appropriate closure relations. On the other hand, the macroscopic model can be derived from the kinetic models by asymptotic methods, like taking hydrodynamic limits. In either case, the continuum model involves the evaluation of pedestrian density, mean velocity and flow variables. Additionally, hyperbolic structures rather than parabolic ones are preferred since it is then possible to write the equations in conservation form and analyse them. Nevertheless, macroscopic models are highly computationally efficient when dealing with larger crowds and provide the necessary information on the flow conditions to use in various crowd management tasks. Hence our focus falls mostly on macroscopic models for pedestrian flow in this thesis.

The introduction of desired velocity, the speed and direction that a pedestrian entity decides to take to reach the target or exit if there were no external influences, was an important step in changing the modelling structures of all scales. Most often, people move in bounded domains towards a certain destination. This defines a *'desired velocity field'* in the domain which essentially gives the velocity each pedestrian would take if they were alone. Pedestrians typically try to move at a speed that is comfortable and efficient for them while also avoiding collisions and navigating around obstacles. Final velocity field is a combination of desired velocity and the interaction velocity. A desired acceleration term is often used to describe how pedestrians adjust their speed and direction of movement based on the behaviour of the crowd around them and in response to changes in the environment, such as the presence of a bottleneck or the opening of a new exit.

An important aspect of any model is how the pedestrians choose their route dynamically. There are two different route choice behaviours modelled in literature - one via a *predictive dynamic user equilibrium (PDUE)* and the other via a *reactive dynamic user equilibrium (RDUE)*. In PDUE [88, 89, 91], the pedestrians are assumed to have complete information of the environment, which they might have accumulated by frequently using the same space for travel over a period of time or have received via other sources. Then the decision making involves a strategy to choose the

route minimizing the total travel cost (time/distance). They predict the future direction along the route to the destination based on current information. While in RDUE, the pedestrians choose a route that minimizes instantaneous travel costs as they have only the immediate flow information available. Huang et al. [92] explains how the potential function in [94] provides an instantaneous cost (calibrated by both the speed and discomfort factor), and hence the model follows a reactive route choice strategy. The pedestrian models in this thesis also satisfy the reactive user equilibrium principle via the eikonal equation. We note that both in predictive and reactive models, the space is fully visible to the pedestrians, either first-hand by direct vision or second-hand through the leader agent they follow.

The challenge in modelling increases when there are obstacles and boundaries in the environment to take care of. Evaluation of desired direction of motion via the Eikonal equation is an effective and brilliant way to incorporate geometry-related information, like the presence of walls and obstacles, into the pedestrian models. This leads to non-local information being available while route choice decisions are made.

To avoid collisions, individuals might adjust their speed or path or both. Collision avoidance is implemented in models in different ways - through force based terms in social force models, by calculating safe directions in velocity-based models and by a future predictive decision-making in anticipation-based models. Providing the geometric information related to stationary or moving obstacles using the Eikonal equation, in the models discussed in this thesis, allows for an easy implementation of collision avoidance via adjustment of path as well as speed. Herein, we have an interplay between trajectory changes using the non-local information about the geometry and velocity changes through interpersonal interactions. Though the social force-based approach has been used widely in pedestrian models, such an approach to consider moving obstacle interactions between themselves and with other pedestrians has not been explored before but is strikingly apt.

On the other hand, when the obstacles are dynamic, that is, they have a mechanism to sense or visually see the pedestrians and try to avoid collisions themselves by suitable adjustments of speed. A protracted way to consider pedestrian interaction with moving obstacles is to recognise that the moving obstacles could be vehicles, with drivers or driver-less and automated. So the whole framework developed to couple obstacle kinematics with the pedestrian model can be extended to consider vehicles following lane-traffic. Then the pedestrian-dynamic obstacle interaction model serves in studying shared spaces. Further extension of the framework can be made to multiple vehicles and change of domain to linear roads with lane-traffic. Once the interactions between the vehicles are modelled via the principles discussed in literature, like the car-following or follow-the-leader models, then we have a pedestrian-vehicular traffic coupled model. We observe that the main mechanism of collision avoidance followed by vehicles is deceleration and braking. Most vehicular traffic models in literature are for lane-based traffic, whereas our model's feature for handling multiple moving obstacles can be utilised for vehicles which do not follow any absolute lanes, like in shared spaces as well as those that follow lane-based traffic.

The pedestrian model can be enhanced to incorporate disease transmission dynamics to allow us to analyse viral spread in dense crowds. Through numerical studies, which allow us to consider

the mobility patterns under the influence of different contact rates and flow conditions in the presence and absence of obstacles, insights into how the disease spreads can be obtained. The effectiveness and efficiency of the model in handling various scenarios and complex geometries are given prominence in this thesis.

An indispensable part of the research in crowd modelling is identifying efficient mathematical tools to analyse the models. In general, numerical methods used in macroscopic simulations are grid-based, which can be laborious to adopt to problems involving complex geometries and moving interfaces. Meshfree methods are hence more suitable for crowd dynamics problems in order to easily handle crowd deformations and the different domain configurations. Moreover, interacting particle systems like crowds have an inherent granular nature and hence a Lagrangian formulation used in meshfree methods such as the Finite Pointset Method (FPM) is apt.

The numerical algorithm involved in solving the pedestrian models in this thesis always involves two major components. First is solving the eikonal equations using a fast marching method over the entire domain of consideration. The solution of the same generates the desired direction of motion for pedestrians, obstacles or vehicles. Second is the solution of the evolution equations for pedestrians and the kinematic equations of obstacles or vehicles coupled to them in a Lagrangian framework. FPM based on Taylor series and least square approximations is applied to solve the model equations, both microscopic and macroscopic. FPM transforms the PDEs (in hydrodynamic model), by approximating the field variables (like density and velocity) and their derivatives, into a system of ODEs that can be solved by time integration algorithms.

As a modification of classical Generalised Finite Difference Method (GFDM), FPM is used to solve Navier-Stokes equations in [164]. It has been extended to problems in solid and fluid mechanics. For example, FPM has been applied to simulations of two-phase immiscible flows in [165], the liquid-liquid flow field in an extractor in [55] and has been used in free surface flows [163] and soil mechanics [127].

In computational fluid dynamics, immersed boundary methods (IBMs) are often used to handle moving geometries in the fluid domain. Since the moving boundaries may not always conform to a structured grid, handling such geometries is a challenging task in grid-based methods. Remeshing is a costly technique, and so IBMs were a necessary development to handle such problems [141]. Moving boundaries are easily handled in meshfree methods since we can independently populate the boundaries with grid points. This allows for the direct implementation of boundary conditions. The numerical code for the simulations in this thesis is written in Fortran. MATLAB has been used for post-processing the data and creating figures used.

1.3 Aims and Objectives

The objective of this thesis is divided into three parts -

1. Develop a mathematical model based on social forces to study pedestrian interaction with moving obstacles and to adapt the meshfree numerical framework to investigate scenarios

with moving geometries. Further, extend this model to include vehicular-pedestrian traffic interaction.

2. Develop a multi-group hydrodynamic model coupled to disease contagion equations to analyze the disease spread in pedestrian crowds. The focus is to study the impact of the presence of stationary or moving obstacles, with special emphasis on the influence of contact times for air-borne diseases.

3. Derive a macroscopic model from a microscopic rational behaviour model and numerically investigate the model and compare it with social force-based models under various density scenarios.

1.4 Structure of the Thesis

Following the objectives outlined above, the thesis is structured as follows :

Chapter 2 reviews the different modelling approaches of pedestrian flow - microscopic (particles-based), mesoscopic (gas-kinetic) and macroscopic (fluid-dynamic) models. The individual based social/behavioural force model and the hydrodynamic Hughes model are explained in detail as they form the basis for the pedestrian models we have considered in the chapters that follow in this thesis. Particular emphasis is given to outlining the bottom-up approach of developing a meso/macro model from a micro model. Further to this, a general idea on meshfree methods, their advantages and limitations, and the purpose of using the method for interacting particle problems are discussed. The finite pointset method (FPM)based on least square approximations is described in detail. Also, we recount the fast marching method (FMM) used for solving Hamilton-Jacobi equations and explain how the eikonal equation can be solved using FMM in the context of meshfree grids.

Chapter 3 describes a mathematical framework to study pedestrian interaction with moving obstacles. We prescribe the hydrodynamic pedestrian model coupled with either passive (one-way coupling) or dynamic (two-way coupling) obstacle kinematics. We explain in detail how this coupling is handled in the numerical framework. The meshfree formulation of equations, the grid management for moving geometries and the procedure to implement boundary conditions are construed. Numerical examples of classical test cases are considered to exhibit pedestrian dynamics in shared spaces.

In **Chapter 4**, we extend the framework developed in Chapter 3 to a pedestrian-vehicular interaction model. The described model is illustrated for different numerical test cases involving one-lane and two-lane roads and various pedestrian crossing scenarios.

Chapter 5 establishes a coupled model to analyse disease contagion in pedestrians. A hydrodynamic multi-group pedestrian model is described starting from a kinetic approach and coupled to an SEIR-based disease model. Scenarios involving uni-directional and bi-directional flow of pedestrians in the absence as well as the presence of static or dynamic obstacles are analysed. The influence of contact time on the infection spread, i.e., for the susceptible to become exposed, is examined thoroughly.

Chapter 6 is a comparative numerical study on models involving social force based interactions against that modelled on cognitive heuristics-based force terms. We show how a macroscopic equivalent of the microscopic rational behaviour model is formally derived via mean-field kinetic theory and moment methods. The interaction force terms in the microscopic and macroscopic models are scrutinised by analysing them in multiple cases - involving just two pedestrians or a group of pedestrians (varying density cases) and obstacles.

Chapter 7 briefly discusses and draws conclusions on the work in this thesis.

II Models and Methods

2 Preliminaries

2.1 Pedestrian Models

Mathematical models for pedestrians can be formulated with different methodologies and categorised based on technicalities and phenomenological observations. For instance, depending on the scale of the independent variable, they are either discrete or continuous. Based on how the process is described, they are either stochastic or deterministic. And based on the scale of the system and level of description, they are either microscopic, mesoscopic or macroscopic. In the work in this thesis, only continuous models of the deterministic type are considered. Continuous models provide information at every instance of time (which is the independent variable in our models); that is, time is regarded as a continuous variable. And deterministic models do not involve any randomness or stochasticity. We use models at different scales of description - micro, meso and macro - in the chapters that follow. To provide a preliminary idea to the reader, we review below the different modelling scales and some models from the literature necessary for our work.

2.1.1 Microscopic Models

Microscopic modelling involves describing the dynamics of every single pedestrian, also called an agent, by considering the influence of their interactions with other pedestrians or the environment and also their own internal motivation to act. These models are also known as individual based models (IBM) or agent based models. The individuals are usually treated as homogeneous particles. Microscopic models are expressed as systems of ordinary differential equations or difference equations, usually non-linear. The position and velocity of each pedestrian act as the dependent variables and define its state in the system. The general form of such second-order systems of ODE for N pedestrians is given as,

$$\dot{\vec{x}}_i(t) = \vec{v}_i(t)\,,\ \dot{\vec{v}}_i(t) = \texttt{acceleration terms}\,,\ i = 1,2,...,N\,. \tag{2.1}$$

Cellular Automata Models

Cellular Automata (CA) models were introduced over two decades ago [27, 67, 130]. Inspired by the motion of ants via chemotaxis [25], floor field CA models were developed, see Refs. [36], [107] and [134]. In these models, the domain is modelled as a regular grid, and the pedestrians are simulated as entities occupying the cells. Rules based algorithms are devised to update the distribution of pedestrians in these cells. Each pedestrian, at any given discrete time step, has a choice to either stay in the same cell or move out of its current cell in any of the directions (usually 8 in a rectangular grid) depending on the probability assigned for the same using a preference matrix. The probability distribution for each pedestrian (entity) is defined and modified according

to the effects of interaction with other entities and obstacles.

Social Force Models

The concept of social forces to model pedestrian dynamics was introduced by [82]. It is based on the theory that pedestrian crowd moves in a social field [117] and they are subject to non-Newtonian forces - the so-called 'social' forces - which describe the self-propelling force towards a target, interaction forces between each other and interactive forces with the environment. The prototypical equations for such a model are the kinematic equations. The temporal change of location r_α of pedestrian α obeys the equation:

$$\frac{dr_\alpha(t)}{dt} = v_\alpha(t). \tag{2.2}$$

And the velocity changes are given by the acceleration equation:

$$\frac{dv_\alpha(t)}{dt} = \mathscr{I}_\alpha(t) + \eta_\alpha(t), \tag{2.3}$$

where $\mathscr{I}_\alpha(t)$ denotes the sum of social forces influencing the pedestrian α and $\eta_\alpha(t)$ are individual fluctuations reflecting unsymmetrical behavioural variations.
Helbing formulated a social force model based on the following observations:

1. Each pedestrian α is trying to reach his or her destination by the shortest possible polygonal path in a desired direction e^0_α with a desired speed v^0_α. The actual velocity v_α gets adapted to the desired velocity in a certain time τ_α.

2. The pedestrians interact with the other pedestrians in their vicinity. In particular, they keep a distance from the others to avoid collisions. This repulsive force is given by appropriate potentials.

3. They repel away from obstacles such as walls and are attracted by objects like window displays and artists.

Thus, the systematic part $\mathscr{I}_\alpha(t)$ of acceleration force is given by:

$$\mathscr{I}_\alpha(t) = \frac{1}{\tau_\alpha}(v^0_\alpha e^0_\alpha - v_\alpha) + \sum_{\beta\neq\alpha} \mathscr{I}_{\alpha\beta}(t) + \sum_B \mathscr{I}_{\alpha B}(t) + \sum_k \mathscr{I}_{\alpha k}(t), \tag{2.4}$$

where $\mathscr{I}_{\alpha\beta}(t)$, $\mathscr{I}_{\alpha B}(t)$ are the repulsive forces towards other pedestrians and obstacles, respectively, and $\mathscr{I}_{\alpha k}(t)$ are the attractive forces towards other objects. The distance-dependent interaction force can be given a simple circular or elliptical specification. For panicking pedestrians, additional physical interaction forces due to friction during collision exists.
The model is capable of handling uni- and multi-directional flows, including intersecting flows. Numerous self-organisation phenomena, like lane formation, stop-and-go flows and stripe formation in intersecting flows, have been described using this model. The spatiotemporal patterns observed emerge due to the nonlinear interactions of pedestrians, while there are no strategies or communication or imitation of behaviour by pedestrians. Moreover, though the model is completely symmetric, all the collective behaviour, like freezing by heating and faster is slower effect, are

symmetry-breaking phenomena. The model has since been revised and extended further to study various events, such as evacuation [80] and panic [81]. A comprehensive review of the different dynamical patterns and phenomena is provided in [40].

Some other microscopic modelling techniques include magnetic force models [135], queuing network models [162], optimal velocity models [132] and heuristics or vision-based models [129]. We observe that the system under consideration is a discrete system with a finite number of particles. Hence, microscopic scale provide the perfect framework for modelling them. But the main drawback of such models is the fact that they are suitable to study only small systems. As the number of pedestrians increases, the models become increasingly computationally expensive and infeasible. Further, deterministic knowledge of minute details of individual behaviour is not practically available for modelling; there are always fluctuations or randomness involved, say in terms of initial conditions.

2.1.2 Kinetic Models

The mesoscopic scale models involve deriving Boltzmann-like equations for the evolution of the probability distribution function of the position and velocity of pedestrians, $f(t,\vec{x},\vec{v})$, where f is totally integrable. This is motivated by the kinetic theory of gases [19, 24]. But while in the kinetic theory of classical particles, the interactions are reversible and follow the conservation of mass, momentum and energy, the interactions in self-propelled particle systems are non-conservative, irreversible, non-linearly additive and non-local. They are hence called 'active' particles [18, 21]], whose motion is dictated by individual/collective social strategies. This is observed in other non-equilibrium systems as well, for instance, biological systems [12]. The collision integral or operator in the Boltzmann equations here is defined using particles' number density balance in any given control volume, which is determined by the microscopic modelling of interactions of any given test particle with the field particles. The macroscopic quantities like density and mean velocity are obtained as moments of the distribution function f. A prototype of kinetic models is given by the following equation:

$$\partial_t f + v.\nabla_x f + \nabla_v.(Ff) = \mathscr{J}[f]$$

The kinetic theory approach, in most cases, involves a continuity assumption, as the state of a system is described using continuous probability density functions. Such an assumption would be valid only in large or medium-sized systems; that is, the pedestrian density should be large enough. To deal with the criticisms on the continuous velocity models, discrete velocity models have been developed too [19]. Further, the kinetic approach has been developed to study dynamics in bounded domains with [102] and without obstacles [8].

2.1.3 Macroscopic Models

The macroscopic approach approximates the system as a continuum flow and describes it using systems of partial differential equations. Herein, the conservation laws for mass and linear momentum provide the evolution equations for macroscopic quantities like density and mean velocity. A

general structure is given as :

$$\begin{aligned} \partial_t \rho + \nabla_{\mathbf{x}}.(\rho \vec{U}) &= 0, \\ \partial_t \vec{U} + (\vec{U}.\nabla_{\mathbf{x}})\vec{U} &= \vec{F}[\rho, \vec{U}]. \end{aligned} \tag{2.5}$$

We need to note that the continuum hypothesis is not entirely realistic in such systems. Further corrections need to be incorporated since they do not, in reality, conserve momentum and energy. Also, the hypothesis is strictly restricted to high-density scenarios.

Classically, if only a continuity equation (conservation of mass) is involved, with an appropriate closure equation linking velocity and density, we have a first-order model [43, 90, 95]. While second-order models involve the continuity and momentum equation coupled together, along with the suitable phenomenological model for the acceleration term $\vec{F}$. Three classes of second-order models differing on how the acceleration term is defined and their qualitative analysis is detailed in [23] and [54]. The distinction revolves around the term either involving acceleration towards an optimal velocity/path or involving a pressure-like density gradient.

Henderson initiated the macroscopic modelling by conjecturing that pedestrian crowds behave similarly to gases or fluids. Henderson's fluid dynamic approach, see [83], was later extended by Hughes via the idea of a potential function in the domain to incorporate more geometric information in a first-order model, see [94, 95]. Additional developments of the same were attempted by [52] and [92].

Hughes Model

Hughes proposes a simple first-order model by considering a homogeneous group of pedestrians in a bounded domain. The 2D model is described using the continuity equation (conservation of mass) of fluid mechanics, given by the first equation of Eqn. (2.5). Hughes makes the following three hypotheses on pedestrian behaviour -

Hypothesis 1 : The walking speed of pedestrians is a function of density of the flow; thatis,

$$u = \mathscr{V}(\rho)\hat{\phi}_x\,,\; v = \mathscr{V}(\rho)\hat{\phi}_y\,,$$

where $\hat{\phi}_x$ and $\hat{\phi}_y$ are the direction cosines.

Hypothesis 2 : Pedestrians have a common purpose-oriented potential ϕ and the motion is always in a direction perpendicular to it, that is,

$$\hat{\phi}_x = \frac{-\dfrac{\partial \phi}{\partial x}}{\sqrt{\left(\dfrac{\partial \phi}{\partial x}\right)^2 + \left(\dfrac{\partial \phi}{\partial y}\right)^2}}\,,\; \hat{\phi}_y = \frac{-\dfrac{\partial \phi}{\partial y}}{\sqrt{\left(\dfrac{\partial \phi}{\partial x}\right)^2 + \left(\dfrac{\partial \phi}{\partial y}\right)^2}}$$

Hypothesis 3 : Pedestrians try to find the shortest time of travel but also try to avoid high-density regions. This is translated to the distance between potentials being proportional to the

pedestrian speed, that means,

$$\frac{1}{\sqrt{\left(\frac{\partial\phi}{\partial x}\right)^2+\left(\frac{\partial\phi}{\partial y}\right)^2}} = \mathscr{D}(\rho)\sqrt{u^2+v^2},$$

where $\mathscr{D}(\rho)$ factors in discomfort at high densities.

Hence, the governing equation is:

$$-\frac{\partial\rho}{\partial t}+\frac{\partial}{\partial x}\left(\rho\mathscr{D}(\rho)\mathscr{V}^2(\rho)\frac{\partial\phi}{\partial x}\right)+\frac{\partial}{\partial y}\left(\rho\mathscr{D}(\rho)\mathscr{V}^2(\rho)\frac{\partial\phi}{\partial y}\right)=0. \tag{2.6}$$

This equation is supplemented with appropriate boundary conditions, and the relations $\mathscr{V}(\rho)$ and $\mathscr{D}(\rho)$ are defined via simple theories following traffic flow. Also, we note the model can be extended for inhomogeneous crowds easily. Hughes also discusses the mathematical properties of the system, flow conditions - supercritical or subcritical and conformal invariance of equations. The model is similar to the Lighthill–Whitham–Richard (LWR) model of traffic flow [118]. The major limitation in such first-order models is the predefined formulation of speed-density relations. It is quite restrictive to assume that speed only depends on the macroscopic quantity. In reality, various factors affect the walking speed of pedestrians. In [92], Huang et al. reformulated this model and described how the potential function could be interpreted as an instantaneous total cost to the destination and hence essentially the hypotheses translates to -

$$||\nabla\phi|| = C(\rho,x,y,t), \tag{2.7}$$

the so-called **"Eikonal Equation"** with cost functional $\mathscr{C}$ with

$$\mathscr{C}(\rho,x,y,t) := \frac{1}{\mathscr{D}(\rho)\mathscr{V}(\rho)}.$$

We later describe in Chapter 3 how this idea of potential functions is explored in the model(s) we use.

More macroscopic models are seen in [60] and [143]. Elaborate reviews of the different models, along with a discussion of their advantages and limitations, can be found in [22] and [81].

Modelling at each scale has its own advantages and limitations, as discussed above. The appropriate modelling scale for each scenario depends on several factors, like the size of the system and what sort of information is required from the system. We refer to [10] for a recent review on the models on kinetic and macroscopic scales.

2.1.4 Hierarchy of Models - Bottom-up Approach

The inquiry into deriving the macroscopic properties of physical systems from the microscopic properties of their constituents (molecules, atoms etc.) led to the foundations of statistical mechanics. The problem was solved mathematically via the kinetic theory of gases, pioneered by [29] and [124]. Kinetic models, which describe the density distribution of particles, act as a bridge between the microscopic and macroscopic scales of models.

For N interacting particles, the Liouville equation governs the evolution of N-particle distribution (probability density function (pdf) f_N) in the phase space of position and velocity. Using integration by parts, the Liouville equation can be converted into a chain of equations called BBGKY (Bogoliubov–Born–Green–Kirkwood–Yvon) hierarchy, where any s-particle pdf is related to the $s+1$-particle pdf. Since these equations are coupled and not closed, we need a closure relation to make sense of the full Liouville equation. In a special case for the one-particle pdf f, the Boltzmann equation is obtained from the Liouville equation by a limiting process using the Boltzmann-Grad limit (radius of hard sphere $\delta \to 0$ and $N \to \infty$). Here, the particle interactions enter the equation via collision operators. There are other approximations which can also truncate the chain and render a solution to the BBGKY form.

Similar to the Boltzmann equation, mean-field approximations for N-body problem leads to an evolution equation for the probability density distribution of a single particle under appropriate scaling and in the limit $N \to \infty$. Under the empirical measure, we get the the mean-field kinetic model, wherein the interactions are modeled through the kernel mappings. A proof of the global existence of the weak solution to the mean-field kinetic equation is provided in [177].

Formal derivation of the fluid models via the hydrodynamic limits of the Boltzmann equations can be provided by applying different perturbation techniques - due to Hilbert [86] or Chapman [39], or Enskog [57]. Later, a method of moments was proposed by Grad [73], which involved deriving the conservation laws by multiplying the kinetic model with v^0, v , v^2 etc. and integrating w.r.t. v. The zeroth moment of f is bulk density ρ, the first moment is momentum $\rho\, u$, and the second moment is energy. A system of equations is obtained through this method, and a state relation is required to close the system. This method of moments is employed in this thesis to derive the continuous macroscopic model from their kinetic equivalents in Chapter 5. The whole idea of a hierarchy of models starting from the individual IBM to the CM discussed here is demonstrated via the detailed derivation in Chapter 6. A similar derivation has been employed in [60] to derive the macroscopic pedestrian model in Section 3.2. We also refer to [49] and [50].

2.1.5 Eikonal Equation

Eikonal equation is a first order partial differential equation describing the propagation of wavefronts in a medium with varying refractive index. The equation takes the form of a Hamilton-Jacobi equation, and its solution gives the phase of the wavefronts, which can be used to determine the direction of wave propagation and the intensity of the wave. Mathematically, the classical eikonal equation is given by,

$$||\nabla \phi(x)||^2 = n^2(x)\,,$$

where $n(x)$ is the refractive index of the medium at point x and ϕ is the wavefront phase. Eikonal equations arise in the study of non-linear Maxwell's equations and provide a link between wave optics and geometric ray optics. Another prominent application of eikonal equations is in approximating the travel times of seismic waves in geophysics [106, 148]. For this formulation, if we

consider an open set Ω with boundary $\partial\Omega$, then the solution ϕ to the equation

$$||\nabla\phi(x)||^2 = \frac{1}{\mathscr{F}(x)}, x \in \Omega, \phi(x) = q(x)x \in \partial\Omega,$$

where $\mathscr{F}$ is speed and q is a Lipschitz continuous cost function and , gives the shortest time of travel from x to $\partial\Omega$. The eikonal equation has many applications in image processing, robotic path planning and in differential games.

2.2 Mesh-free Methods

Numerous methods have been developed over the years to solve partial differential equations (PDEs), many of them being general methods and some being special to the class of PDEs, say hyperbolic or elliptic, we have to solve. There are two main approaches for these numerical methods - one direct, called strong form methods and one indirect, called weak form methods. Strong form methods discretise and solve the PDEs directly, and weak form methods establish an equivalent system, usually in integral form, that governs the physical problem and solves them. The finite difference method (FDM), finite volume method (FVM) and collocation method are examples of strong form methods, while the finite element method (FEM) is a weak from method. Methods like FDM and FVM use fixed grids for the discretisation, with the dependent variables being evaluated at grid points (also called cell centres in the case of FVM).

On the other hand, meshfree methods do not involve predefined meshes. They essentially use a set of scattered nodes within the problem domain and the boundaries. The functional values are approximated locally using these nodes. And a set of algebraic equations are devised for the domain. To approximate the unknown function, 'shape (basis) functions' are used. These basis functions are locally supported, only a small set of nodes in the immediate neighbourhood are used for evaluation and the shape function is considered zero outside this local neighbourhood. Such shape functions are said to have 'compact support', and the local neighbourhood is called the support domain or influence neighbourhood. The shape functions can be defined in integral, differential or even series form. In meshfree methods, both strong and weak forms exist. There are a variety of meshfree methods using local nodes for function approximation, like Smooth Particle Hydrodynamics (SPH) method, meshless local Petrov–Galerkin (MLPG) method, the point interpolation method etc. See [119] for details on different kinds of meshfree methods. One of the categories of meshless methods is particle methods, and the one described here has a strong formulation.

Meshless methods have numerous advantages over grid-based methods. Grid-based methods typically require a structured or unstructured grid, and this process of grid generation can be time-consuming, especially for complex geometries. Meshless methods are better suited for handling complex geometries, and they lead to fewer problems with accuracy or stability around irregular boundaries or regions with strong gradients. Additionally, they are more easily adaptable to moving boundary problems, such as those involving fluid-structure interaction. Further to this, meshless methods utilize less memory than mesh-based methods, and this proves beneficial when we need

to scale the grid to higher dimensions. Mesh-based methods are quite impractical, as they lead to an exponential growth in the number of grid points required to maintain accuracy in such cases. Moreover, meshfree methods are better suited for parallel computing and cause lesser issues, like load balancing between nodes involved in distributed computing, in large-scale problems. All of these factors make meshfree methods computationally less expensive than traditional grid-based methods. Apart from this, we see that meshless methods do not have connectivity constraints, that is, nodes can be located anywhere, and hence they can easily handle singularities. The use of interpolation techniques leads to smoother solutions and also helps in handling discontinuities.
While meshless methods offer a significant number of advantages over mesh-based methods, they have limitations too. They may lead to higher computational costs for some particular problems, as they can involve numerical integration over unstructured domains. Since these methods are often dependent on smoothing parameters that determine the size of the influence domain, the choice of these parameters can have an impact on the accuracy and stability. Moreover, finding optimal values of these parameters is a challenge. Similarly, as the method relies heavily on the distribution of data points and their sampling density, it is prone to errors if the data distribution is not reflective of the underlying system. Lastly, as these methods are relatively new, they lack well-established standards and conventions like traditional methods. Hence, it is sometimes difficult to establish practices for using it in different applications.

2.2.1 Finite Point Set Method

The finite point set method is a generalised finite difference method. In this method, a point cloud in the computational domain acts as numerical grid points. FPM is a strong formulation and models differential equations by the direct approximation of differential operators.

Point Cloud

Let Ω be a computational domain with boundary Γ. We discretise the interior of the domain with a set of particles, called interior particles or interior points/nodes, and the boundary with a set of particles, called boundary particles or boundary points/nodes. The initial distribution of the point cloud is typically random (can be structured too), but whose resolution is prescribed by a smoothing length, $h = h(x,t)$.
The boundary is discretised first, by considering it as piece-wise linear segments (lines or triangles or quadrilaterals) and populating these segments starting from their midpoint. Once the boundary is discretised, layer of interior particles are initialised inside the domain in accordance with the distance criterion. We successively create such layers of particles from the already available layers of points till the centre of the domain is reached.

Approximations

Let x be an arbitrary point in the domain where we need to evaluate an unknown function $Z(x)$ and its spatial derivatives from the neighbouring particles. We consider a weight function w with compact support, such that the particles closer to x have a larger influence than those away from it.

Here, we use a truncated Gaussian weight function,

$$w(x_j) = \begin{cases} \exp\left(-\dfrac{\alpha\,||x_j - x||^2}{h^2}\right) & \text{, if } x_j \leq h \\ 0 & \text{, elsewhere} \end{cases}$$

where α is a positive constant and $x_j \in \mathscr{N}(x)$ with $\mathscr{N}(x)$ being the set of 'm' neighbours of x. Consider the Taylor series approximations of $Z(x_j)\,, j = 1,2,...m$ about x:

$$Z(x_j) = Z(x) + \sum_{k=1}^{2} Z_k(x)(x_{kj} - x_k) + \frac{1}{2}\sum_{k,l=1}^{2} Z_{kl}(x)(x_{kj} - x_k)(x_{lj} - x_k) + e_j\,. \tag{2.8}$$

These can be written in matrix form as: $M\mathbf{a} = \mathbf{b} - \mathbf{e}$, that is,

$$M = \begin{pmatrix} 1 & 1 & 1 & 1 & 1 & 1 \\ 1 & dx_{11} & dx_{21} & \frac{1}{2}dx_{11}^2 & dx_{11}dx_{21} & \frac{1}{2}dx_{21}^2 \\ 1 & dx_{12} & dx_{22} & \frac{1}{2}dx_{12}^2 & dx_{12}dx_{22} & \frac{1}{2}dx_{22}^2 \\ \vdots & \vdots & \vdots & \vdots & \vdots & \vdots \\ 1 & dx_{1m} & dx_{2m} & \frac{1}{2}dx_{1m}^2 & dx_{1m}dx_{2m} & \frac{1}{2}dx_{2m}^2 \end{pmatrix},$$

and

$$\mathbf{a} = \begin{pmatrix} Z(x) \\ Z_1(x) \\ Z_2(x) \\ Z_{11}(x) \\ Z_{12}(x) \\ Z_{22}(x) \end{pmatrix}, \mathbf{b} = \begin{pmatrix} Z(x_1) \\ Z(x_2) \\ \vdots \\ Z(x_m) \end{pmatrix}, \mathbf{e} = \begin{pmatrix} e_1 \\ e_2 \\ \vdots \\ e_m \end{pmatrix}.$$

Since in most cases we ensure that $m > 6$, this is an over-determined system if we consider to take $\mathbf{e} = 0$. So, to find the unknowns, method of weighted least squares is used. We minimize the functional (quadratic form):

$$J = \sum_{j=1}^{m} w_j e_j^2\,.$$

If we considered a weighted matrix $W = \delta_{ij} w_j$, then

$$J = (M\mathbf{a} - \mathbf{b})^T W (M\mathbf{a} - \mathbf{b})\,.$$

The minimization of J gives,

$$\mathbf{a} = (M^T W M)^{-1}(M^T W)\mathbf{b}\,.$$

Each row of $\mathbf{a}$ gives the derivatives' values as a linear combination of the known values of the function at the neighbouring points in $\mathscr{N}(x)$. The neighbour lists are usually large, i.e. m is large, and so we have a sparse linear system. And the system can be solved by any of the iterative solvers.

Neighbour Searching

The efficiency of neighbour-searching algorithms is imperative in particle methods. For each particle x_i, the set of nodes at a distance less than h from it are considered the nearest neighbours. But the crude way of computing pairwise distances for each pair of particles and then finding the neighbour list is extremely expensive. In order to avoid this, the domain is split into cells such that each particle is assigned a cell. Neighbours are then detected by only considering the nodes within the same cell or adjacent ones sharing an edge.

Addition and Deletion/Merging of Points

In order to establish the quality and initial density of the cloud, it is ensured that no two points are closer than $r_{min}h$ distance apart and that every sphere of radius $r_{max}h$ has at least one point. This implies that the distance between any point and its nearest neighbour (inter-point distance) lies within the range (r_{min}, r_{max}). But the movement of the point cloud according to the dynamics of the fluid may sometimes result in them coming too close, forming clusters, or moving far apart, creating holes in the domain. To emend such anomalies, we include additional particles in the holes or remove particles from the clustered ones. On addition of particles, we need to approximate the physical quantities there. Again, we use interpolation from the neighbouring particles for this. Removing particles is pretty straightforward; we either add one particle at the centre of mass of the two particles or remove one out of them. Also, we mention that when a particle needs to be removed, boundary (rigid or free surface) particles have a higher preference to be retained than the interior ones. For further details, we refer to [164], [159] and [158].

2.3 Solving the Eikonal Equation

Eikonal equation can be solved via different approaches depending on the specific problem being solved. One approach involves converting the eikonal equation into a time-dependent level-set equation which can be solved by higher-order methods. Finite volume methods [6], Galerkin methods [17] or non-oscillatory methods [138] can be used to solve this time-dependent Hamilton-Jacobi equation. These methods are conditionally stable and require a lot of time for convergence in the entire domain due to the finite speed of propagation. Convergence to a weak solution can be seen as limits of viscosity solutions for Hamilton-Jacobi equations [44]. The level set method was developed to solve these higher-order equations in [137]. A second approach is to consider the equation as a stationary boundary value problem and devise algorithms to solve the non-linear system of equations on discretisation. In this case, finite difference methods can be applied directly for upwind approximations, and the discretised equations can be solved iteratively. Fast level set techniques for solving stationary problems have been developed. Amongst the various methods available in literature for solving the eikonal equation, the front marching methods like fast sweeping method [178, 179] and fast marching methods are popular because they are fast and unconditionally stable. The fast sweeping method is an iterative algorithm and uses non-linear upwinding along with Gauss-Seidel like iterative procedure for alternating sweeping in predefined

directions. We use the fast marching method, as described below, in the numerical computations in this thesis work.

We mention that solving the Eikonal equation by the classical method of characteristics is possible in the local sense. But global solutions cannot be obtained due to intersecting characteristics causing shocks. Hence, we devote to finding viscosity solutions. A crucial feature of the Eikonal equation is that the trajectory of characteristics and the gradient lines of the viscosity solution coincide. With respect to the numerical approximations of solutions, this feature has helped with the development of Dijkstra-like algorithms, such as, the level set method.

2.3.1 Fast Marching Method

Fast marching method (FMM) is a single-pass algorithm for solving the Eikonal equation without any iteration. It uses the "causality" principle where information propagates in a single direction from smaller values of the function to larger ones, from one grid point to another. The solution is obtained by moving "upwind" from the boundary. The technique involves upwind finite difference approximations of the eikonal operators in such a way that the causality relationship is reflected. The algorithm is fast because of computations being restricted to a narrow band around the front. The narrow band is marched forward while the evaluated points are frozen, and new points are added to the band. The algorithm, as described in [153], involves the following steps:

1. Tag all the points in boundary where value is known as 'Known'.
2. Add all the neighbours of points in 'Known' to the 'Narrow' band. Add all other points to 'Far' band.
3. Let A be the trial point with the minimum value.
4. Add A to 'Known', remove it from 'Narrow' band.
5. Update 'Narrow' band - find neighbours of A , if any of them is in 'Far', remove them from 'Far' and add to 'Narrow'.
6. Recompute the values at all the points in 'Narrow'.
7. Return to Step 3.

The efficiency of the algorithm depends heavily on the method used to identify the grid point with the smallest value in the 'Narrow' band. A min-heap data structure is an efficient scheme discussed in [155] and utilised here. Given M_n points in the heap, this data structure sorts the heap in $O(\log M_n)$ steps. So the total computational time of the FMM for a mesh with M_n points is $O(M_n \log M_n)$ steps as each mesh point is visited once to add to 'Known' and every time the heap is reordered. The fast marching method was introduced for solving static Hamilton-Jacobi equations in rectangular or triangulated grids. We describe below how the least square approximations of the FPM approach can be adapted to solve the Eikonal equation on any grid - orthogonal, non-orthogonal or meshfree.

2.3.2 Using FPM

Consider the Eikonal equation:

$$||\nabla\Phi(x)||^2 = \mathscr{F}^2(x)\,, x \in \Omega\,. \tag{2.9}$$

Suppose the domain Ω is discretised by m points $X_1, X_2, ..., X_m$. Let $\mathscr{A}$ be the set of nodes where the solution Φ is already available or computed. Consider a node $\tilde{X}$ where we need to compute Φ. Let $N_{\tilde{X}}$ be the set of neighbours of $\tilde{X}$ in a ball of radius h and $N_{\tilde{X}\mathscr{A}} = N_{\tilde{X}} \cap \mathscr{A}$.
If $|N_{\tilde{X}\mathscr{A}}| = 1$, say, $N_{\tilde{X}\mathscr{A}} = \{X_1\}$, then the value of Φ at $\tilde{X}$ is given as

$$\Phi(\tilde{X}) = \Phi(X_1) + \mathscr{F}(\tilde{X})||\tilde{X} - X_1||\,.$$

If $|N_{\tilde{X}\mathscr{A}}| \geq 2$, say, $N_{\tilde{X}\mathscr{A}} = \{X_1, X_2, X_3, ..., X_m\}$, then we can approximate the value of Φ at $\tilde{X}$ via Taylor series similar to the description in Section 2.2.1. For $j = 1, 2, ..., m$, denote $\Phi(X_j) = \Phi_j$ and $\Phi(\tilde{X}) = \tilde{\Phi}$, then we have,

$$\Phi_j = \tilde{\Phi} + \sum_{k=1}^{2} \tilde{\Phi}_k dX_{kj} + e_j,$$

where $dX_{kj} = X_{kj} - \tilde{X}_k$, e_j is the error and $\tilde{\Phi}_1$ and $\tilde{\Phi}_2$ are $x-$ and $y-$ partial derivatives of $\tilde{\Phi}$, respectively.
Now, we can write the equation in matrix form as:

$$M.a = b, \tag{2.10}$$

where

$$M = \begin{pmatrix} dX_{11} & dX_{21} \\ dX_{12} & dX_{22} \\ \vdots & \vdots \\ dX_{1m} & dX_{2m} \end{pmatrix}, \mathbf{b} = \begin{pmatrix} \Phi_1 - \tilde{\Phi} \\ \Phi_2 - \tilde{\Phi} \\ \vdots \\ \Phi_m - \tilde{\Phi} \end{pmatrix}, \mathbf{a} = \begin{pmatrix} \Phi_1 \\ \Phi_2 \end{pmatrix}.$$

Now, we multiply both sides of Eqn. (2.10) with $M^T W$, where $W = diag(w_1, w_2, \ldots, w_m)$, with Gaussian weights. Then, we get the equation,

$$P.\mathbf{a} = \tilde{\mathbf{b}},$$

where

$$P = \begin{pmatrix} \sum_j w_j dX_{1j}^2 & \sum_j w_j dX_{1j} dX_{2j} \\ \sum_j w_j dX_{1j} dX_{2}j & \sum_j w_j dX_{2j}^2 \end{pmatrix} \text{and} \tilde{\mathbf{b}} = \begin{pmatrix} \sum_j w_j dX_{1j}(\Phi_j - \tilde{\Phi}) \\ \sum_j w_j dX_{2j}(\Phi_j - \tilde{\Phi}) \end{pmatrix}.$$

Let $Q = P^{-1}$. Then, we get, $a = Q.\tilde{\mathbf{b}}$, so that,

$$\tilde{\Phi}_1 = l_{11} + l_{12}\tilde{\Phi} \text{and} \tilde{\Phi}_2 = l_{21} + l_{22}\tilde{\Phi},$$

where

$$l_{11} = \sum_j w_j(Q_{11}dX_{1j} + Q_{12}dX_{2j})\Phi_j\,, l_{12} = \sum_j w_j(Q_{11}dX_{1j} + Q_{12}dX_{2j})\,,$$

and

$$l_{21} = \sum_j w_j(Q_{21}dX_{1j} + Q_{22}dX_{2j})\Phi_j\,,\; l_{22} = \sum_j w_j(Q_{21}dX_{1j} + Q_{22}dX_{2j})\,.$$

Substituting in the Eikonal equation, we get the quadratic equation in $\tilde{\Phi}$,

$$(l_{12}^2 + l_{22}^2)\tilde{\Phi}^2 + 2(l_{11}l_{12} + l_{21}l_{22})\tilde{\Phi} + l_{11}^2 + l_{21}^2 = \mathscr{F}^2.$$

The quadratic equation has two solutions. Considering the upwind structure of the equation and method, the information propagates from smaller to larger values of Φ. So, we take the larger value out of the two solutions, which would be the front moving outwards from the $N_{\tilde{X},\mathscr{A}}$. Moreover, we need to check the causality conditions :

$$\tilde{\Phi} \geq \Phi_j \,\text{and}\, \nabla\tilde{\Phi}.\nabla\Phi_j > 0\;\forall X_j \in N_{\tilde{X},\mathscr{A}}.$$

2.4 Velocity-Density Relation / Fundamental Diagrams

A fundamental relation between the macroscopic variables flow rate, density and mean velocity : $q = v\rho$, is an important equation in the modelling of traffic and crowd flow. If flux q is plotted as a function of density ρ, we have what is referred to as the 'fundamental diagram'. And the plot of velocity v as a function of density ρ is called the 'velocity diagram'.
In the context of traffic modelling, this equation serves as a closure relation for the first-order macroscopic models, which are often obtained from conservation laws. Also, the equilibrium velocity is modelled via such velocity-density relations in homogeneous equilibrium traffic flow. We mention some simple models from literature here [110, 151].
Greenshield's model: A linear model proposed by Greenshield [75] -

$$V(\rho) = V_{max}\left(1 - \frac{\rho}{\rho_{max}}\right). \tag{2.11}$$

Greenberg's model: Greenberg, in [74], proposed a logarithmic relation -

$$V(\rho) = \lambda \ln\left(\frac{1}{\rho}\right). \tag{2.12}$$

Bonzanni-Mussone's model from [30] -

$$V(\rho) = \exp\left[-\alpha\left(\frac{\rho}{1-\rho}\right)\right]. \tag{2.13}$$

Kühne's model from [115]

$$V(\rho) = V_{max}\left(1 - \left(\frac{\rho}{\rho_{max}}\right)^{n1}\right)^{n2}. \tag{2.14}$$

The above models were deduced from experimental studies for different traffic situations. As the macroscopic modelling of pedestrian crowd followed from the traffic models, these relations are employed in the speed-density relations for pedestrian models, for example, the relation f in the

Hughes model. Also, the fundamental diagram is a quantitative benchmark for pedestrian models. Virkler and Elayadath [167] studied the fundamental relation and compared various speed-density models - Greenshields, Greenbreg, bell shape, 2- and 3-regime linear - using video recordings in a pedestrian tunnel. Lam et al. [116] investigated speed-density-flow conditions for different pedestrian facilities such as walkways, crosswalks and stairways in transit stations. Their studies concluded that no single model fits all facilities, and different kinds of speed–density models should be adopted for different pedestrian facilities.

3 Pedestrian Obstacle Interaction

3.1 Introduction

In a social environment, humans encounter stationary or moving obstacles while manoeuvring various spaces to reach their destinations. Different voluntary and involuntary strategies are used by humans to avoid collisions in such scenarios. An understanding of when and whether a collision will occur is essential; see [47]. This information forms the basis of collision avoidance models, as seen in [35]. Numerous experimental studies have been conducted to understand pedestrian collision avoidance behaviour [108].

A major problem which led to the research into obstacle avoidance was the improvement of evacuation efficiency. It has been seen via experimental studies that the presence of a stationary obstacle at bottlenecks can improve evacuation efficiency [156]. The obstacle's position, size and shape all play a role in the evacuation strategy. Moving obstacles have a similar effect [174]; now, their speed also plays a factor. These moving obstacles, such as robots, are used to regulate the flow or navigate to proper exits [169, 175]. Extensive research on pedestrian interactions with moving obstacles is still limited.

Agent-based models taking inspiration from robot motion planning techniques have been used for collision avoidance in literature [64]. Such a velocity-obstacle-based approach models the obstacle as a region to be avoided and makes velocity-based predictions to prevent collisions [46]. The concept of a dynamic potential field to navigate a domain with obstacles without explicit collision avoidance was proposed in [166].

In this work, we propose a model to study such interactions in shared environments. The macroscopic model for pedestrian motion is combined with the proposed kinematic equations of obstacle motion wherein the feedback force terms are modelled via Hughes's approach of potential functions obtained through an eikonal equation. For the numerical solutions, an immersed boundary approach is used along with the mesh-free particle method, as seen in [60].

The chapter is organised as follows: in Sections 3.2 and 3.3, we describe the models for pedestrian and obstacle motion; Section 3.4 explains the numerical method in detail, and we see some results of the numerical simulation for different cases in Section 3.5.

3.2 Pedestrian Model

We consider the pedestrian model developed in [60], which combines a social force model [82] to a Hughes-type model [94]. See Sections 2.1.1 and 2.1.3 for a brief description of these models.

3.2.1 Microscopic Model

The microscopic model for N pedestrians with positions x_i, $i = 1,2,\ldots N$ and velocities v_i, $i = 1,2,\ldots,N$ is

$$\begin{aligned} dx_i &= v_i\,dt, \\ dv_i &= \sum_{i\neq j} I(x_i - x_j, v_i - v_j)dt + G(x_i, v_i, \rho_i)\,dt. \end{aligned} \tag{3.1}$$

The function I denotes the interaction force term between the pedestrians. I is given as the gradient of an interaction potential. And the function G is the desired acceleration term which is based on the eikonal solution ϕ. Here, as the eikonal solution dictates the trajectory of the pedestrians, G is given as,

$$G(x,v,\rho) = \frac{1}{T}\left(-V(\rho(x))\frac{\nabla\phi(x)}{\|\nabla\phi(x)\|} - v\right). \tag{3.2}$$

These equations are coupled to an eikonal equation,

$$V(\rho(x))\,||\nabla\phi|| = 1\,, \qquad x\in\Omega\,, \tag{3.3}$$

where V is a density dependant velocity function (cf. Section 2.4).

Interaction Forces

The interaction forces between pedestrians, I, in Eqn. (3.1), are modelled similar to the social forces concept as described in Section 2.1.1. $I(x_i - x_j, v_i - v_j)$ is the interaction force between pedestrians at positions x_i and x_j moving with velocities v_i and v_j, respectively. The force can be modelled as a pure repulsive force so that,

$$I(x,v) = \frac{C_r}{l_r}\exp\left(-\frac{\|x\|}{l_r}\right)\hat{n}\,, \tag{3.4}$$

where C_r is a repulsive strength and l_r a length scale. Or it could be a linearly varying repulsive force combined with dissipative effects, similar to that given in [60] as below:

$$I(x,v) = \left(k_n(2R_r - x)\hat{n} - \mu_n\langle v,n\rangle\hat{n} - \mu_t\langle v,n^{\perp}\rangle n^{\perp}\right)H(2R_r - x), \tag{3.5}$$

where H is a Heaviside function and R_r is an interaction radius. k_n is the interaction strength. μ_n and μ_t are the frictional coefficients, and $\hat{n}$ and $n^{\perp}$ are the unit vectors, in the normal and perpendicular directions, respectively.

Relaxation Time

The relaxation time T denotes how fast the pedestrians can correct their current velocity to the desired velocity.

> **Remark 3.1** The values for the parameters maximal density ρ_{max}, maximal velocity V_{max} and relaxation time T in the above model are chosen from the literature on experimental studies [34].

3.2.2 Hydrodynamic Model

The basic hydrodynamic model for pedestrian motion, comprising of the continuity and momentum equations, coupled to the eikonal equation in Eqn. (3.3), is:

$$\begin{aligned} \partial_t \rho + \nabla_x.(\rho U) &= 0\,, \\ \partial_t U + (U.\nabla_x)U &= G(x,U,\rho) + \hat{I}(\rho,U)\,, \\ V(\rho(x))\,||\nabla\phi|| &= 1\,, \qquad x \in \Omega\,. \end{aligned} \tag{3.6}$$

The macroscopic variables ρ and U here denote the density and average velocity of the pedestrians (as a fluid). The detailed derivation from the microscopic model in Eqn. (3.1) to the macroscopic model in Eqn. (3.6) via mean-field kinetics is provided in [60].

3.3 Equations for Moving Obstacle

We classify the obstacles into two - passive and dynamic and model their dynamics using simple ODEs governing the movement of their centre of mass.

3.3.1 Passive Obstacles

For the purpose of our study, we consider those obstacles as "passive", which do not have a feedback interaction. That is, these obstacles move along fixed trajectories and do not change their path or speed depending on the presence/absence of the pedestrians in their vicinity. It means that there is no need to provide any self-driven force to these obstacles. Their motion, as the motion of centre of mass of the rigid obstacle, can be modelled independently as:

$$\begin{aligned} dx &= vel_{tot}\,dt\,, \\ vel_{tot} &= A\,cos(\omega t), \end{aligned} \tag{3.7}$$

where A is the amplitude and ω, the frequency of oscillatory motion of the obstacle, which defines the velocity vel_{tot} of the obstacle.

3.3.2 Dynamic Obstacles

We consider those obstacles as "active", which have a feedback interaction. They intake the information from the environment and change their path and speed in order to avoid collisions with other obstacles and pedestrians while moving towards a predefined and specific target/exit. Here, the interaction between the pedestrians and moving active obstacle(s) is additionally modelled by kinematic equations using a repulsive potential similar to the pedestrian-pedestrian interactions. Also, a second eikonal equation is integrated for computing the path of the obstacle towards its destination. The velocity update equation for the obstacle in this case based on these forces is given as:

$$\begin{aligned} dx_i^O &= v_i^O dt\,, \\ dv_i^O &= \sum_{j \in N_p} I^O(x_i^O - x_j, v_i^O - v_j)dt + G^O(x_i^O, v_i^O, \rho_i)dt\,, \end{aligned} \tag{3.8}$$

where x_i^O and v_i^O are the position and velocity of the i^{th} obstacle's centre of mass (see Fig. 3.3), N_p is a neighbour list of pedestrians in the immediate vicinity of the obstacle, x_j and v_j are the position and velocity of the j^{th} pedestrian neighbour and ρ_i is the interpolated density of pedestrians at x_i^O. I^O is specified as a negative gradient of an interaction potential $I^O = -\nabla P^O$ and desired acceleration G^O is obtained from the gradient of the eikonal solution ϕ^O for the obstacle. For a density dependant velocity function V^O, we have,

$$G^O(x^O, v^O, \rho) = \frac{1}{T^O}\left(-V^O(\rho(x^O))\frac{\nabla\phi^O(x^O)}{||\nabla\phi^O(x^O)||} - v^O\right),$$

coupled to the eikonal equation

$$V^O(\rho(x))\,||\nabla\phi^O|| = 1\,, \qquad x \in \Omega\,. \tag{3.9}$$

Here, we take, P^O as a pure repulsive Morse potential:

$$P^O(x) = C_r^O \exp\left(-\frac{||x||}{l_r^O}\right), \tag{3.10}$$

so that, we have I^O similar to Eqn. (3.4),

$$I^O(x,v) = \frac{C_r^O}{l_r^O}\exp\left(-\frac{\|x\|}{l_r^O}\right)\hat{n}\,. \tag{3.11}$$

The coupling of the kinematic equations of the moving obstacle to the hydrodynamic model of pedestrian motion is through the eikonal equation solving for ϕ^O with density ρ of pedestrians.

3.4 Numerical method

For the purpose of the numerical simulation of the described model(s), we use a meshfree particle method which is based on least square approximations [164], as described in Section 2.2.1.

3.4.1 Space and Time Discretization

For the numerical simulations, a Lagrangian formulation of the hydrodynamic equations in Eqn. (3.6) is used in this method with the material derivatives as below:

$$\begin{aligned}
\frac{dx_i}{dt} &= U_i\,,\\
\frac{d\rho_i}{dt} &= -\rho_i \nabla_x . U_i\,,\\
\frac{dU_i}{dt} &= G(x_i, U_i, \delta\star\rho) + I\star\rho\,.
\end{aligned} \tag{3.12}$$

And this system is coupled to the obstacle's kinematic equations Eqn. (3.8). The convolution integral of the interaction potential is evaluated by a first order integration rule:

$$\hat{I}(\rho, U) = I\star\rho \approx \sum_{j\in N} I(x-x_j, U-U_j)\,\rho_j\,dV_j,$$

where dV_j is the local area around a particle. The resultant equations are solved by an explicit Euler time discretization method in our simulations.

3.4.2 Grid

A mesh-free cloud of particles (mesh-free grid) is used to solve the pedestrian flow equations in Lagrangian form, as described above. A separate fixed structured or unstructured grid is used to solve the eikonal equation in the domain considered. The information from the irregular point cloud, like density and velocity, is interpolated to the stationary eikonal grid to solve the eikonal equation. See Section 2.3 for details on solving the eikonal solution. And the spatial derivatives of the eikonal equation at any grid point of the mesh-free cloud are computed from the values of its neighbouring grid points of the eikonal grid, using a weighted least-squares method as described in Section 2.2.1.

To handle the moving obstacle, we use an immersed boundary approach. The grid points are activated or deactivated according to the position of the moving obstacle, as shown in Fig. 3.1. The points of the eikonal grid, which are completely inside the boundary of the obstacle, are deactivated for calculations, and the points outside the boundaries are activated.

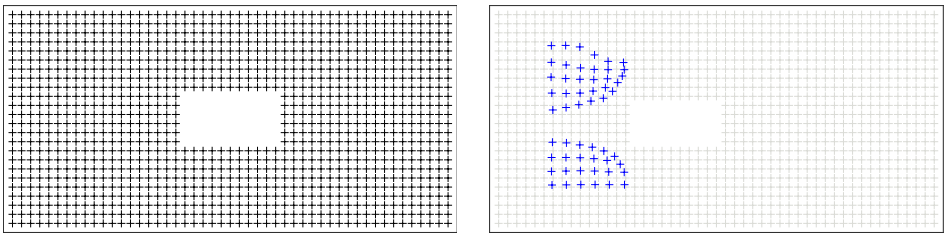

Figure 3.1 – Eikonal Grid with a Rectangular Obstacle (left) and Mesh-free Cloud (right)

3.4.3 Eikonal Equation

The eikonal equation is solved by a fast marching method [154] on the separate structured mesh, see Section 2.3.1.

In the case of the passive obstacle, one eikonal equation pertaining to the pedestrian motion is solved (see Eqn. (3.6)), while in the case of the active obstacle, two eikonal equations, one for pedestrians and one for obstacle(s) (see Eqn. (3.9)), are solved.

The eikonal solution essentially incorporates the model's hypothesis that the information about the environment is available to the pedestrians/obstacles at any given time. This information includes the position of the pedestrian cloud or obstacle/vehicles, the position of the walls, the position of the exit doors and the edges of the roads. These pieces of information are mathematically provided either as boundary condition(s), say for exit space in the domain, or via the density-dependant function $V(\rho)$ and $V^O(\rho)$. A cost to avoid higher density regions in the crowd is provided via V/V^O.

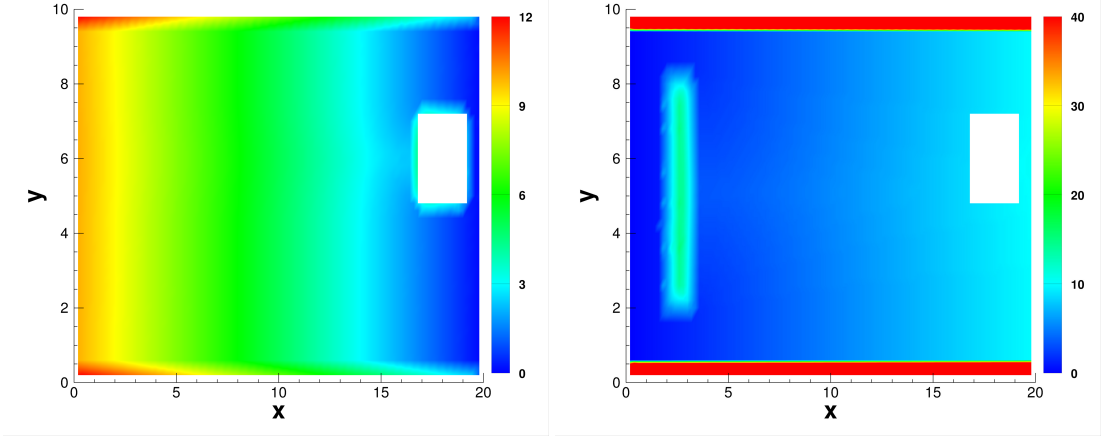

Figure 3.2 – Eikonal Solution for pedestrians (left) and for obstacles (right)

Velocity-Density Relations

While solving for ϕ, the eikonal solution for pedestrians, as in Fig. 3.2 (left), we take (see Greenshield's model in Eqn. (2.11)),

$$V(\rho(x)) = V_{max}(1 - \rho(x)/\rho_{max})\,.$$

Here, $\rho(x)$ is the density of pedestrians interpolated at a given location x or it is the artificial density at a given location x if x is a point on the boundary walls or edges of the obstacle.
While solving for ϕ^O, the eikonal solution for obstacle, as in Fig. 3.2 (right), we take for $n1 > 0$ (see Kühne's model in Eqn. (2.14)),

$$V^O(\rho(x)) = V^O_{max}(1 - (\rho(x)/\rho_{max})^{n1})\,.$$

Here, $\rho(x)$ is again the value of the density of pedestrians interpolated at a given location x or it is the artificial density at a given location x if x is a point on the boundary walls.
The choice of this relation reflects the hypothesis that even if the density of the pedestrians is very low at a given location, the obstacle changes its path or slows down to avoid the potential collision. This is because a moving obstacle colliding with a pedestrian is far more dangerous than a pedestrian-pedestrian collision. For example, the collision would be catastrophic in a real situation with a vehicle as a moving obstacle, .

Boundary conditions for eikonal equation

1. *Pedestrians:* The inflow boundary of pedestrians is assigned a free boundary condition. The outflow boundary is assigned a Dirichlet boundary condition with the value of ϕ assigned to zero. The other boundaries of the domain and the boundaries of the obstacles are either assigned Dirichlet boundary conditions with a high value for ϕ or considered as a no-slip boundary after assigning a high artificial density on the boundaries to be reflected in the velocity-density relations. The domain of the eikonal equation and, correspondingly, the boundaries vary depending on the simulation scenario under consideration.

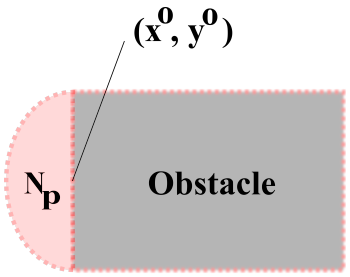

Figure 3.3 – Centre of Mass

2. *Obstacle:* The inflow boundary of the obstacle(s) is assigned free boundary condition. The outflow boundary is assigned a Dirichlet boundary condition with the value of ϕ^O assigned to zero. The boundaries of the obstacles are not considered for solving ϕ^O. The other boundaries are treated similarly to how they are treated while solving for ϕ.

3.4.4 Velocity Assignment of Active Obstacle

The motion of the rigid obstacle is mathematically considered as the motion of its centre of mass. Here, we consider the centre of mass of the obstacle or vehicle to be the midpoint of the leading edge of the moving obstacle, that is, the edge of the moving rectangular or square obstacle with its outward normal same as the $x-$component of the unit velocity vector at a given instant of time. Although physically, the centre of mass of the solid obstacle is different. For an obstacle moving to the left direction, the centre of mass (x^O, y^O) is shown in Fig. 3.3.
The model equations for the obstacle or vehicle(s) are essentially the equations for the position and velocity of their individual centre of mass. In our model, the gradient of the eikonal solution ϕ^O for the force term G^O is evaluated at the centre of masses. While evaluating the interactive force I^O, we can either evaluate it at the centre of mass directly or take an average of the same around the boundary of the obstacle.

3.4.5 Solution Procedure

To numerically solve the hydrodynamic pedestrian model coupled with the obstacle dynamics, we use the following procedure -

1. Initialise the structured eikonal grid with initial conditions and boundary conditions for ϕ. And initialise the meshfree particle cloud in the interior of the domain with initial density and velocity. Further, initialise the boundary particles with the boundary conditions. In the presence of dynamic obstacles, a second set of initial and boundary conditions for ϕ^O is assigned.

2. Activate or deactivate the eikonal grid based on the position of the obstacle(s), treating it like an immersed boundary.

3. Interpolate the density of pedestrians ρ from the meshfree particles onto the eikonal grid. For each eikonal grid point, only the nearby neighbours are used for interpolation.

4. Solve the eikonal equation for pedestrians Eqn. (3.3) and find ϕ. For moving obstacles, find ϕ^O by solving Eqn. (3.9).

5. Evaluate the gradient values $\nabla\phi$ at the meshfree particle points $i = 1,2,...,N$ in the interior of the domain to evaluate the acceleration term G in the RHS of Eqn. (3.12).

6. Also, evaluate the interaction force I at each particle i.

7. Update U_i using Eqn. (3.12).

8. Update the density ρ_i using Eqn. (3.12).

9. Update the position of particles x_i using Eqn. (3.12).

10. Update the position of moving obstacle(s). If the obstacle(s) are passive, update its position and velocity using Eqn. (3.7). If we have dynamic obstacle(s), update using Eqn. (3.8).

11. Update time (here, fixed time steps are used). Repeat steps $2-10$ for moving obstacles until the final time is reached. For static obstacles, perform steps $2-5$ only once at the initial time. And then repeat steps $6-9$ until the final time.

3.5 Numerical Results

Using the numerical method described above, we solved the model equations in Section 3.2 to analyze the collision-avoidance behaviour of pedestrians and moving passive or dynamic obstacles. In all the figures representing numerical simulations, note that the mesh-free particles used in solving the hydrodynamic equations are shown as green circles. These do not represent pedestrians physically.

In all our simulations, we consider a two-dimensional domain, a platform or corridor which is $100\,m$ long and $50\,m$ wide. The top and bottom boundaries are rigid walls without any entry or exit. The right boundary is the exit for pedestrians, and the left boundary is the exit for obstacles. Initially, pedestrians are, for simplicity, concentrated in a rectangular region in the domain near the left boundary and they intend to move towards the exit. And the obstacles considered are rectangular in shape, $20\,m$ long and $10\,m$ wide for the passive case. The dynamic obstacles are $10\,m \times 5\,m$. The initial density of the pedestrians is taken as $\rho = 1\,ped/m^2$. For the present simulations, we do not consider any continuous inflow of pedestrians. The computational details are as given in Table 3.1, if not otherwise stated. We initialize the pedestrians with a distance of $2.1\,m$. The mesh size for the eikonal grid is $\Delta x = 1.0\,m$. Explicit time integration with a fixed time step size of $0.002\,s$ is used in our simulations.

Parameter	Value	Parameter	Value
V_{max}	$2\ m/s$	V^O_{max}	$3\ m/s$
T	$0.001\ s$	T^O	$0.1\ s$
ρ_{max}	$10\ \text{ped}/m^2$	C_r	$4\ m^2/s^2$
$n1$	0.1	l_r	$1\ m$

Table 3.1 – Computational Details for Results in Section 3.5

3.5.1 Case 1: Passive Obstacle

Passive moving obstacles do not have a feedback interaction with the pedestrians and follow predefined trajectories. We considered two different scenarios, pure translation ($A \neq 0, \omega = 0$) and translation combined with oscillation ($A \neq 0, \omega \neq 0$), and compared them with the case of a stationary obstacle ($A = 0, \omega = 0$). The left and middle subfigures in Fig. 3.4 show the case where a pedestrian group interacts with a passive obstacle in translation.

We observe that when pedestrians interact with a passive obstacle(s), they adjust their path to avoid collision with the obstacle. When the position of the static obstacle is available, the potential given by the eikonal equation adjusts the path of the pedestrians. In the case of a moving obstacle, while computing the numerical solution, the velocity of the obstacle is prescribed at each time step, and the obstacle position is updated as in Eqn. (3.7). The pedestrians again gain information about the moving obstacle through the eikonal solution in the domain. And they navigate the domain accordingly. The path adjustment is made well in advance than the time instance of a head-on collision, using the information available via the eikonal solution.

The presence of a moving obstacle slows down the pedestrians in terms of the time taken to navigate the domain when compared to their behaviour in the presence of a static obstacle. This implies that the pedestrians exit the domain faster in the presence of a stationary obstacle. Hence, the total number of pedestrians in the domain decreases faster with time, as seen in the plot in Fig. 3.4. This is expected as they have to adjust their path and speed continuously to move forward. Also, a larger area around the moving obstacle (in the direction of its oscillation) is avoided by pedestrians.

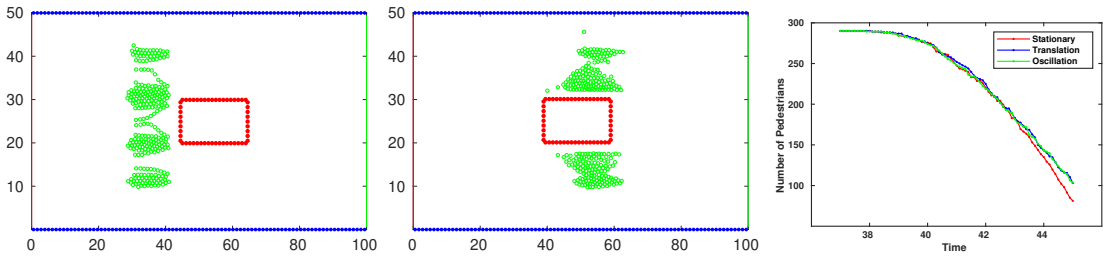

Figure 3.4 – Pedestrian interaction with a passive moving obstacle shown as red rectangle at time $t = 10\,s$ (left) and $t = 20\,s$ (middle). (Right) Number of pedestrians-time graph for the three different cases - stationary obstacle, passive obstacle in translation, passive obstacle in translation and oscillation.

3.5.2 Case 2: Dynamic Obstacle

In the case of a dynamic moving obstacle, both the obstacle and pedestrians actively try to avoid collisions with each other since there is a feedback interaction via the force terms (cf. Eqn. (3.6) and Eqn. (3.8)). Fig. 3.5 shows a scenario wherein a group of pedestrians interact with a dynamic obstacle. We observe that, though pedestrians and obstacles undergo path and speed changes, the collision avoidance mechanism is primarily via a change of path by pedestrians and a change of speed by obstacles. It is observed that when the obstacle faces the pedestrian crowd head-on, it first avoids the collision and then later moves ahead on a direct path and with a constant speed when the pedestrians have cleared the space ahead. Owing to the two-way interactions here, in comparison to one-way interaction in the case of passive obstacle, the changes in trajectory of pedestrians is more smoother, continuous and less abrupt. This leads to a lesser tendency of having a high-density of pedestrian crowd near the corners of the leading edge of the obstacle, relative to a passive obstacle. Nevertheless, the presence of any obstacle involves the crowd leading to high density near their corners.

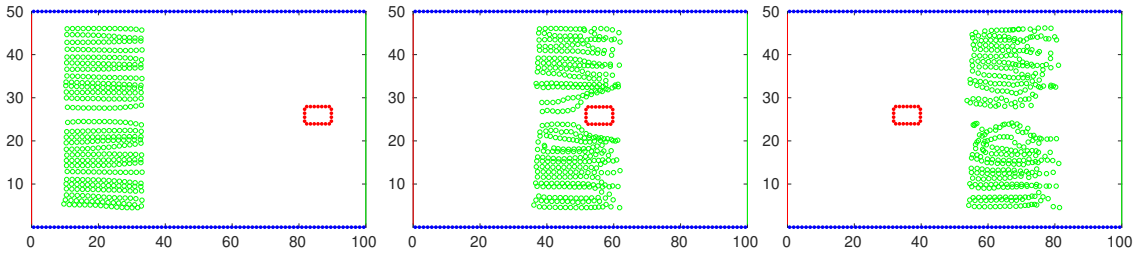

Figure 3.5 – Pedestrian interaction with a dynamic moving obstacle (red rectangle) at time $t = 5\,s$ (left), $t = 20\,s$ (middle) and $t = 30\,s$ (right). Note that the green markers denote the Lagrangian mesh-free grid points and not the physical pedestrians.

3.6 Grid Convergence

In order to understand the accuracy of our numerical method for the pedestrian model, we consider the numerical simulation of pedestrian interaction with a static obstacle for different initial meshfree particle spacing (see Fig. 3.6), say $(\Delta x)_p$, keeping the mesh size of eikonal grid fixed at $\Delta x = 1.0\,m$ and smoothing length h varying according to $(\Delta x)_p$. We consider a reference mesh and evaluate the errors relative to the values of the concerned function/variable on this reference grid. For our purposes, we choose a reference particle spacing with $(\Delta x)_p = 0.25\,m$ and $h = 0.625$. The density profiles for the different cases are compared at various time instances in Fig. 3.7. We see that the densities match quite well for the finer and coarser grids of sizes $(\Delta x)_p = 0.25\,m$ and $(\Delta x)_p = 0.5\,m/1.0\,m$.

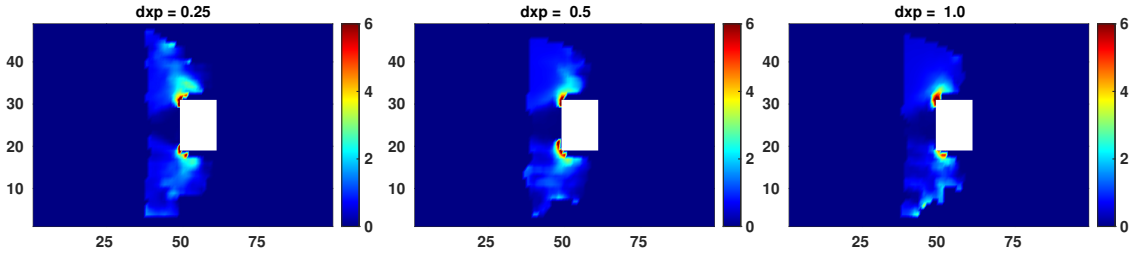

Figure 3.6 – Density plots for pedestrian interaction with a static obstacle at time $t = 20\,s$ for different particle spacing.

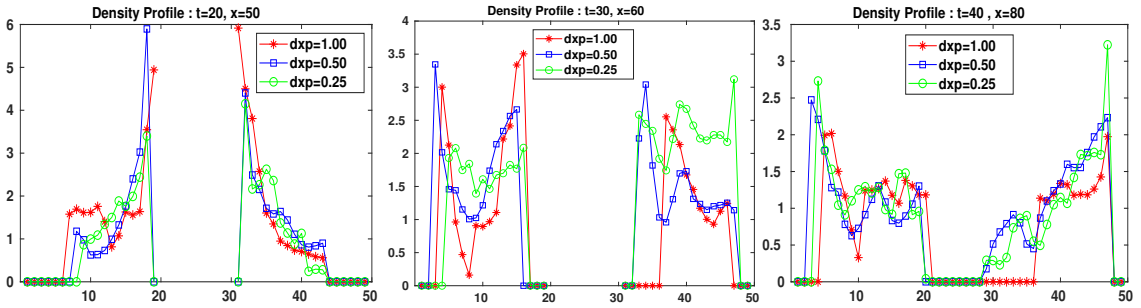

Figure 3.7 – Comparison of density profiles for the different mesh spacing at time $t = 20\,s$ (left), $t = 30\,s$ (middle) and $t = 40\,s$ (right).

3.7 Conclusion

We have successfully coupled a hydrodynamic model for pedestrian motion with simple kinematic equations for moving obstacles via eikonal equations. Our model satisfactorily replicates the collision-avoidance patterns observed in experimental scenarios like in [93]. But being a macroscopic model, only moderate to high-density scenarios can be studied, and it is not possible to analyze microscopic behavioural patterns. We can further study the path and speed changes observed and make quantitative comparisons with other data, for example, in [68] and [160]. Also, exhaustive studies by changing the size or shape of the obstacle and of the domain can be conducted. We note here that the numerical method used is particularly efficient to employ in complex environments and changes in geometries. For more accurate results, parameters need to be estimated from experimental or real data.

III Applications

4 Pedestrian Vehicular-Traffic Interaction

4.1 Introduction

'Shared spaces' is rapidly becoming an inevitable part of urban street design and safety. Understanding how pedestrians and vehicles interact in such realms is hence essential for ensuring the proper functioning of such facilities [11]. Additionally, with the automation of vehicles, challenging research problems in this area are numerous and waiting to be tackled by mathematicians and engineers alike. Hence, it is imperative to develop modelling techniques to combine pedestrian and vehicular traffic models to arrive at hybrid models and demonstrate methods to analyse them analytically or computationally.

Traffic flow modelling approaches can vary depending on how we choose to define the time scale, continuous or discrete, as well as the description detail - microscopic, mesoscopic or macroscopic. At the microscopic scale, the long-established way is the car following theory, wherein each individual vehicle's acceleration is prescribed in accordance with the stimulus provided via interaction with the other vehicles analogous to particles in Newtonian mechanics. Different models, either first or second-order ODEs, arise based on how the interactions are defined using speed of vehicles, relative distance or relative velocity between vehicles, see Refs. [37, 38, 66, 70, 84, 144]. Follow-the-leader models assume that the acceleration response of a driver depends only on the velocity of the leading vehicle. However, these models have difficulty distinguishing the free flow and congested flow behaviour of traffic. In optimal velocity models, the desired speed of each vehicle is a function of the headway-distance [16]. See [32] for a review of car-following models. Cellular automata models describe the vehicles by discrete lattice points and discrete speeds, see [98]. In our work, we postulate the interaction terms based on a generalised follow-the-leader approach with the anisotropic assumption, wherein each vehicle interacts with all (not just one) of the vehicles leading it but do not interact with the ones behind it.

The notion of viewing traffic flow as analogous to fluid flow, and describing the vehicle density via the Euler/Navier-Stokes equation(s), was proposed in the early works of [118] and [150]. Some of the early models had deficiencies, for example, presence of negative speeds and violation of anisotorpy principle in [140, 171], as critiqued in Refs. [48] and [14]. Refined first-order (only continuity equation) and second-order (equations for evolution of both density and mean velocity) models have been developed ever since [101, 172]. Moreover, an attempt to develop a macroscopic model from the microscopic theories is seen in [13]. The macroscopic equations, though similar to fluid equations, have ancillary terms to describe properties specific to vehicular interactions. For instance, vehicles accelerate to achieve a desired velocity, and their interactions do not conserve energy or momentum.

Models based on statistical mechanics, that is, kinetic models for traffic, were developed initially in [146] and [139], who modelled the collision operator based on a relaxation term and an interaction term. Later in [133], a kinetic description was developed for acceleration in place of the relaxation type term used in the earlier models. Further to this, Enskog-type kinetic model was introduced in [109], which can handle inhomogeneous traffic as well, in contrast to the earlier models, which handled only homogeneous flows and restricted backward propagation of perturbations. Early kinetic descriptions faced criticisms related to the continuity assumption of the probability distribution function over the space and velocity variable [48]. A novel approach to consider a discrete velocity space to elucidate the granular nature of vehicular traffic was developed by [51]. Further, a framework with double discretization of both velocity and space variables is seen in [63]. A comprehensive review of the continuum models, both kinetic and macroscopic, is provided in [142].

The objective presented in this chapter is to develop a model to study the interaction between pedestrians and vehicles in lane-traffic at intersections. A non-local macroscopic pedestrian dynamics model is coupled to a microscopic vehicular traffic model in 1D through eikonal equations. We again use the mesh-free particle method to solve the hydrodynamic equations in Lagrangian form, which can then be easily combined with the kinematic equations. The numerical method is as explained in Section 3.4. We demonstrate the model by solving it numerically in three traffic scenarios; one, at an uncontrolled crossing in a single-lane road; second, at a zebra crossing in a single-lane road and finally, at a crossing with a traffic island in a two-lane road.

In this chapter, we describe a microscopic one-dimensional system of equations for vehicular traffic in Section 4.2. These are combined with the pedestrian evolution equations described in Section 3.2.2. The numerical results are detailed in Section 4.3.

4.2 Vehicular Traffic Model

The model for interaction with active moving obstacles in Chapter 3 can be further extended to consider pedestrian-vehicular interaction. For the simplest case, we consider a single-lane vehicular traffic scenario modelled by appropriate interaction terms as in [31]. Like in the case of moving obstacles, the information of the environment (road) and the destination of the obstacles (here vehicles) is provided via the boundary conditions of the eikonal equation. The difference is that here we need only solve a one-dimensional eikonal equation for the single-lane vehicular motion. The interaction between the pedestrians and vehicle(s) is modelled in the eikonal force itself via the velocity-density function. The kinematic equations for the vehicles are:

$$\begin{aligned} dx_i^V &= v_i^V\,dt\,, \\ dv_i^V &= \sum_{j<i} I^V(x_i^V - x_j^V, v_i^V - v_j^V)dt + G^V(x_i^V, v_i^V, \rho_i)dt\,, \end{aligned} \tag{4.1}$$

where x_i^V and v_i^V are the position and velocity of the i^{th} vehicle's centre of mass and ρ_i is the interpolated density of pedestrians at x_i^V. Note that x_i^V and v_i^V are in 1D here and are taken as the

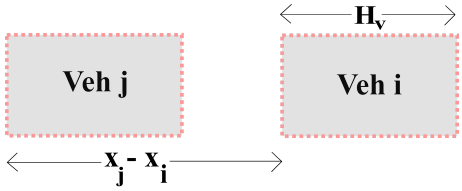

Figure 4.1 – Interaction Lengths between vehicles

midpoint of the leading edge of the respective vehicle instead of its physical centre of mass, similar to the moving obstacle in Fig. 3.3. For the interaction between vehicles of length H^V, the force term I^V with interaction range r^V is given as,

$$I^V(x_j^V - x_i^V, v_i^V - v_j^V) = c^V \frac{v_j^V - v_i^V}{|x_j^V - x_i^V - H^V|} \left[\frac{1}{r^V\sqrt{\pi}} \exp\left(- \left(\frac{(x_j^V - x_i^V) - r^V/2}{r^V} \right)^2 \right) \right].$$

The desired acceleration term G^V similar to the obstacle's case is given here as:

$$G^V(x^V, v^V, \rho) = \frac{1}{T^V} \left(-V^V(\rho(x^V)) \frac{\nabla \phi^V(x^V)}{||\nabla \phi^V(x^V)||} - v^V \right),$$

$$V^V(\rho(x))\,||\nabla \phi^V|| = 1, \qquad x \in \Omega. \tag{4.2}$$

Note that here $\nabla \phi^V$ is just a 1D derivative, and we take for $n1 > 0$, the velocity-density relation similar to obstacle's case in Section 3.4.3 as:

$$V^V(\rho(x)) = V_{max}^V(1 - (\rho(x)/\rho_{max})^{n1}).$$

Here, $\rho(x)$ is obtained as an average of interpolated density of pedestrians along the perpendicular direction within the boundaries of the road.

Remark: V/V^V is chosen based on the assumption that the velocities should be low when the density of pedestrians is high at a particular location. The additional factor $n1$ appears in V^V because we want the velocity of vehicles to be significantly lower compared to the velocity of pedestrians given by V. Also, note that other choices of functions can be made instead of a linearly varying V, see Section 2.4.

4.3 Numerical Results

To study the pedestrian interaction with vehicular traffic, we consider for simplicity vehicular traffic in one dimension. We consider three different scenarios based on different right of way on the road – a single-lane road with an uncontrolled crossing, a single-lane road with a zebra crossing and a two-lane road with a traffic island. Similar to the description in Section 3.4.1, the hydrodynamic model is written in a Lagrangian form and coupled to the system of equations for vehicles Eqn. (4.1) ($2m$ equations for m vehicles in the domain).

As explained in Section 3.4.2 and Section 3.4.3, the eikonal equations are solved by a fast marching method on the structured grid. In the case of vehicles, a 1D eikonal equation is solved, see Eqn. (4.2), in the domain of the road. The eikonal equation for the pedestrians Eqn. (3.3) is solved on the whole domain with appropriate boundary conditions identifying the edges of the road. In the case of zebra crossing, only a vertical strip of crossing on the road is part of the eikonal domain for pedestrians, while the rest of the road is neglected. For the case of two-way traffic flow, two sets of eikonal equations (for pedestrians and vehicles) are solved on the two different halves of the domain of the road, one above the traffic island and another below the traffic island. The information on the environment, like the position of vehicles, edges of the road and exit for the pedestrians/vehicles, are provided via the boundary conditions of the eikonal equations. For Eqn. (3.3), high boundary values of eikonal variable ϕ are assigned to the edges of roads and boundaries of vehicles to ensure repulsion from them and a low value to the exit at the bottom of the domain (green) for attraction towards it. While for the vehicles, high boundary values of eikonal variable ϕ are assigned to the edges of roads and a low value to the exit (red) at the left or right of the domain.
Moreover, similar to the obstacle's scenario, an immersed-boundary like method is used to identify and activate or deactivate the eikonal grid points based on the vehicle's position on the road. At each time step, the eikonal grid points falling within the boundaries of any vehicle are deactivated while the points outside are active. Also, any point outside the boundaries of the road is either deactivated throughout the simulation or not considered as a part of the eikonal domain at all.
A solution procedure similar to the one in Section 3.4.5 is used here. The parameter values for the below numerical cases are provided in Table 4.1. We have chosen here $V^V_{max} = 10\,km/h \approx 3\,m/s$ as we are more interested in the dynamics of slow-moving traffic usually observed in traffic-restricted areas or shared spaces. The equations are solved using an explicit Euler time discretization with a fixed time step of $0.001\,s$ in all cases.
In all scenarios, we consider a domain 100 units long and 50 units wide. In the first two cases with only one-way traffic, the centre of the domain consists of a road which is 20 units wide, and the traffic flows from the right boundary to the left in a single lane. In the two-way traffic case, the domain consists of a road which is 30 units wide with single-lane traffic flow in opposite directions on either side of the road. The single-lane traffic flows are modelled in 1D as given in Eqn. (4.1). The boundaries of the road are marked by black dashed lines, and the exit for vehicles is marked by red on the left boundary of the domain. A group of pedestrians are occupying the domain on one side of the road (on the top of the domain) with the intention of crossing the road and arriving at the exit (marked in green) at the bottom of the domain on the other side of the road.

4.3.1 Pedestrian interaction with single-lane traffic – uncontrolled crossings

In this scenario, as shown in Fig. 4.2, both the vehicles and pedestrians have equal right of way on the road. The pedestrians avoid collisions by adjusting their path, and the vehicles slow down to avoid collisions. A plot of the velocity changes of the vehicles against time is shown in Fig. 4.4 (left). The initially accelerating vehicles slow down when the pedestrian group enters the road, a little after 25 s. The vehicles do not stop completely. They move slowly at a constant low velocity between

Parameter	Value	Parameter	Value
V_{max}	$2\ m/s$	V^V_{max}	$3\ m/s$
T	$0.001\ s$	T^V	$0.1\ s$
R	$0.1\ m$	H^V	$4\ m$
ρ_{max}	$10 ped/m^2$	r^V	$4\ m$
$n1$	0.05	c^V	$1e^3\ m^2/s^2$

Table 4.1 – Computational Details for Results in Section 4.3

the time 40 s and $100/120$ s. They later accelerate again once the road ahead is clear of pedestrians.

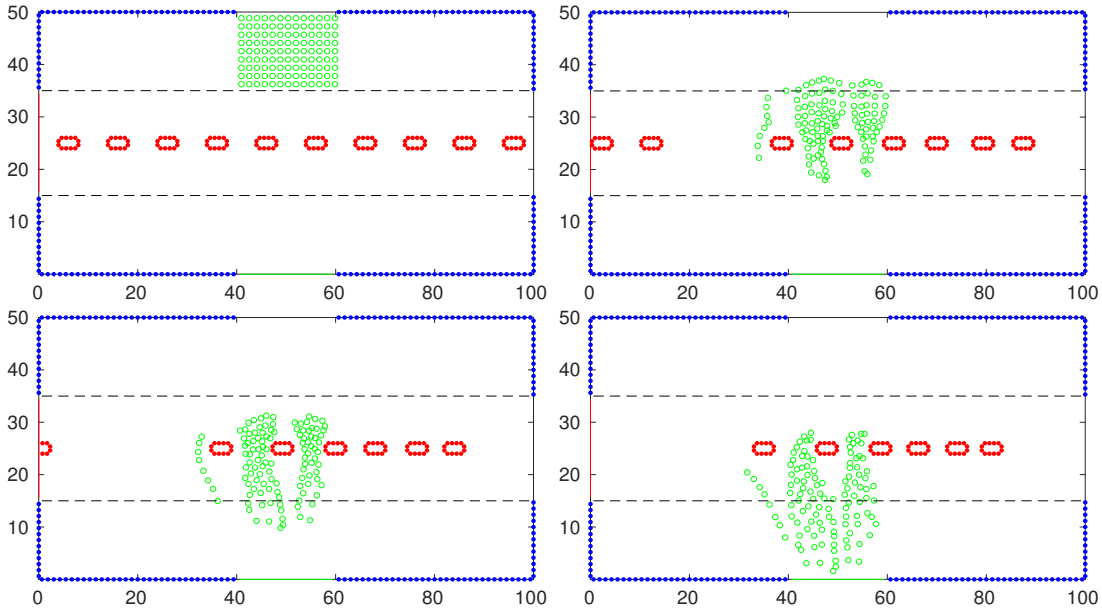

Figure 4.2 – Pedestrian interaction with single-lane traffic – uncontrolled crossings

4.3.2 Pedestrian interaction with single-lane traffic – Zebra crossing

In this case, the pedestrian group is trying to cross the road along the zebra crossing. A 20 units wide zebra crossing is provided in the middle of the road, as shown in Fig. 4.3, with its boundaries marked by blue dotted-dashed lines. Here, the pedestrians have the right of way on the road at the zebra crossing. The velocity plot of the vehicles is shown in Fig. 4.4 (right). We see that the accelerating vehicles slow down and come to a halt at the crossing. They wait while the pedestrian group crosses the road and then later accelerate again towards the exit of the road.

4.3.3 Pedestrian interaction with two-way traffic and traffic island

Here, we consider a two-lane road with vehicles travelling in opposite directions on each lane of width 10 units. A traffic island 20 units wide is in the middle of the two lanes, as shown in Fig. 4.5,

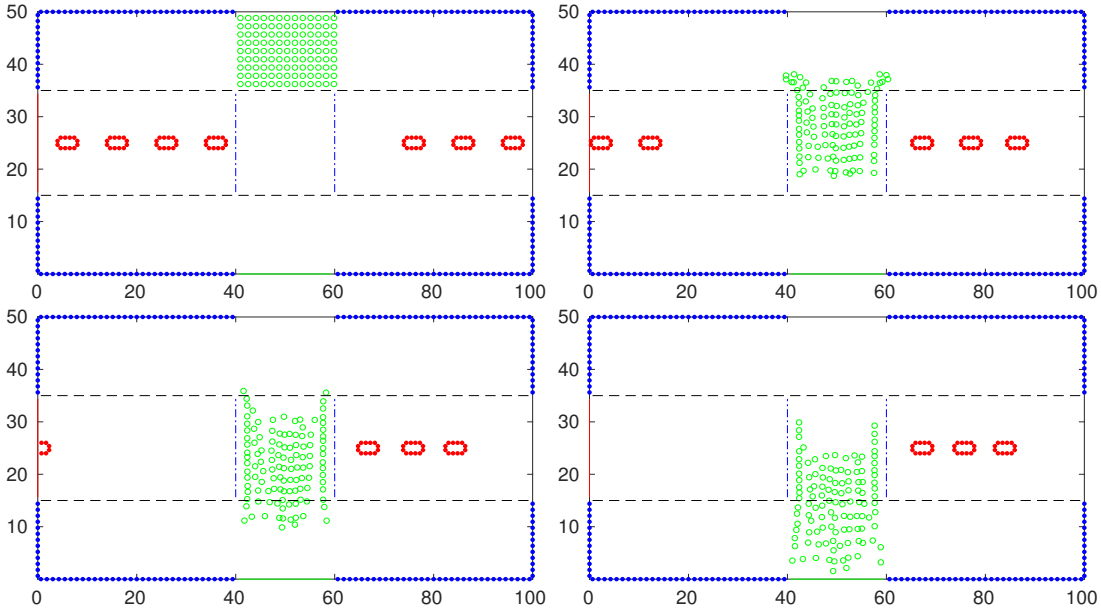

Figure 4.3 – Pedestrian interaction with single-lane traffic – zebra crossing

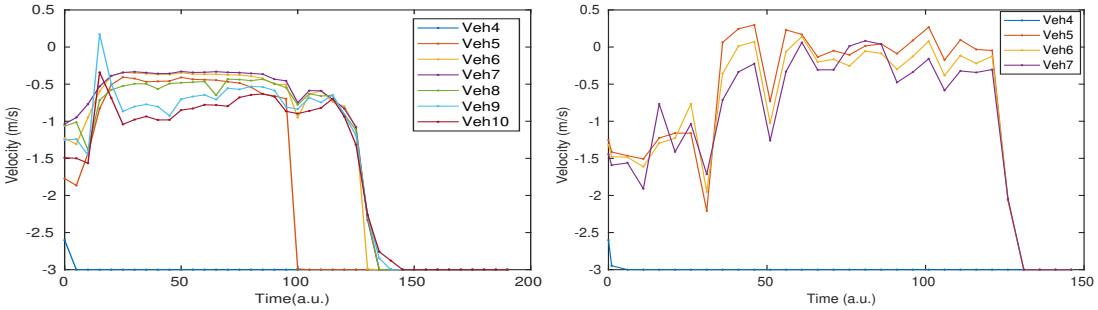

Figure 4.4 – Change in velocity of vehicles at uncontrolled crossing (left) and zebra crossing (right). The leading vehicle at the left end of the simulation setup is Veh1 and they are numbered sequentially.

marked by a green line. In this case, the pedestrians and vehicles both have equal right of way. But in most cases, the concept of a traffic island is to help the pedestrians stop in between the two lanes for ease of crossing after checking the traffic. We again observe that the vehicles slow down and allow the pedestrians to pass. The pedestrians tend to interact with each lane of traffic separately and take a halt at the traffic island after crossing first lane. Vehicles in each lane wait while the pedestrian group crosses that particular lane and then later accelerate again towards the exit of the road.

4.4 Conclusion

We have efficiently coupled a hydrodynamic pedestrian model to a one-dimensional vehicular interaction model. The coupling through eikonal equations is effective in incorporating the non-local information about the domain, like the presence of boundary walls, the position of obstacles/vehicles

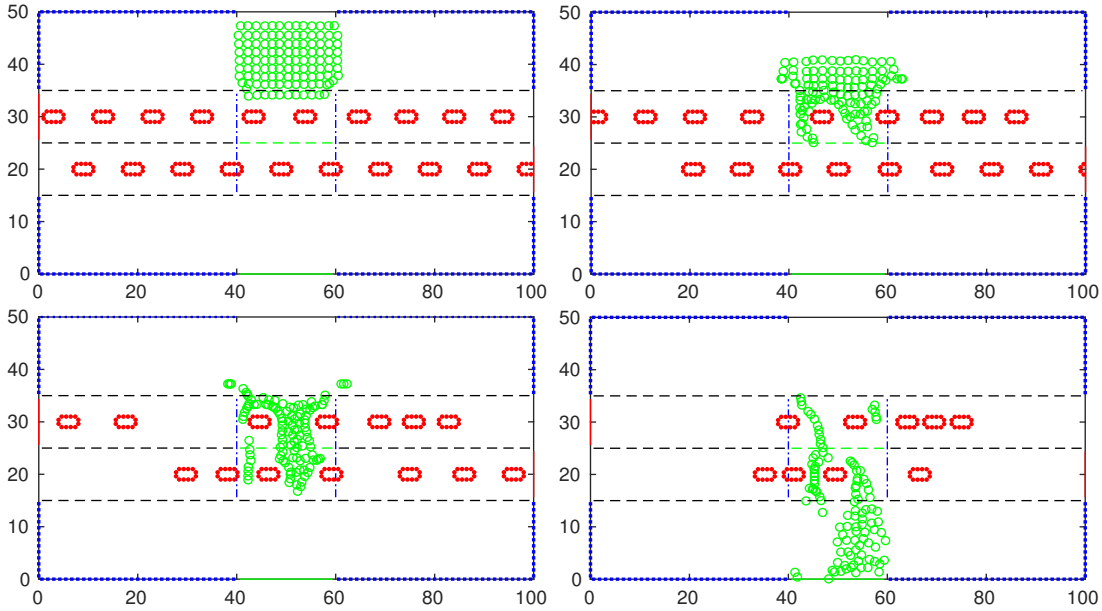

Figure 4.5 – Pedestrian interaction with two lane traffic - traffic island

and the density of pedestrians via boundary conditions or source functions. We remark that the microscopic equations for vehicular traffic presented here in Section 4.2 can be used to develop the corresponding kinetic and macroscopic equations via an approach similar to [49] or [60].
We demonstrate through three different numerical test cases that the coupled model is successful in replicating physically realistic scenarios. We note that since the pedestrian model is macroscopic, individual behavioural patterns cannot be extracted. However, it is particularly adequate for high-density scenarios. Moreover, the mesh-free numerical method is computationally efficient (see [111]) and robust to deal with high densities and complex geometries. Further quantitative studies to understand the effect of vehicle speed and interaction range on the behaviour of pedestrians need to be carried out. We remark that the developed framework can be used to consider pedestrian and automated vehicle interactions in future.

5 Disease Contagion in Pedestrian Crowds

5.1 Introduction

The COVID-19 pandemic and the surge of infections caused havoc worldwide, with countries trying to prevent their healthcare systems from complete collapse. Severe acute respiratory syndrome coronavirus 2 (SARS-CoV-2) causes COVID-19, a respiratory infectious disease (RID) with a high transmission rate. Before vaccines were invented, the major plans contrived for controlling disease spread were wearing masks and social distancing as preventive measures, together with extensive testing and quarantine of infectious individuals [41, 62]. While global initiatives to control large-scale migration of the population within and between countries, like restrictions on travel via flights or trains, were established, reducing contact through lockdown of cities or towns and restrictions on social gatherings were the norms locally [168]. It hence is essential to study disease spread dynamics in smaller domains as well as on a larger scale. This pandemic clearly led to an increased interest in mathematical and statistical models of diseases, which can present us with valuable information regarding the spatiotemporal dynamics of disease spread to aid governmental agencies with appropriate assessment and decision-making in disease prevention, detection, control, and treatment. The research efforts for the same have been multi-disciplinary, involving epidemiologists, molecular biologists, computational scientists, applied mathematicians and sociologists alike.

Various analytical approaches have been used in the literature to model the spread of infectious diseases [85, 157]. Compartmental models are a class of deterministic models which are population-based and non-spatial [33]. The seminal work(s) of [100] commenced this class of epidemiological models, which divides the population into distinct categories (compartments) and provides a system of ODEs for their masses (either in proportions or counts). Classically, the compartments used are Susceptible(S), Exposed(E), Infected(I) and Recovered/Removed(R). Depending on which of these compartments are chosen in a model and how the transition rates from one state to another are defined in the set of differential equations, the models are named SIR, SEIR, SEIS, SEIRS and others. For a recent review, refer [161]. We note that the major limitations of such models are their unrealistic 'well-mixed' assumption and that they neglect the heterogeneity amongst the individuals in their interactions or mobility patterns. Alternate modelling approaches to rectify some limitations are explored, for example, in [26] and [72]. We refer to [28], [113] and [126] for a small selection of papers related to the work presented in this chapter.

Recently, there have been some efforts to link epidemiological modelling and crowd modelling,

which have heretofore been considered independent. Special interest has been shown in models suited to explore infectious diseases transmitted via airborne particles and requiring proximity of individuals to spread, e.g. influenza A, tuberculosis, pneumonia or COVID-19, which is our focus too. On the microscopic scale, a social force model is combined with contact tracking to study the spread of a highly infectious airborne disease amongst individuals moving in a confined environment in [149]. Another notable agent-based approach developed in [65] combines a diffusion-based contagion-immunity coupling and the pedestrian equations of motion to analyse the disease spread and immune reaction of COVID-19 in moving crowds. It is crucial to study the disease spread at this scale as it provides more intricate and low-level information essential for more targeted responses towards disease control but in a small population.

For intermediate-size populations, a coupled kinetic model for pedestrians and disease contagion was presented in [103]. Further, a kinetic theory approach using tools of game theory to model interactions between individuals and with the surroundings was adopted to study such populations occupying a confined environment for a short duration of time in [104] and [105]. [9] considers an SEIR approach to provide a pure kinetic model for disease contagion in a crowd evacuation scenario in a bounded domain, while we use an SEIS approach for our model in Section 5.2. We remark here that the time scale for movement or evacuation from a room (bounded domain) is in the order of minutes while the duration for an exposed individual to become infectious, called the *disease latency period*, is usually in the order of days. Hence, a transition from exposed to infected usually does not take place during the evacuation. Such features of the SEIS model we use are highlighted appropriately wherever necessary in the text. The significance of our work is that we formulate a multi-group hydrodynamic model which can handle larger densities of crowds and provide macroscopic information. Indeed, the continuity assumption in such fluid-like crowd models is still criticised. It would be ideal to look at multi-scale models like in [20]. The presented model allows us to assess the effect of geometry on infection transmission by considering dynamics in the presence of obstacles. Attempts have been made earlier in this regard, which has been more specific to design and spatial layout of specific areas like restaurants [42] or offices [125] or hospitals [56]. However, the need is to discern the actual mechanism of disease transmission conditional to various factors, including individual factors like the contact time and relative velocities as well as physical factors like size of obstacles [45].

Our main objective is to include a kinetic disease spread model in the form of a multi-group equation into a kinetic pedestrian dynamics model, derive hydrodynamic approximations and provide an efficient numerical simulation of the coupled model for complex two-dimensional geometries. For the pedestrian flow model, we consider a kinetic equation for multi-group pedestrian flow based on a social force model coupled with an eikonal equation to model the geometry and goals of the pedestrians. This model is coupled with a non-local SEIS contagion model for disease spread, where local contacts, as well as the influence of contact time, are included. We also extend the model to situations with more complex geometries and moving objects in the computational domain. This follows from the way we detailed the interaction of pedestrians with larger geometrically extended objects like cars in a shared space environment, as in Section 3.3.2 and Chapter 4. The

numerical simulation is based on mesh-free particle methods for the solution of the Lagrangian form of the hydrodynamic equations, similar to what is detailed in Section 3.4.
The chapter is organized in the following way: in Section 5.2, a kinetic model for pedestrian dynamics with disease spread is presented. The section also contains the associated hydrodynamic equations derived from a moment closure approach. In Section 5.3, numerical solutions of the macroscopic equations are presented for different physical situations and parameter values, including uni- and bi-directional flow in a two-dimensional passage without obstacles and with fixed and moving obstacles.

5.2 Coupled Model for Disease Contagion

We use a kinetic model for the evolution of the distribution functions of susceptible, exposed and infected pedestrians as a starting point and derive associated hydrodynamic equations.

5.2.1 Kinetic Evolution Equation for Disease

We consider an equation for the evolution of pedestrian distribution functions $f^{(k)} = f^{(k)}(x,v,t), k = S,E,I$. Here f^S stands for the distribution of susceptible pedestrians, f^E for the exposed pedestrians and f^I for the infected pedestrians. The evolution equations are given by

$$\partial_t f^k + v \cdot \nabla_x f^k + R f^k = T^k, \tag{5.1}$$

with $k = S,E,I$. The operators R and T^k are given by the following definitions.

$$R f^k(x,v) = \nabla_v \cdot \left([G(x,v,\rho) - \nabla_x \mathscr{U} \star \rho(x)] f^k \right),$$

with

$$\rho = \rho^S + \rho^E + \rho^I,$$

where

$$\rho^k(x) = \int f^k(x,v) dv.$$

Here, $\mathscr{U}$ is an interaction potential describing the local interaction of the pedestrians and $\star$ denotes the convolution. Common choices for the interaction potential are purely repelling potentials like spring-damper potentials or attractive-repulsive potentials like the Morse potential. Here, we have, for simplicity, considered a Morse potential without attraction given by

$$\mathscr{U} = C_r exp\left(-\frac{|x-y|}{l_r} \right), \tag{5.2}$$

where C_r is the repulsive strength and l_r the length scale. The part of the forcing term involving G describes the influence of the geometry on the pedestrian's motion and a potentially long-range interaction between the pedestrians; see below for a detailed description. The operators T^k are defined using a SEIS-type kinetic disease spread model leading to

$$\begin{cases} T^S = \nu f^I - \beta_I f^S \\ T^E = \beta_I f^S - \theta f^E \\ T^I = \theta f^E - \nu f^I \end{cases} \tag{5.3}$$

with constants ν, θ, see Remark 5.3 below, and the non-local infection rate $\beta_I = \beta_I(x, v; f^S(\cdot), f^E(\cdot), f^I(\cdot))$ depending in a non-local way on the rate of infected persons; compare Refs. [28] and [103] for similar approaches. We define

$$\beta_I = \int \frac{1}{\rho(y)} \int K_\phi(x-y, v-w) f^I(y,w) dw dy. \tag{5.4}$$

The kernel K_ϕ in the infection rate is chosen as

$$K_\phi = K_\phi(x,v) = i_o \phi_X(x) \phi_V(v). \tag{5.5}$$

with $\int \phi_X(x)dx = 1 = \int \phi_V(v)dv$. Here, ϕ_X is determined as a decaying function of $|x|$ to take into account the effect that infections between pedestrians are more probable the closer pedestrians are approaching each other. ϕ_V is chosen in a similar way depending on $|v|$ to take into account the fact that infections are more probable the longer the interacting pedestrians stay close to each other, that is, the smaller their relative velocities are. The parameter i_o is determined by the infectivity. We refer to the section on numerical results for the exact definition of these kernels.
Finally, G is given, as in Eqn. (3.2), by

$$G(x,v,\rho) = \frac{1}{T}\left(-V(\rho(x)) \frac{\nabla\phi(x)}{\|\nabla\phi(x)\|} - v\right), \tag{5.6}$$

where ϕ is determined by the coupled solution of the eikonal equation

$$V(\rho)\|\nabla\phi\| = 1. \tag{5.7}$$

This describes the tendency of the pedestrians to move with a velocity given by a speed $V(\rho)$ and a direction given by the solution of the eikonal equation. The eikonal equation essentially includes all information about the boundaries and the desired direction of the pedestrians via the boundary conditions. These boundary conditions for the eikonal equation are chosen in the following way, as also described in Section 3.4.3. For walls or the boundaries of obstacles in the domain, we set the value of ϕ at the boundary to a numerically large value. For inflow boundaries, free boundary conditions for ϕ are chosen. Whereas for outflow boundaries, where the pedestrians aim to go, we set $\phi = 0$.
We note again that, on the one hand, the eikonal equation includes the geometrical information via boundary conditions. On the other hand, it models a global reaction of pedestrians to avoid regions of dense crowds via the term $V(\rho)$ in Eqn. (5.7).

Remark 5.1 The parameters in the above formulas, particularly in the definition of Eqn. (5.7) and Eqn. (5.2) have to be chosen consistent with empirical data [24, 99].

Remark 5.2 Instead of the social force model used here, one could use more sophisticated interaction models; see, for example, Refs. [15], [49] and [121]. We note that the differences between these models in the present hydrodynamic context are small. The behaviour of the solutions is rather dependent on the choice of the parameters. In this context, Chapter 6 provides a numerical study to anlayse differences between the social force based model used here and the model presented in [15].

Remark 5.3 The dynamical system called the SEIS model with constant infection rate is given by

$$\begin{cases} \frac{d\tilde{S}}{dt} &= -\beta\tilde{I}\tilde{S} + \nu I \\ \frac{d\tilde{E}}{dt} &= \beta\tilde{I}\tilde{S} - \theta\tilde{E} \\ \frac{d\tilde{I}}{dt} &= \theta\tilde{E} - \nu\tilde{I} \end{cases}$$

where β is the infection rate, ν the recovery rate and θ the rate with which exposed pedestrians are becoming infected. Pedestrians are potentially becoming exposed when they are in contact with infected pedestrians.However, exposed pedestrians are only becoming infectious at a certain rate θ. Exposed pedestrians do not infect other pedestrians. Usually, in the situations and on the time scales under consideration here, ν and θ are very small and set to zero in numerical simulations such that the number of infected pedestrians remains constant during the simulation.

Remark 5.4 A key difference between other agent-based models [28] is the dependence of the infection on the relative velocity of the agents. This has direct implications on the process of infection during the dynamics, as can be seen in the case studies.

5.2.2 Multi-group Hydrodynamic Model

Integrating the kinetic equation against dv and $v\,dv$ and using a mono-kinetic distribution function to close the resulting balance equations, i.e. approximating f^k as:

$$f^k \sim \rho^k(x)\delta_{U(x)}(v)\,,$$

one obtains a continuity equation for group k

$$\partial_t\rho^k + \nabla_x\cdot(\rho^k U) = \int T^k dv \tag{5.8}$$

and the momentum equation

$$\partial_t U + (U\cdot\nabla_x)u = G(x,U,\rho) - \nabla_x\mathscr{U}\star\rho \tag{5.9}$$

with the total density ρ given as

$$\rho = \rho^S + \rho^E + \rho^I.$$

Moreover,

$$G(x,U,\rho) = \frac{1}{T}\left(-V(\rho(x))\frac{\nabla\phi(x)}{\|\nabla\phi(x)\|} - U\right),$$

where ϕ is determined by solving the eikonal equation Eqn. (5.7):

$$V(\rho)\|\nabla\phi\| = 1.$$

The continuity equations are explicitly written as

$$\begin{cases} \partial_t\rho^S + \nabla_x\cdot(U\rho^S) = \nu\rho^I - \beta_I\rho^S \\ \partial_t\rho^E + \nabla_x\cdot(U\rho^E) = \beta_I\rho^S - \theta\rho^E \\ \partial_t\rho^I + \nabla_x\cdot(U\rho^I) = \theta\rho^E - \nu\rho^I \end{cases} \tag{5.10}$$

with $\beta_I = \beta_I(x;\rho^S(\cdot),\rho^E(\cdot),\rho^I(\cdot),U(\cdot))$, where now

$$\beta_I = \int K_\phi(x-y,U(x)-U(y))\frac{\rho_I(y)}{\rho(y)}dy. \tag{5.11}$$

Remark 5.5 Multi-group models for pedestrian flows have also been used in different contexts. For example, a hydrodynamic multi-group model for pedestrian dynamics with groups of different sizes has been developed and analysed in [122].

5.2.3 Hydrodynamic model using volume fractions

For numerical computations, this is rewritten using volume fractions, that means we solve the continuity equation

$$\partial_t\rho + \nabla_x\cdot(\rho U) = 0 \tag{5.12}$$

and the momentum equation

$$\partial_t U + (U\cdot\nabla_x)U = G(x,U,\rho) - \nabla_x\mathscr{U}\star\rho. \tag{5.13}$$

Then, we compute the volume fractions $\alpha^S,\alpha^E,\alpha^I$ with $\alpha^S+\alpha^E+\alpha^I = 1$ as

$$\begin{cases} \partial_t\alpha^S + U\cdot\nabla_x\alpha^S = \nu\alpha^I - \beta_I\alpha^S \\ \partial_t\alpha^E + U\cdot\nabla_x\alpha^E = \beta_I\alpha^S - \theta\alpha^E \\ \partial_t\alpha^I + U\cdot\nabla_x\alpha^I = \theta\alpha^E - \nu\alpha^I \end{cases} \tag{5.14}$$

with $\beta_I = \beta_I(x;\alpha^I(\cdot),U(\cdot))$ defined by

$$\beta_I = \int K_\phi(x-y,U(x)-U(y))\alpha^I(y)dy. \tag{5.15}$$

Finally, one computes

$$\rho^I = \alpha^I\rho, \rho^S = \alpha^S\rho, \rho^E = \alpha^E\rho.$$

5.3 Numerical Results

We have performed numerical simulations of equations Eqn. (5.12) to Eqn. (5.15) and Eqn. (3.8) for different scenarios. Like in the earlier chapters, we solve the hydrodynamic model by combining the Lagrangian formulation with the obstacle's kinematic equations, if necessary. The numerical method follows the same ideas described in Section 3.4 regarding handling the grid and solving the eikonal equation. In all our simulations, we consider a computational domain given by a platform or corridor of size $100\,m \times 50\,m$. The top and bottom boundaries are rigid walls without any entry or exit. Right and left boundaries are exits for pedestrians and obstacles depending on the situation under consideration. We consider uni- as well as bi-directional flow of pedestrians. Initially, the pedestrian particles are distributed as shown in Fig. 5.1 with a distance of $1.575\,m$ from each other. We consider the cases with and without obstacles, which are either fixed or moving. We initialize the infected pedestrians (coloured in red) with $\alpha_I = 1, \alpha_S = 0, \alpha_E = 0$ and the susceptibles (coloured in green) by $\alpha_I = 0, \alpha_S = 1, \alpha_E = 0$. Note that we refer to the meshfree Lagrangian particles as 'pedestrians' and 'particles' interchangeably. The macroscopic particles in the numerical setup are not physical pedestrians; rather, they are grid points carrying the information of averaged quantities like pedestrian density and velocity at that particular position in the domain.

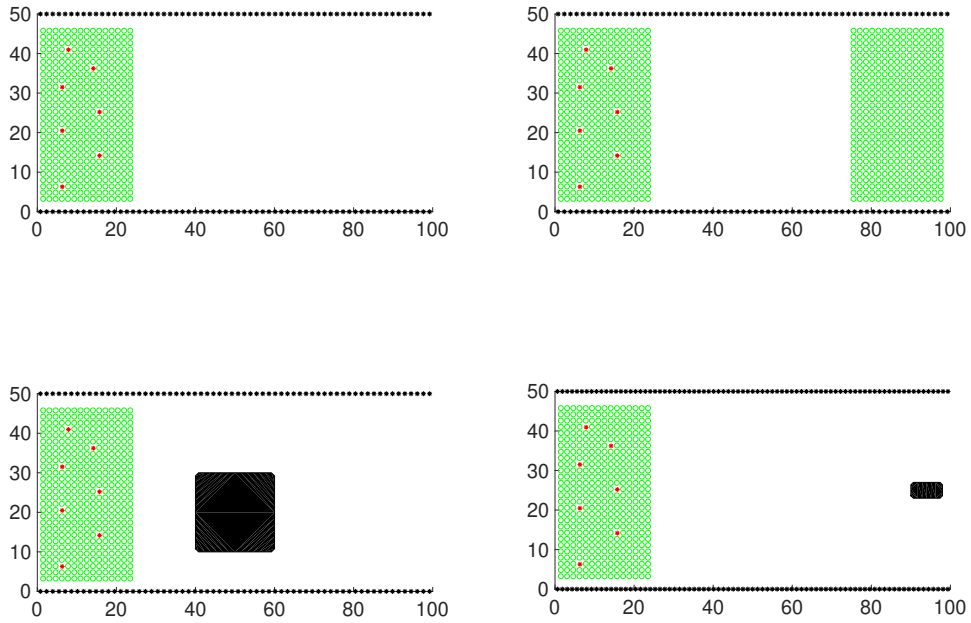

Figure 5.1 – Initial situation at $t = 0$. Top row: Uni-directional (left) and bi-directional (right) flow. Bottom row: Fixed obstacle (left) and moving obstacle (right). Red indicate infected, green indicate susceptible pedestrians.

We have used for the infection rate β_I, the functions $\phi_X = \exp(-|x-y|^4)$ and $\phi_V = \exp(-|u-v|^6)$. Moreover, we choose $V(\rho) = V_{max}\left(1 - \frac{\rho}{\rho_{max}}\right)$, and $V^O(\rho)$ is chosen in the same way with V_{max}

substituted by V_{max}^{O}. For the parameters, we have used the values given in Table 5.1.

Variable	Value	Variable	Value
V_{max}	$2\ m/s$	ρ_{max}	$10\ ped/m^2$
V_{max}^{O}	$3\ m/s$	T	$0.001\ s$
$C_r = C_r^O$	$50\ m^2/s^2$	l_r	$2\ m$
l_r^O	$1\ m$	i_o	$0.04\ m^2/s^2$

Table 5.1 – Computational Details for Results in Section 5.3

During the evolution, infected pedestrians are coloured in red, susceptibles in green and exposed pedestrians in blue according to the values of α^k. If $\alpha^E > 0.05$, the colour switches from green to blue, meaning that the probability of being exposed has exceeded a certain threshold. The red pedestrians remain red throughout the simulations since the recovery rate ν is set equal to 0 in the simulations. Moreover, since θ is also set to 0, exposed pedestrians are not becoming infected and cannot infect others in the simulations.

The fixed and the moving obstacle considered are rectangular in shape and initially located as shown in Fig. 5.1.

Explicit time integration of the equations in Lagrangian form is done with a fixed time step size of $0.001\ s$ in our simulations.

5.3.1 Test-case 1: Fixed Obstacle

In this first test case, we considered a fixed obstacle and compared the results to a situation without an obstacle. We consider bi-directional flow without an obstacle and uni- and bi-directional flow with an obstacle. This is done for the case $\phi_V = 0$ (no influence of contact time) and the case where ϕ_V is chosen as defined above, which means for a situation where the influence of the contact time is included. The present initial configuration, i.e. the initial distances between the pedestrians, is chosen in such a way that there is no increase in the number of probably exposed pedestrians if a uni-directional flow without obstacle is considered with or without the influence of the contact time. Figures 5.2 to 5.5 show the time evolution of the moving grid particles and the associated infection labels with influence (left column) and without influence (right column) of contact time. Row 1 shows bi-directional flow without an obstacle; row 2 shows uni-directional flow around an obstacle and row 3 shows bi-directional flow around an obstacle. Red indicates infected, green susceptible and blue exposed pedestrians.

Here one observes, e.g. in Fig. 5.4 or 5.5, that in situations with bi-directional flow (top- and bottom row), the number of exposed pedestrians is strongly reduced if the contact time is taken into account. For uni-directional flow, the differences are much smaller. A more detailed discussion is given below.

Comparing row 2 in Fig. 5.4 or 5.5, i.e. the uni-directional flow with an obstacle and the uni-directional case without an obstacle (no exposed pedestrians), one observes that the number of exposed pedestrians is considerably increased due to the denser pedestrian crowd surrounding the

obstacle. A similar observation can be made comparing row 1 and row 3 in these figures. The flow is becoming denser due to the pedestrians surrounding the obstacle, increasing the number of exposed pedestrians. The results show that the geometry of the domain plays a major role in the infection rate.

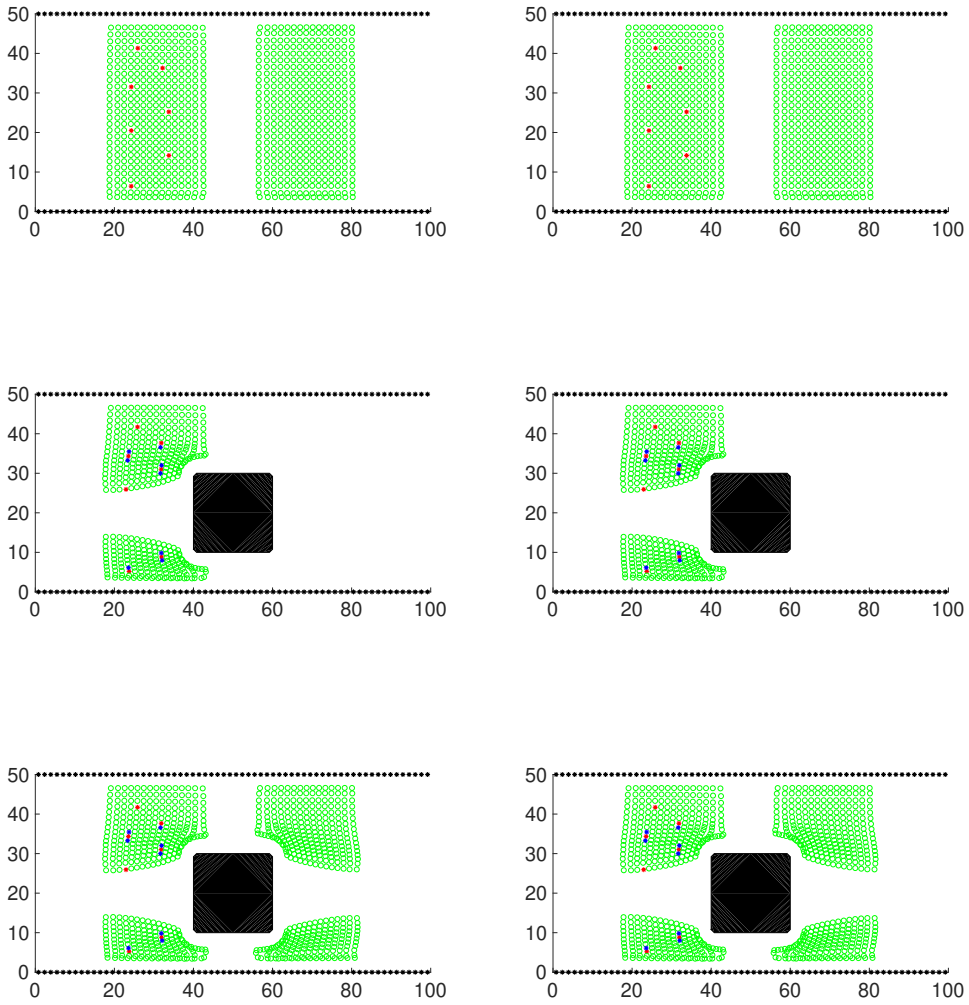

Figure 5.2 – Pedestrian dynamics at time $t = 10$ with influence (left) and without influence (right) of contact time. Row 1: Bi-directional flow. Row 2: Uni-directional flow around obstacle. Row 3: Bi-directional flow around obstacle. Red indicate infected, green indicate susceptibles and blue indicate probably exposed pedestrians.

In Fig. 5.6, we have plotted the number of pedestrians with a higher probability of being exposed versus time. One can again observe that, in bi-directional flows, the number of these pedestrians is much higher if the influence of the contact time is neglected. This is as expected since, even if pedestrians are coming close to each other, they pass each other quickly, and the contact time is short such that contagion is less probable. On the other hand, in the case of unidirectional flow,

pedestrians are walking in the same direction, such that the effect of neglecting the contact time is comparably small.

In general, we mention that the contagion model is based on very simple assumptions, and the above findings are purely qualitative. Obviously, for more accurate results, the parameters of the contagion model have to be adapted to experimental findings. We refer again to Ref. [103] for similar investigations.

Finally, in Fig. 5.7, we show the macroscopic density of the pedestrians at times $t = 10\ s, 20\ s, 30\ s$ and $40\ s$ for the flow around the obstacle.

5.3.2 Test-case 2: Moving Obstacle

In this subsection, we consider the interaction of pedestrians with a moving obstacle, e.g. a vehicle in a shared space. We consider the same computational domain as in test-case 1 with pedestrians, which are initially located as in Fig. 5.1 (right bottom). Their destination is the right exit. The moving obstacle of size $4\ m \times 8\ m$ is located on the right, with the left exit as the destination. Typically in a restricted traffic area, the vehicle has a low speed limit. We have chosen $10\ km/h \sim 3\ m/s$. The maximum speed of the pedestrians is chosen as $2\ m/s$.

In Fig. 5.8, we have plotted the positions of pedestrians and the obstacle at different times $t = 8\ s, 14\ s, 18\ s$ and $22\ s$. We observe an interaction of pedestrians and the obstacle between times $t = 14\ s$ and $t = 22\ s$. Moreover, one observes a slight increase in the number of exposed pedestrians, which is less pronounced than in the case of the larger fixed obstacle studied in test-case 1.

Moreover, in Fig. 5.9, we have plotted the x-velocity component of the obstacle along its centre of mass. One observes that the obstacle (coming from the right) accelerates and maintains almost its maximum speed. When it encounters the pedestrian crowd, it reduces its speed. Finally, it accelerates again when there are no pedestrians anymore in its surroundings.

5.4 Conclusion

We have presented a multi-group macroscopic pedestrian flow model combining a dynamic macroscopic model for pedestrian flow and an SEIS compartmental-based kinetic disease spread model. The mesh-free particle method to solve the governing equations is used for the computation of several numerical examples analyzing different situations and parameters. The dependence of the solutions and, in particular, the dependence of the number of exposed pedestrians on geometry and parameters is investigated and discussed and shows qualitatively consistent results.

Findings indicate that, particularly in bi-directional flow, it is important to take into account the contact time for a realistic description of the flow. This is expected since pedestrians pass each other quickly and the contact time is short, such that contagion is, in reality, less probable. For uni-directional flow, the effect of neglecting the contact time is comparably small. Moreover, we find that for flow with an obstacle, the number of exposed pedestrians is considerably increased due to the denser pedestrian crowd surrounding the obstacle. Since the density in these flow situations increases, the number of exposed pedestrians increases. The numerical results show the importance

of the geometry of the domain for the rate of infection.
Finally, we mention that the awareness of contagion might change the trajectories computed by the eikonal equation and the preferred distances between the pedestrians. Incorporating such aspects leads to changes in the definition of the eikonal equation and the interaction potential.

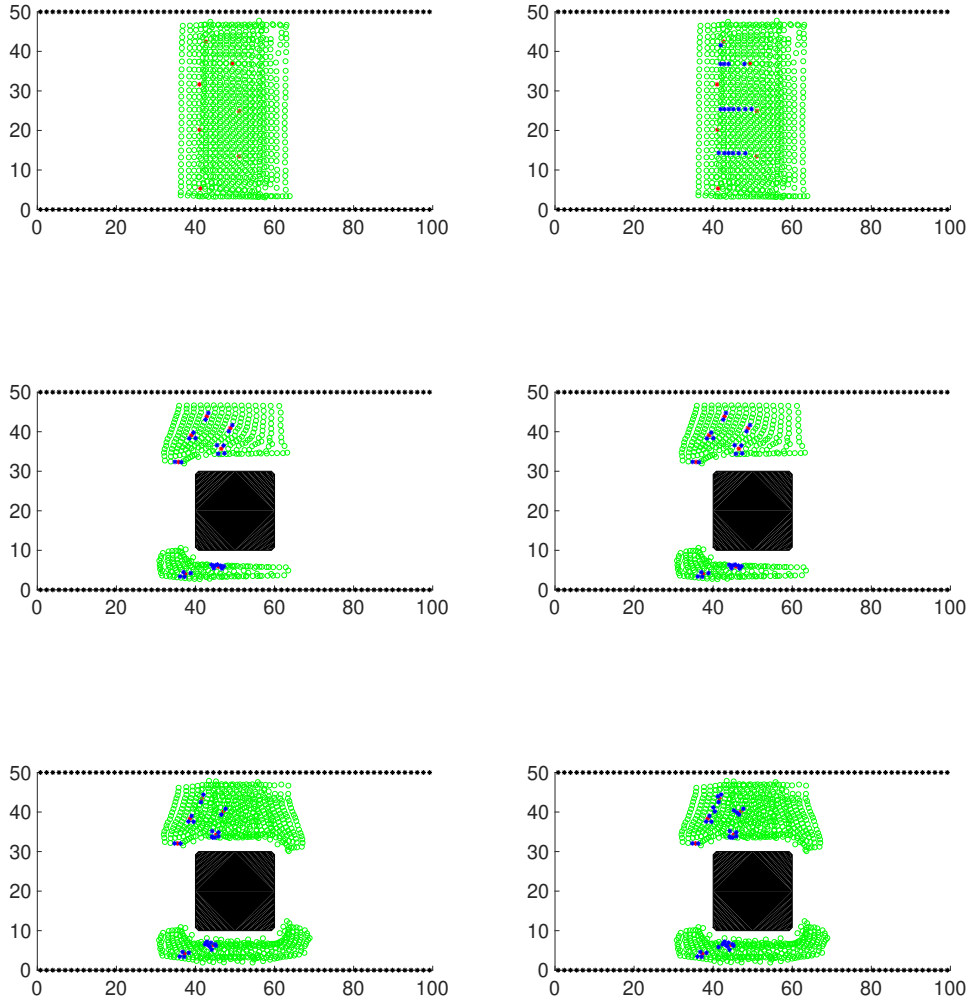

Figure 5.3 – Pedestrian dynamics at time $t = 20$ with influence (left) and without influence (right) of contact time. Row 1: Bi-directional flow. Row 2: Uni-directional flow around obstacle. Row 3: Bi-directional flow around obstacle. Red indicate infected, green indicate susceptibles and blue indicate probably exposed pedestrians.

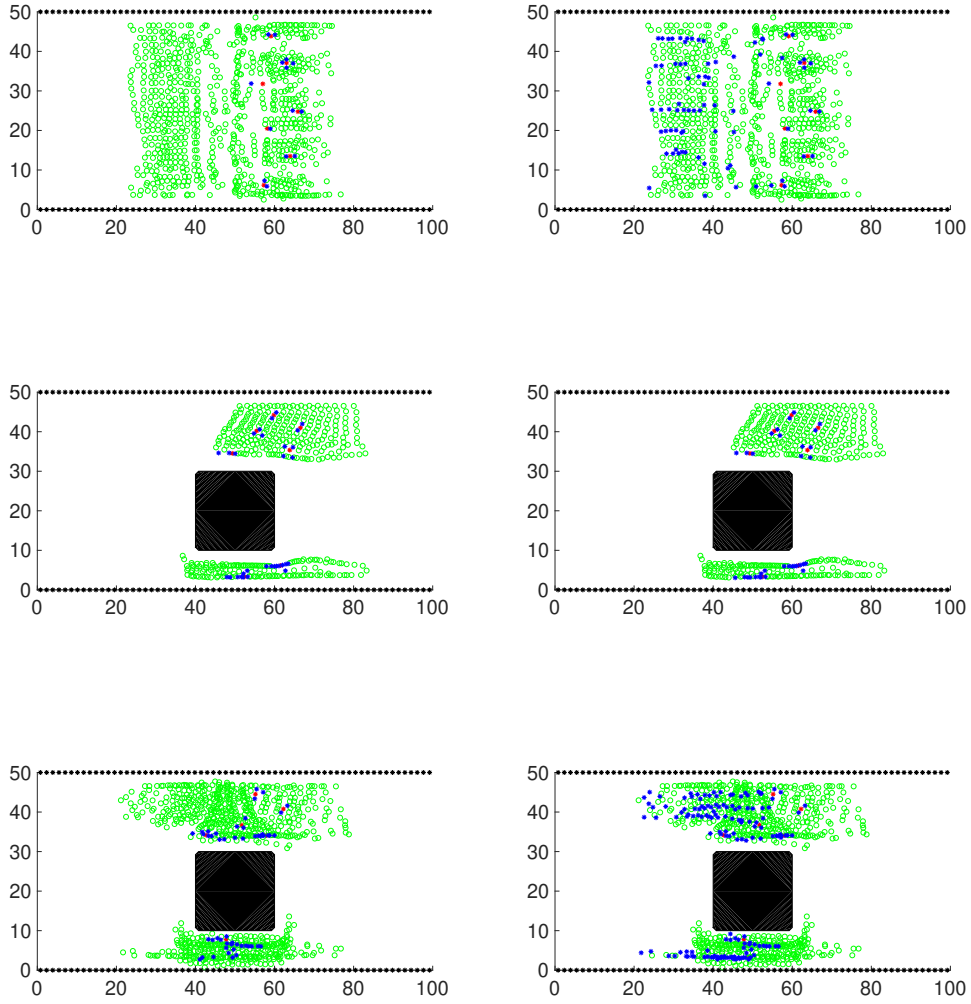

Figure 5.4 – Pedestrian dynamics at time $t = 30$ with influence (left) and without influence (right) of contact time. Row 1: Bi-directional flow. Row 2: Uni-directional flow around obstacle. Row 3: Bi-directional flow around obstacle. Red indicate infected, green indicate susceptibles and blue indicate probably exposed pedestrians.

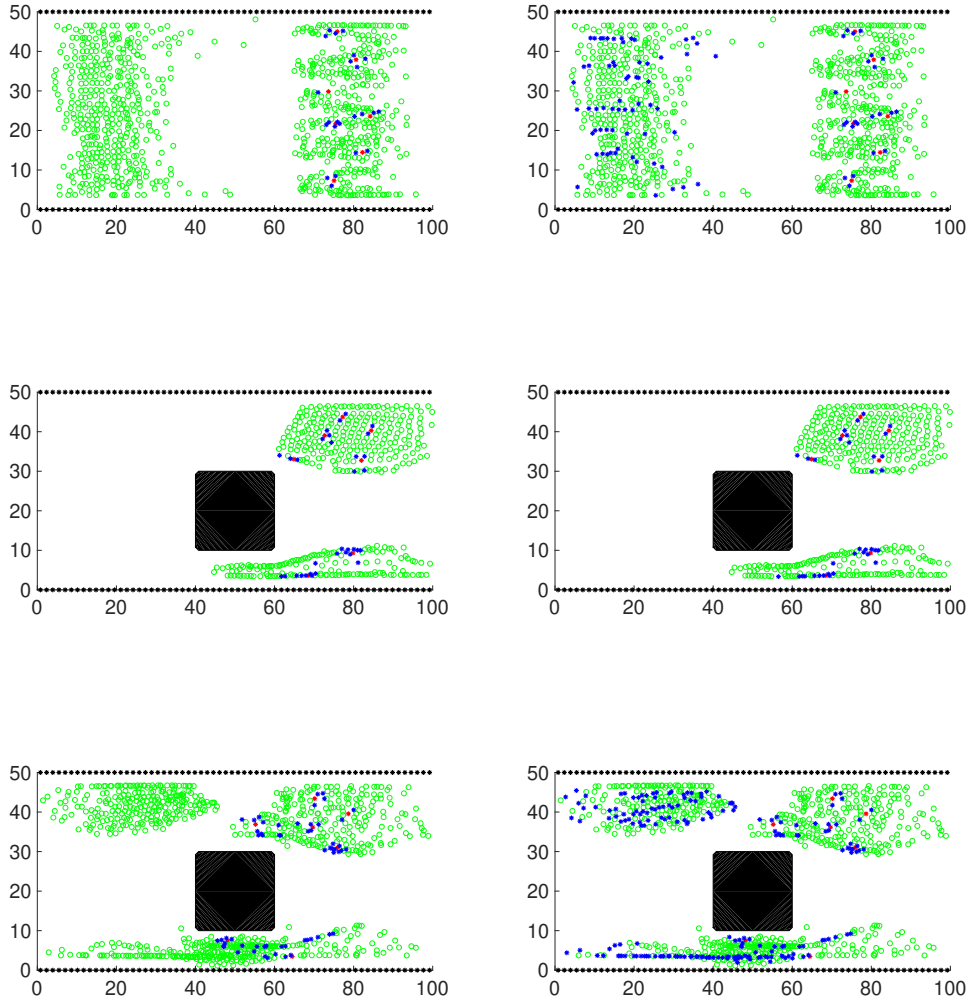

Figure 5.5 – Pedestrian dynamics at time $t = 40$ with influence (left) and without influence (right) of contact time. Row 1: Bi-directional flow. Row 2: Uni-directional flow around obstacle. Row 3: Bi-directional flow around obstacle. Red indicate infected, green indicate susceptibles and blue indicate probably exposed pedestrians.

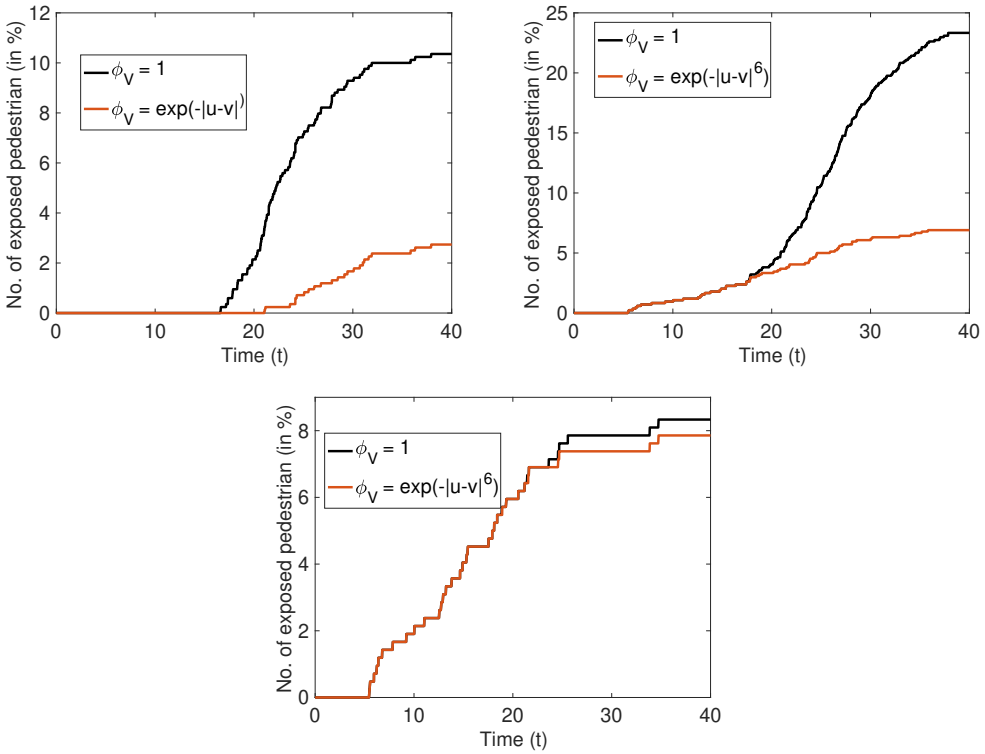

Figure 5.6 – Number of pedestrian with an increased probability of being exposed (in %) vs time. First row bi-directional flow without obstacle (left) and with obstacle (right). Second row: uni-directional with obstacle.

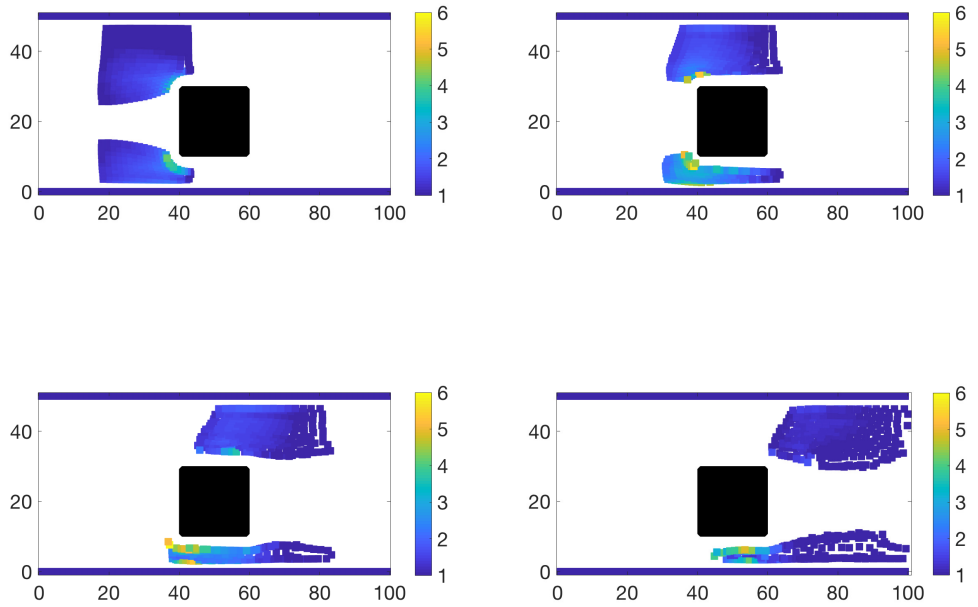

Figure 5.7 – Macroscopic density ρ of pedestrian dynamics at times $t = 10, 20, 30, 40$ with influence of contact time for uni-direction flow with fixed obstacle.

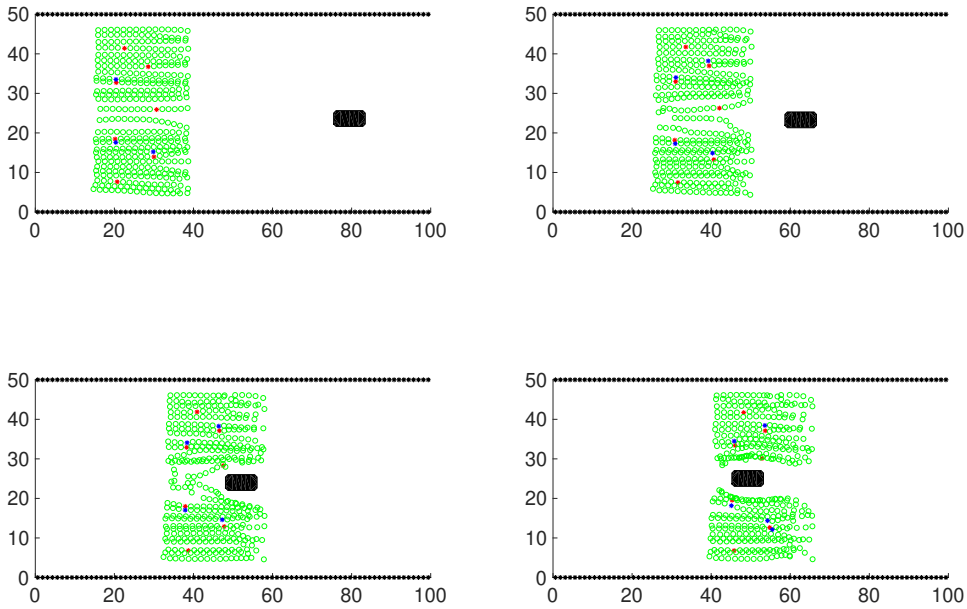

Figure 5.8 – Positions of pedestrian and obstacle at $t = 8s, 14s$ (first row) and $t = 18s, 22s$ (second row). Red indicate infected, green indicate susceptibles, blue indicate probably exposed pedestrians.

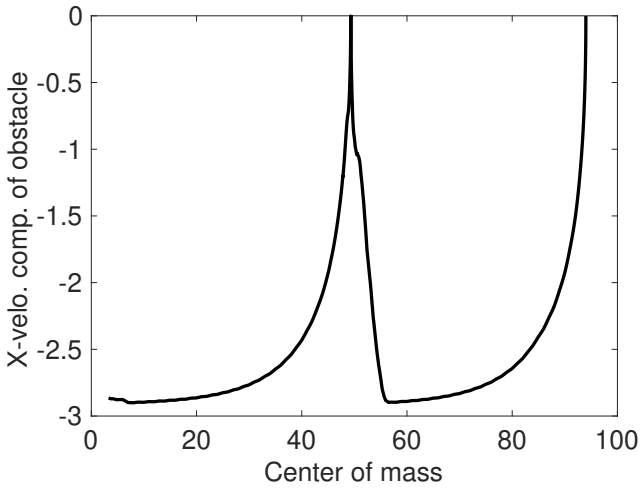

Figure 5.9 – The velocity of the obstacle along the center of mass.

6 Rational Behaviour Model in different density scenarios

6.1 Introduction

The question of how humans interact with the environment and make decisions to move through their environment has motivated research in the direction of behavioural dynamics. Any evolved behavioural pattern is preceded by a dynamics of perception and action. Perception involves the interaction of an agent with its environment and collection of information via 'laws of ecological optics' [71] and processing that information into actionable behaviour via 'laws of control' [170]. A dynamical model was developed in [61] based on these principles to predict route choice behaviours. A recent attempt to include rational behaviour of pedestrians in an agent based model was made by the development of a heuristics based rational behaviour model in [129] and later improved in [15] based on vision based models as developed in [136]. In these works, as well as in [49], the rational behaviour interaction models have been investigated. A hierarchy of models ranging from microscopic, over kinetic models to macroscopic models has been established in [49].
In the present chapter, we consider the extended rational behaviour model from [15] and state a related kinetic and hydrodynamic model following and extending slightly the procedure outlined in [49], we also refer to Section 2.1.4. Section 6.2 discusses these models and also how geometries and moving obstacles are included via a coupling to an eikonal equation. The hierarchy of rational behaviour models is numerically investigated for different density situations with fixed and moving geometries in Section 6.3. We investigate the differences between the rational behaviour interaction model and interaction models based on the classical social force based models [82], [87] and compare the different models on the microscopic and the macroscopic level. For the numerical experiments we use the mesh-free particle method [111, 164] to solve the macroscopic model equations in a Lagrangian sense. The microscopic equations are solved using the same numerical framework. See Section 3.4 for the details on using the numerical method for solving the pedestrian models.

6.2 Pedestrian Flow Model based on rational behaviour

We consider here a slightly modified version of the hierarchy of pedestrian models formulated in [49] and [15] . The microscopic pedestrian model formulated in [49] and [15] is based on a collision avoidance model combined with a social force type environmental coercion term. The collision avoidance model consists of two stages - perception stage and decision stage. The

perception stage is described by an interaction region for each pedestrian and the definition of two functionals, the distance to interaction and the distance of closest approach as defined below. Consider a pair of pedestrians i and j. Assume that agent i is aware of it's own position x_i and velocity v_i and can also perceive j's x_j and v_j accurately. In the perception stage, the observables are:

- Time to interaction of i and j, $\tau_{i,j}$:
  Time that minimizes the distance $d_{i,j}$ between the pedestrians.
$$\tau_{i,j} = -\frac{(x_j - x_i)\,.\,(v_j - v_i)}{||v_j - v_i||^2}$$
- Point of closest approach of i to j, $p_{i,j}$:
  The point along the trajectory of i where the agents will be closest.
$$p_{i,j} = x_i + v_i\,\tau_{i,j}$$
- Distance to interaction (DTI) of i and j , $D_{i,j}$:
  The distance of i to $p_{i,j}$.
$$D_{i,j} = -\frac{(x_j - x_i)\,.\,(v_j - v_i)}{||v_j - v_i||^2}||v_i||$$
- Distance of closest approach (or minimum distance (MD)) of i and j , $C_{i,j}$:
$$C_{i,j} = \left(||x_j - x_i||^2 - \frac{(x_j - x_i)\,.\,(v_j - v_i)}{||v_j - v_i||^2}\right)^{1/2}$$

6.2.1 Time-continuous Model

In the decision stage, a decision on the velocity is made based on the above observables via a decision potential Φ and an associated cost functional. With some simplifications, this leads to the collision avoidance term F_i in the model described below. The so called environmental coercion effects are included in the model via a social force type approach and lead to the term E_i below. The resulting time-continuous model for N pedestrians ($i = 1, 2, ..., N$) with location $x_i = x_i(t)$ and velocity $v_i = v_i(t)$ at time t is

$$\begin{aligned} \frac{dx_i}{dt} &= v_i\,, \\ \frac{dv_i}{dt} &= F_i + E_i\,, \end{aligned} \tag{6.1}$$

where

$$F_i = -\nabla_{\tilde{v}}\Phi_i(v_i) \tag{6.2}$$

and

$$E_i = E_{g,i}(x_i) + E_{\mu,i}(x_i, v_i). \tag{6.3}$$

Note that here and in the following, we do not explicitly write the dependencies on t for the sake of a simpler presentation.

The decision potential Φ is defined as follows. Define first

$$X_{ij} = x_j - x_i,\ V_{ij} = v_j - v_i.$$

Let T_i be the set of pedestrians approaching the pedestrian at x_i and belonging to the i^{th} pedestrian interaction region defined as the angular sector centred at x_i, with axis v_i, semi-angle $\nu/2$ and radius r_i, which means

$$\begin{aligned} T_i = \Big\{ & j \in \{1,2,...,N\}, i \neq j \mid ||X_{ij}|| \leq r_i \text{ and} \\ & \frac{X_{ij} \cdot v_i}{||X_{ij}||\,||v_i||} > \cos(\nu/2) \text{ and } X_{ij} \cdot V_{ij} < 0 \Big\}. \end{aligned} \tag{6.4}$$

For every $j \in T_i$, we compute the distance to interaction (DTI) of i and j, denoted by D_{ij} and the distance of closest approach or minimum distance (MD) of i and j, denoted as C_{ij}, as given in [15], as

$$C_{ij} = \min \left\{ \left[||X_{ij}||^2 - \frac{(X_{ij} \cdot V_{ij})^2}{||V_{ij})||^2} \right]^{1/2}, R \right\}$$

and

$$D_{ij} = \min \left\{ \frac{-X_{ij} \cdot V_{ij}}{||V_{ij}||^2} ||v_i||, L \right\},$$

where the constant parameters L and R are the maximal DTI and the maximal MD, respectively. The expressions for C_{ij} and D_{ij} are obtained by considering the distance of two pedestrians with the respective locations and velocities versus time and determining the time to interaction as well as the point of closest approach. We refer to [15] for details. As in [49], we define the overall heuristics considering the harmonic average to approximate the minimum DTI:

$$D_i^{-1} = \frac{1}{\#T_i} \sum_{j \in T_i(t)} D_{ij}^{-1}. \tag{6.5}$$

Moreover, slightly changing the expression in [15], we define the weighted average of the MD as

$$C_i = \frac{1}{\#T_i} \sum_{j \in T_i} C_{ij}\ w_{ij}, \tag{6.6}$$

where the weights are given by

$$w_{ij} = \frac{D_{ij}^{-1}}{D_i^{-1}}.$$

Then the i^{th} pedestrian potential function is given by,

$$\Phi_i(\tilde{v}) = \frac{k}{2} ||D_i C_i \tilde{v} - LR v_i^*||^2 + \frac{\tilde{k}}{2} \left(||\tilde{v}||^2 - ||v_i^*||^2 \right)^2, \tag{6.7}$$

where $v_i^\star$ is the target velocity associated with the i^{th} pedestrian.
The environmental coercion terms are as in classical social force models [82] on the one hand given by an interaction potential and the related force E_g is given as,

$$E_{g,i}(x_i) := \sum_{j \neq i} g(||X_{ij}||) n_{ij}$$

with the interaction normal

$$n_{ij} = \frac{X_{ij}}{||X_{ij}||}.$$

Here, g denotes the absolute value of a radial repulsive force depending on the distance of the interacting pedestrians. On the other hand the friction term including tangential and normal friction during an encounter is given by,

$$E_{\mu,i}(x_i, v_i) := -\sum_{j \neq i} \left(\mu_n V_{ij} \cdot n_{ij} n_{ij} + \mu_t V_{ij} \cdot n_{ij}^{\perp} n_{ij}^{\perp} \right) w_\mu(\|X_{ij}\|).$$

Here, μ_n, μ_t are normal and tangential friction coefficients during the interactions and w_μ concentrates the interaction friction to particles undergoing an interaction, see the discussion in [15] and [60].

Finally, for future use, we define the microscopic number density as,

$$\rho_i = \frac{\#S_i}{\pi s_i^2}, \tag{6.8}$$

where

$$S_i = \left\{ \; j \in \{1, 2, ..., N\} \mid ||X_{ij}|| \leq s_i \; \right\}$$

with an observation radius s_i.

6.2.2 Mean-field Kinetic Model

For the passage from the microscopic model to the mean-field equation, we simplify the following considerations by assuming that the target velocity $v_i^\star(t)$ is given by a function $v^\star(x,t)$ via $v_i^\star(t) = v^\star(x_i(t),t)$, that means it depends only on the location. Then, we describe the system using a number density distribution $f(x,v)$ with $x, v \in \mathbb{R}^2$, where we again neglect the dependence on t for simplicity of presentation. Let $f(x,v)\,dx\,dv$ be the number density of pedestrians in a small physical volume dx around the point x, within an angular neighbourhood dv of v. Then f formally satisfies the Fokker-Planck equation:

$$\partial_t f + v.\nabla_x f + \nabla_v.(Ff) + \nabla_v.(Ef) = 0, \tag{6.9}$$

compare, for example, [49] and [60].

The force term F is given by the continuous equivalent of Eqn. (6.2) and written as,

$$F(x,v) = -\nabla_{\tilde{v}} \Phi_{(x,v)}(v),$$

where the potential Φ is given by,

$$\Phi_{(x,v)}(\tilde{v}) = \frac{k}{2} ||D_{(x,v)} C_{(x,v)} \tilde{v} - LRv^*||^2 + \frac{\tilde{k}}{2} \left(||\tilde{v}||^2 - ||v^*||^2 \right)^2.$$

To compute DTI denoted by $D_{(x,v)}$ and MD denoted by $C_{(x,v)}$ of pedestrians located at position x with velocity v, we first define the interaction region

$$T(x,v) = \Big\{ y \in \mathbb{R}^2, u \in \mathbb{R}^2 \;\; | \;\; ||y-x|| \leq r(x), \\ \frac{y-x}{||y-x||} \cdot \frac{v}{||v||} \geq \cos(\nu/2) \text{and } (y-x) \cdot (u-v) < 0 \Big\}.$$

Now the continuous equivalents of Eqns. (6.5) and (6.6) are

$$D^{-1}_{(x,v)} = \frac{\int_{T(x,v)} \tilde{D}^{-1}_{(x,v)}(y,u) f(y,u) dy\, du}{\int_{T(x,v)} f(y,u)\, dy\, du}$$

and

$$C_{(x,v)} = \frac{\int_{T(x,v)} \tilde{C}_{(x,v)}(y,u) \tilde{D}^{-1}_{(x,v)}(y,u) f(y,u)\, dy\, du}{D^{-1}_{(x,v)} \int_{T(x,v)} f(y,u)\, dy\, du},$$

which is equal to

$$\frac{\int_{T(x,v)} \tilde{C}_{(x,v)}(y,u) \tilde{D}^{-1}_{(x,v)}(y,u) f(y,u)\, dy\, du}{\int_{T(x,v)} D^{-1}_{(x,v)} f(y,u)\, dy\, du}.$$

The quantities $\tilde{D}_{x,v}(y,u)$ and $\tilde{C}_{x,v}(y,u)$ are the elementary DTI and MD of a pedestrian located at position x and velocity v in the encounter with a particle located at y and having velocity u. They are given by,

$$\tilde{C}_{x,v}(y,u) = \min\left\{ \left[||y-x||^2 - \frac{((y-x).(u-v))^2}{||u-v||^2} \right]^{1/2}, R \right\}$$

and

$$\tilde{D}_{x,v}(y,u) = \min\left\{ \frac{||(y-x).(u-v)||}{||u-v||^2} ||v||, L \right\}.$$

The continuous equivalent of the environmental coercion term is $E = E(x,v)$ with $E = E_g + E_\mu$. Here, E_g is

$$\begin{aligned} E_g(x) &= \int_{y\in\mathbb{R}^2} \int_{u\in\mathbb{R}^2} g(||y-x||) n(x,y) f(y,u)\, dy\, du \\ &= \int_{y\in\mathbb{R}^2} g(||y-x||) n(x,y) \rho(y)\, dy, \end{aligned} \tag{6.10}$$

where $n(x,y) = \dfrac{y-x}{||y-x||}$ and $\rho(x)$ is the local density

$$\rho(x) = \int_{v\in\mathbb{R}^2} f(x,v)\, dv.$$

Moreover, E_μ is given as,

$$E_\mu(x,v) = \int_{y\in\mathbb{R}^2} \int_{u\in\mathbb{R}^2} \mu(x,y,v,u) w_\mu(\|y-x\|) f(y,u)\, du\, dy \tag{6.11}$$

where

$$\mu(x,y,v,u) = \mu_n(u-v)\cdot n(x,y) n(x,y) + \mu_t(u-v)\cdot n(x,y)^\perp n(x,y)^\perp.$$

Local Approximation of Kinetic Model

Assume that there exists a small dimensionless quantity $\eta << 1$ such that,

$$r = \eta\, \hat{r}, R = \eta\, \hat{R}, L = \eta\, \hat{L},$$

where all hat quantities are assumed to be of $\mathcal{O}(1)$. By the same assumptions as in [49] we have

$$\eta^2 k = \hat{k} = \mathcal{O}(1).$$

Now, since we have to consider only local interactions, let $y = x + \eta\,\xi$, with $\xi \in \mathbb{R}^2$, in the mean field equations. In this scaling, our kinetic model with all unknowns now depending on η is:

$$\partial_t f^\eta + v.\nabla_x f^\eta + \nabla_v.(F^\eta f^\eta) + \nabla_v.(E^\eta f^\eta) = 0, \tag{6.12}$$

with

$$F^\eta(x,v) = -\nabla_{\tilde{v}}\Phi^\eta_{(x,v)}(v)$$

and

$$E^\eta(x,v) = E^\eta_g(x,v) + E^\eta_\mu(x,v)$$

Now, $y \in T(x,v) \equiv \xi \in \hat{T}_{v,v,\hat{r}}$, where

$$\hat{T}_{v,v,\hat{r}} = \left\{ \xi \in \mathbb{R}^2, u \in \mathbb{R}^2 \;\mid\; ||\xi|| \le \hat{r}, \frac{\xi}{||\xi||}.\frac{v}{||v||} \ge \cos(v/2), \xi.(u-v) < 0 \right\}.$$

Then we have, the elementary quantities

$$\tilde{C}_{(\xi,u,v)} = \frac{1}{\eta^2}\hat{C}(\xi,u,v), \tilde{D}_{(\xi,u,v)} = \frac{1}{\eta}\hat{D}(\xi,u,v)$$

where

$$\hat{C}(\xi,u,v) = \min\left\{ \left[||\xi||^2 - \frac{(\xi.(u-v))^2}{||u-v||^2} \right]^{1/2}, R \right\}$$

$$\hat{D}(\xi,u,v) = \min\left\{ \frac{||\xi.(u-v)||}{||u-v||^2}||v||, L \right\}.$$

Consequently, we get,

$$D^{-1}_{(x,v)} = \frac{1}{\eta}\breve{D}^{-1}_{(x,v)}, C_{(x,v)} = \frac{1}{\eta^2}\breve{C}_{(x,v)}$$

where,

$$\breve{D}^{-1}_{(x,v)} = \frac{\int_{\hat{T}_{v,v,\hat{r}}} \hat{D}^{-1}(\xi,u,v) f(x+\eta\,\xi,u)\,d\xi\,du}{\int_{\hat{T}_{v,v,\hat{r}}} f(x+\eta\,\xi,u)\,d\xi\,du} \tag{6.13}$$

$$\breve{C}_{(x,v)} = \frac{\int_{\hat{T}_{v,v,\hat{r}}} \hat{C}(\xi,u,v)\hat{D}^{-1}(\xi,u,v) f(x+\eta\,\xi,u)\,d\xi\,du}{\breve{D}^{-1}_{(x,v)} \int_{\hat{T}_{v,v,\hat{r}}} f(x+\eta\,\xi,u)\,d\xi\,du} \tag{6.14}$$

Since, f is assumed to evolve on large scales and $\eta << 1$, we need only consider the leading order term in the Taylor expansion of f in Eqns. (6.13) and (6.14). We have,

$$f(x+\eta\,\xi,v) = f(x,v) + (\eta\,\xi)\,f_x(x,v) + \mathcal{O}((\eta\,\xi)^2).$$

This leads to the following expressions of $\breve{D}^{-1}$ and $\breve{C}$:

$$\breve{D}^{-1}_{(x,v)} = \frac{\int_{u\in\mathbb{R}^2}\int_{\xi\in\hat{T}_{v,v,\hat{r}}} \hat{D}^{-1}(\xi,u,v)\,d\xi\,f(x,u)\,du}{\int_{\xi\in\hat{T}_{v,v,\hat{r}}} d\xi \int_{u\in\mathbb{R}^2} f(x,u)\,du} \tag{6.15}$$

and

$$\breve{C}_{(x,v)} = \frac{\int_{u\in\mathbb{R}^2}\int_{\xi\in\hat{T}_{v,v,\hat{r}}} \hat{C}(\xi,u,v)\hat{D}^{-1}(\xi,u,v)\,d\xi\,f(x,u)\,du}{\breve{D}^{-1}_{(x,v)} \int_{\xi\in\hat{T}_{v,v,\hat{r}}} d\xi \int_{u\in\mathbb{R}^2} f(x,u)\,du}. \tag{6.16}$$

Hence, the potential is:

$$\Phi_{(x,v)}(\tilde{v}) = \frac{\hat{k}}{2}||\breve{D}_{(x,v)}\breve{C}_{(x,v)}\tilde{v} - LRv^*||^2 + \frac{\tilde{k}}{2}\left(||\tilde{v}||^2 - ||v^*||^2\right)^2 .$$

The environmental coercion force terms are given as,

$$\begin{aligned} E_g^{\eta}(x,v) &= \int_{\xi\in\mathbb{R}^2\setminus\{0\}}\int_{u\in\mathbb{R}^2} g(||\xi||)\, n(\xi)\, f(x+\eta\,\xi,u)\, d\xi\, du \\ &= \int_{\xi\in\mathbb{R}^2\setminus\{0\}}\int_{u\in\mathbb{R}^2} g(||\xi||)\, n(\xi)\, f(x,u)\, d\xi\, du \\ &= \int_{\xi\in\mathbb{R}^2\setminus\{0\}} g(||\xi||)\, n(\xi)\, N(x)\, d\xi \end{aligned}$$

and

$$E_{\mu}^{\eta}(x,v) = \int_{\xi\in\mathbb{R}^2}\int_{u\in\mathbb{R}^2} \mu(\xi,v,u) w_{\mu}(\|\xi\|) f(x,u)\, d\xi\, du,$$

where,

$$\mu(\xi,v,u) = \mu_n(u-v)\cdot n(\xi)n(\xi) + \mu_t(u-v)\cdot n(\xi)^{\perp}n(\xi)^{\perp}$$

with $n(\xi) = \dfrac{\xi}{||\xi||}$.

***Special Case**:*

If we consider the case when $\nu = 2\pi$, that is, there is no blind zone. Then, $\hat{T}$ is the disc:

$$B_{\hat{r}} = \left\{\xi \in \mathbb{R}^2 \;\middle|\; ||\xi|| \le \hat{r}\right\}.$$

Then, we get,

$$\breve{D}_x^{-1} = \frac{\int_{u\in\mathbb{R}^2}\int_{\xi\in B_{\hat{r}}} \hat{D}^{-1}(\xi,u,v)\, d\xi\, f(x,u)\, du}{Area(B_{\hat{r}})\int_{u\in\mathbb{R}^2} f(x,u)\, du}$$

and

$$\breve{C}_x = \frac{\int_{u\in\mathbb{R}^2}\int_{\xi\in B_{\hat{r}}} \hat{C}(\xi,u,v)\, d\xi\, \hat{D}^{-1}(\xi,u,v) f(x,u)\, du}{\breve{D}_x^{-1} Area(B_{\hat{r}})\int_{u\in\mathbb{R}^2} f(x,u)\, du}.$$

Hence, potential Φ also does not depend on v and is written as:

$$\Phi_x = \frac{\hat{k}}{2}||\breve{D}_x\breve{C}_x\tilde{v} - LRv^*||^2 + \frac{\tilde{k}}{2}\left(||\tilde{v}||^2 - ||v^*||^2\right)^2 .$$

The environmental coercion terms are:

$$E_g^{\eta}(x) = \int_{\xi\in\mathbb{R}^2\setminus\{0\}} g(||\xi||)\, n(\xi)\, N(x)\, d\xi$$

and

$$E_{\mu}^{\eta}(x,v) = -\mu(\tilde{\rho}(x,t))vE_{\mu}^{\eta}(x) = \int_{\xi\in\mathbb{R}^2}\int_{u\in\mathbb{R}^2} \mu(\xi,v,u) w_{\mu}(\|\xi\|) f(x,u)\, d\xi\, du$$

with

$$\tilde{\rho}(x) = \frac{2R^2}{\hat{r}^2} Area(B_{\hat{r}}) \int_{u\in\mathbb{R}^2} f(x,u)\, du$$

6.2.3 Hydrodynamic Model

Proceeding as in [49] or [60], one derives the associated hydrodynamic model using a moment closure method wherein we start with the mean field kinetic model and integrate it against functions of particle velocity v. The equations we obtain involve the macroscopic quantities, density $\rho(x)$ and average velocity $U(x)$ of pedestrians, where

$$U(x) \quad = \quad \frac{1}{\rho(x)} \int_{v\in\mathbb{R}^2} v f(x,v)\, dv.$$

Integrating the kinetic model in Eqn. (6.9) against dv and $v\,dv$, we get the continuity equation

$$\partial_t \rho + \nabla_x \cdot (\rho U) = 0 \tag{6.17}$$

and an equation for the momentum

$$\partial_t(\rho U) + \nabla_x . \left(\int_{v\in\mathbb{R}^2} v \otimes v f\, dv \right) = \int_{v\in\mathbb{R}^2} F\, f\, dv + \int_{v\in\mathbb{R}^2} E\, f\, dv\,. \tag{6.18}$$

To close the equations we use the monokinetic closure Ansatz,

$$f(x,v) = \rho(x)\, \delta_{U(x)}(v).$$

Then, Eqn. (6.18) changes to

$$\partial_t(\rho U) + \nabla_x \cdot (\rho U \otimes U) = \rho F_x^M + \rho E_x^M$$

with

$$F_x^M = -\nabla_{\tilde{v}} \Phi_x^M(U(x)),$$

where Φ_x^M is defined as

$$\Phi_x^M(\tilde{v}) = \frac{k}{2} ||D_x^M C_x^M \tilde{v} - LRv^*||^2 + \frac{\tilde{k}}{2} \left(||\tilde{v}||^2 - ||v^*||^2 \right)^2.$$

And D_x^M is given by

$$(D_x^M)^{-1} = \frac{\int_{T^M(x)} D^{-1}_{(x,U(x))}(y,U(y))\rho(y) dy}{\int_{T^M(x)} \rho(y)\, dy},$$

where

$$T^M(x) = \Big\{ y \in \mathbb{R}^2 \;\mid\; ||y-x|| \le r(x)\,, \\ \frac{y-x}{||y-x||} \cdot \frac{U(x)}{||U(x)||} \ge \cos(\nu/2) \text{ and } (y-x)\cdot(U(y)-U(x)) < 0 \Big\}.$$

Analogously,

$$C_x^M = \frac{\int_{T^M(x)} C_{(x,U(x))}(y,U(y)) D^{-1}_{(x,U(x))}(y,U(y))\rho(y)\, dy}{\int_{T^M(x)} D^{-1}_{(x,U(x))}(y,U(y)))\rho(y)\, dy}.$$

Finally, we have,

$$E_x^M = E_g + E_\mu^M$$

with E_g as in (6.10) and E_μ^M as

$$E_\mu^M = -\int_{y\in\mathbb{R}^2} \mu(x,y,U(x),U(y))\; w(\|y-x\|)\rho(y)\; dy.$$

6.2.4 Including geometries using the eikonal equation

In addition to the local interaction forces F_i and E_i, we add another component to the force for the velocity update in Eqn. (6.1). In a scenario where there are other elements in the environment which affect the movement of pedestrians, like walls/obstacles, we need a force which directs them away from these and towards the target. A classical approach is given by using the eikonal equation as in [94], [95] and [123]. We refer to [60] for a combination of social force models and the eikonal equation in the context of a macroscopic equation.

The revised time-continuous model is:

$$\begin{aligned} \frac{dx_i}{dt} &= v_i\,, \\ \frac{dv_i}{dt} &= F_i + E_i + G_i\,, \end{aligned} \tag{6.19}$$

with F_i and E_i given by Eqn. (6.2) and Eqn. (6.3) as before and

$$G_i = \frac{1}{T}\left(-V(\rho_i)\,\frac{\nabla\phi(x_i)}{||\nabla\phi(x_i)||} - v_i\right) \tag{6.20}$$

with ρ_i given in Eqn. (6.8). And, T is a reaction time, which is here assumed to be constant and ϕ being the solution of the eikonal equation,

$$V(\rho(x))\,||\nabla\phi(x)|| = 1, \tag{6.21}$$

with V a density dependent velocity function and $\rho(x)$ is given by a continuous interpolation of ρ_i, which is as defined in Eqn. (6.8). The geometry enters via the boundary conditions imposed on the eikonal equation. For boundaries, one usually chooses a Dirichlet boundary condition with a very large value. For exits, a Dirichlet condition with the value zero is chosen.

With the same procedure as before, we derive the continuity equation and the associated momentum equation,

$$\partial_t(\rho U) + \nabla_x\cdot(\rho U\otimes U) = \rho F_x^M + \rho E_x^M + \rho G_x^M \tag{6.22}$$

with F_x^M and E_x^M as above and G_x^M as

$$G_x^M = \frac{1}{T}\left(-V(\rho(x))\,\frac{\nabla\phi(x)}{||\nabla\phi(x)||} - U(x)\right), \tag{6.23}$$

which is coupled to Eqn. (6.21).

Remark 6.1 We note that, there are several works discussing well-posedness for the Hughes model, i.e. the continuity equation coupled to the eikonal equation. As an example, we refer to [52]. However, we are not yet aware of any attempts to prove this for a hydrodynamic system coupled to the eikonal equation.

6.2.5 Determining the target directions

Instead of predefining the target directions $v_i^\star(t) = v^\star(x,t)$, it seems more reasonable to adapt them as well via an eikonal equation and determine $v^\star(x,t)$ via

$$\frac{dv^\star}{dt} = \frac{1}{T^\star}\left(-\frac{\nabla\phi^\star(x)}{||\nabla\phi^\star(x)||} - v^\star\right). \tag{6.24}$$

with

$$||\nabla\phi^\star(x)|| = 1. \tag{6.25}$$

Here, the target directions can be adapted to the geometry via the eikonal equation and $T^\star$ is again a reaction time.

6.2.6 Modelling the motion of an obstacle

The motion of the obstacle is described similarly to the procedure outlined in Section 3.3.2. The obstacle is moving towards a predefined and specific target/exit given by an eikonal equation. Moreover, information from the environment is taken into account, and the moving obstacle changes its path and speed in order to avoid collisions with pedestrians. The equation for the obstacle is given as:

$$\begin{aligned}\frac{dx^O}{dt} &= v^O\,,\\ \frac{dv^O}{dt} &= E^O(x^O,v^O) + G^O(x^O,v^O)\,,\end{aligned} \tag{6.26}$$

where x^O and v^O are the position and velocity of the obstacle's centre of mass and E^O is computed from the interaction with pedestrians with density ρ in the immediate vicinity of the obstacle. A pure repulsion force of the form Eqn. (6.10) is used. The force G^O is obtained from the gradient of the eikonal solution ϕ^O for the obstacle. Explicitly, we define

$$G^O(x^O,v^O) = -\frac{1}{T^O}\left(V^O(\rho(x^O))\frac{\nabla\phi^O(x^O)}{||\nabla\phi^O(x^O)||} - v^O\right),$$

where ϕ^O is the solution of

$$V^O(\rho(x))\,||\nabla\phi^O(x)|| = 1\,, \qquad x\in\Omega.$$

Here, T^O is chosen as constant and, rather than being a reaction, describes the weighting between the reaction of the obstacle to neighbouring pedestrians and the importance of following its predefined goal.

The model for the pedestrian motion is coupled to the moving obstacle's kinematic equations via the eikonal equation for the obstacle, which includes the density ρ of pedestrians, and also via the interaction term in Eqn. (6.26). On the other hand, the moving obstacle model is coupled to the pedestrian flow equations via the eikonal equation for pedestrians, which includes the moving geometry into the model. Finally, we note that multiple obstacles could be described in a similar way, including an interaction term between the obstacles.

6.3 Numerical Investigation

6.3.1 Numerical Method

In our numerical studies, we compare the different models in detail on the microscopic as well as the macroscopic level. For a comparison between microscopic and macroscopic results in the case of a social force type interaction term, we refer to [111]. We also refer to [111] for a detailed comparison of the computation times of microscopic and macroscopic simulations for social force type interactions and the potential gain in CPU time using the macroscopic modelling.

For the microscopic model equations, pair-wise interactions are considered to evaluate the interaction forces. It is computationally costly to consider and evaluate the force term for each possible pair in a simulation scenario involving a large number of microscopic pedestrian particles. Hence, we choose to consider only nearest neighbour interactions within a specific radius as considered in [60].

For the macroscopic equations, a meshfree particle method based on least square approximation is used, see Section 2.2.1. The method is based on a Lagrangian formulation of the hydrodynamic equations. These Lagrangian equations are then solved on a mesh-free cloud of particles, see Section 3.4 for more details. Note that, physically speaking, the macroscopic grid particles do not represent a single pedestrian but rather a local average of pedestrians. The gain in computational efficiency of the macroscopic method versus the microscopic one is essentially due to the fact that the number of macroscopic grid particles does not have to be chosen of the same size as the number of microscopic particles. It is usually much smaller.

In both, microscopic and macroscopic cases, the eikonal equations are solved on a fixed structured grid using a fast-marching method [154], see Section 2.3. Note that alternatively, a fast-sweeping method could be applied [147]. The variable values like those of density are interpolated from the mesh-free cloud onto this fixed grid. The spatial derivatives of the eikonal function are again obtained from nearest neighbours via a weighted least square algorithm.

Including a moving obstacle requires a coupling of these equations to the obstacle's kinematic equations. In this case, one has additionally to activate and deactivate the eikonal grid points depending on the obstacle's position in a manner similar to an immersed boundary method, see Section 3.4. When the obstacle is fixed, this needs to be done only once at the beginning of the time evolution. Otherwise, the activation-deactivation of grid points needs to be performed at every time step of evolution for moving obstacles. For the time discretization, we use an explicit scheme with time step as specified in the results section for each case.

6.3.2 Interaction Models

To analyse the effect of different interaction potentials or forces on collision avoidance, we consider various scenarios. First, a head-on two particle collision, then a collision avoidance scenario where a particle is navigating a group, and finally, situations with boundaries and larger rigid obstacles (stationary and moving).

We investigate and compare 4 types of interaction models. First, the model based on rational behaviour presented above in Section 6.2 by Eqns. (6.1)-(6.3) and $E = 0$, i.e. without a repulsive

force, is considered. Second, we consider the rational behaviour model combined with a repulsive force $E = E_g$, where g is as in [15] given by,

$$g(\|x\|) = -D_r \left(\frac{2}{s_r^2} + \frac{1}{\|x\|^2} \right) exp\left(-\frac{\|x\|^2}{s_r^2} \right). \tag{6.27}$$

Here, D_r is a repulsive strength and s_r a length scale. Third, a social force model as described in [60] is considered, given by the equations Eqns. (6.1)-(6.3) with $F = 0$ and a purely repulsive force $E = E_g$ with

$$g(\|x\|) = \frac{C_r}{l_r} exp\left(-\frac{\|x\|}{l_r} \right). \tag{6.28}$$

Again C_r is a repulsive strength and l_r a length scale. As a final example, we use a social force model with a repulsive force E_g given by a linearly varying force

$$g(\|x\|) = k_n(2R_r - \|x\|)H(2R_r - \|x\|), \tag{6.29}$$

where H is the Heaviside function and R_r an interaction radius. This force is used together with an additional dissipative force E_μ given by nonzero friction coefficients μ_t, μ_n and a function $w_\mu(\|x\|) = H(2R_r - \|x\|)$ restricting the friction to the interaction range. The parameters used in the different models are collected in Tables 6.1 and 6.2. For a further discussion of the parameters in social force models, we refer to [152]. Each of these models is considered with and without the eikonal force term.

Interaction Force	Parameters
Rep., $E = E_g$ with g from (6.28)	$C_r = 2\frac{m^2}{s^2}$, $l_r = 0.2m$
Collision Avoidance $F = -\nabla_v \Phi$	$k = 2\frac{1}{sm^4}$, $\tilde{k} = 1\frac{s}{m^2}$, $L = 2m$, $R = 1m$
Rep.-Dissip., $E = E_g + E_\mu$ with g from (6.29)	$k_n = 10\frac{1}{s^2}$, $R_r = 0.42m$, $\mu_n = 5\frac{1}{s}$, $\mu_t = 1\frac{1}{s}$
Collision Avoidance + Rep., $F + E_g$ with g from (6.27)	$k = 2\frac{1}{sm^4}$, $\tilde{k} = 1\frac{s}{m^2}$, $L = 2m$, $R = 1m$, $D_r = 1\frac{m^3}{s^2}$, $s_r = 1m$

Table 6.1 – Parameter list for the different interaction force terms for Sections 6.3.3 and 6.3.5. Parameters not listed are set to zero.

6.3.3 Two particle collision avoidance

In this scenario, we consider two particles, one heading to the right with an initial velocity $v_1^{(0)} = (1,0)\,m/s$, and the second heading to the left with an initial velocity $v_2^{(0)} = (-1,0)\,m/s$ as shown in Fig. 6.1(left). The target velocities in the collision avoidance model are accordingly $v_1^\star = (1,0)\,m/s$

for the pedestrian moving to the right and $v_2^\star = (-1,0)\,m/s$ for the one moving to the left. The particles start at a distance of $1\,m$ between them. We study the collision avoidance behaviour for the models described above in Section 6.3.2, including pure collision avoidance (rational behaviour), pure repulsive force and the repulsive/dissipative social force model. Additionally, we study the effects obtained from simulations with and without the eikonal force term in the different cases. For the eikonal term G_i in Eqn. (6.20), we use $V = V_{max}(1 - \frac{\rho}{\rho_{max}})$ with $V_{max} = 1\,m/s$, $\rho_{max} = 5\,ped/m^2$ and $T = 0.1\,s$. For the calculation of microscopic number density ρ_i, as given in Eqn. 6.8, we use $s_i = 0.5\,m$. The details of the other parameters used in the different cases are shown in Table 6.1 in the first three rows. Explicit time integration with a fixed time step size of $0.01\,s$ is used for this simulation.

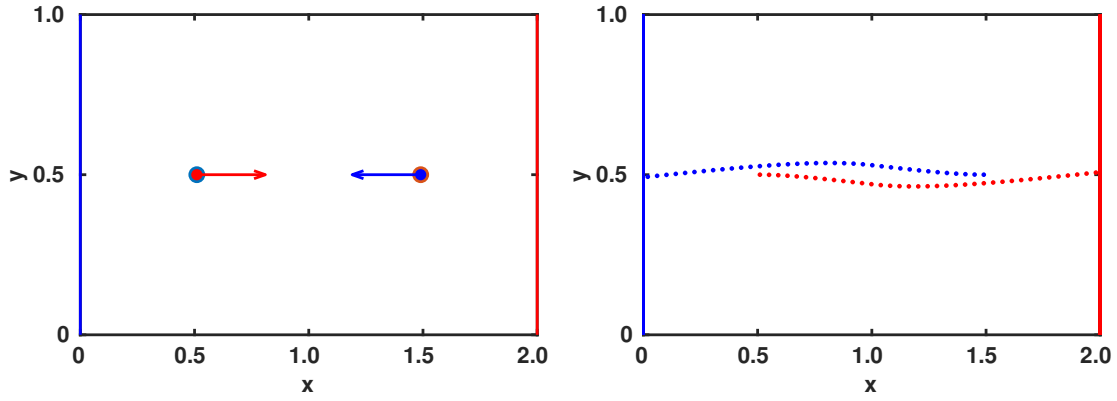

Figure 6.1 – Two-particle collision avoidance scenario

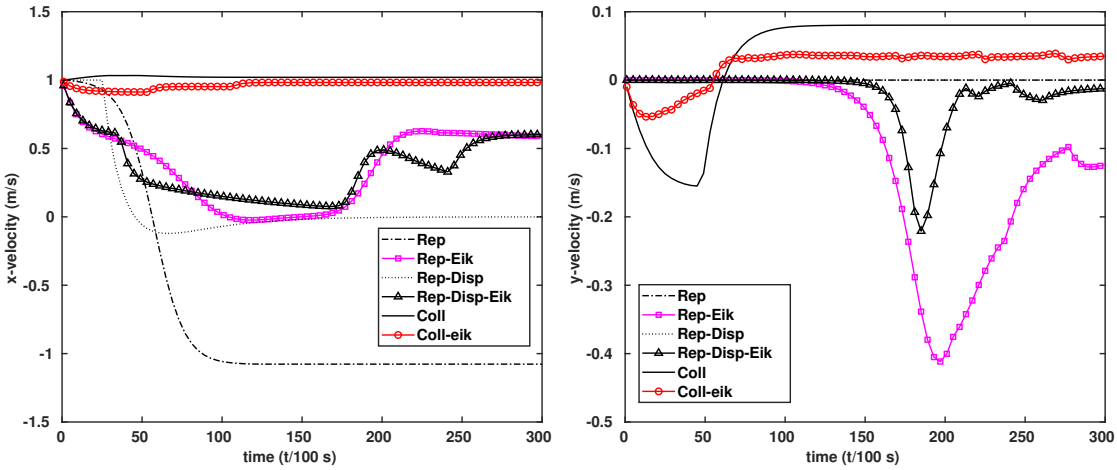

Figure 6.2 – Velocity-time graphs of particle moving to the right for 3 different interaction rules including pure repulsion, repulsion/dissipation and collision avoidance. In each case, the models are used with and without eikonal force.

A sample plot of trajectories of the particles with the collision avoidance model, where a collision is successfully avoided, is shown in Fig. 6.1(right). The velocity-time graphs of the particle moving

to the right are shown in Fig. 6.2. We observe, from the x-velocity graphs in Fig. 6.2 (left), that purely repulsive or repulsive and dissipative social force terms lead to pedestrians bouncing and moving opposite to their desired direction once they encounter a potential collision from a distance. On bouncing back, they either come to a stop or even move in the opposite direction, depending on the strength of the residual social force. Hence the additional eikonal term is essential to counter the social force and keep the particles moving forward. The eikonal terms are not essential in the case of the collision avoidance models. In this case, the pedestrian keeps its speed and only changes slightly its direction to avoid the collision, as can be seen from the y-velocity graphs in Fig. 6.2 (right). We also observe that for the pure social force models, there is no change in the y-direction of the particle heading to the right to avoid a head-on collision.

Moreover, we see from the velocity-time graphs in Fig. 6.2 that for the case of social force models combined with the eikonal equation, the collision is avoided. The particles initially slow down when they predict the collision and then slowly modify their direction. Once the collision is avoided, they accelerate again and move in the target direction. On the other hand, the rational behaviour collision avoidance model guarantees collision avoidance while maintaining the target velocity without relying on the eikonal equation. There is no abrupt bouncing or change of direction here, but a gradual change in direction and velocity because of the anticipatory behaviour. Adding an eikonal force term is not a necessity in this case.

In conclusion, purely repulsive or repulsive-dissipative social forces are not sufficient for a reasonable collision avoidance behaviour, while using just the potential Φ in the collision avoidance models as given in Eqn. (6.2) is enough to obtain a physically reasonable solution without additional eikonal or social force terms. The model works perfectly fine in the case considered in this subsection.

6.3.4 Comparison with experimental data - one pedestrian avoiding a stationary pedestrian

We consider the controlled experiment of a pedestrian avoiding a stationary pedestrian (at the centre) in a corridor of length $7.88\,m$ and width $1.75\,m$, as described in [128]. In Fig. 6.3, the averaged trajectory of the pedestrian from experiments is compared against the trajectory predicted from the model in Eqn. (6.1) with collision avoidance force F. For our numerical setup, we consider the initial position of the pedestrian as in the experiment. The parameter for the relaxation time in the eikonal equation is chosen as $T = 0.5\,s$ and $V_{max} = 1.3\,m/s$, as considered in the model in [128]. That means we do not fit the parameters to the experimental trajectory but rather use experimentally determined parameter values. We see that for the chosen parameters, the trajectory agrees well. The largest displacement from the centre, corresponding to the peak in the trajectory from experimental data, is $0.411\,m$ and in the simulated trajectory is $0.526\,m$.

6.3.5 Collision avoidance - one particle against a group of particles

To study how collision avoidance behaviour is affected when there is a higher density of pedestrians rather than a one-to-one head-on scenario, we consider a group of pedestrians described by the

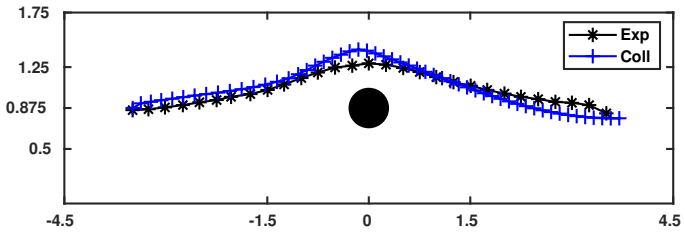

Figure 6.3 – Comparsion of average trajectory from controlled experiment (labeled Exp) in [128] with the trajectory obtained from the model (labeled Coll) in Eqn. (6.1) using collision avoidance from Eqn. (6.2) with parameter values $k = 2\,\frac{1}{sm^4}$, $\tilde{k} = 1\,\frac{s}{m^2}$, $L = 3.5\,m$, $R = 0.5\,m$. The data for the average trajectory was extracted, from the figure in the publication [128], using the online tool - [145]

microscopic equations moving to the right, each with an initial velocity $v_i^{(0)} = (1,0)\,m/s, i = 2,\ldots N$ and a single pedestrian heading to the left with an initial velocity $v_1^{(0)} = (-1,0)\,m/s$ (see Fig. 6.4(left)). The target velocities are chosen accordingly.

We consider again the models described at the beginning in Section 6.3.2 with parameters given in Table 6.1. For the eikonal term G_i, we use $V = V_{max}(1 - \frac{\rho}{\rho_{max}})$ with $V_{max} = 1\,m/s$, $\rho_{max} = 5\,ped/m^2$ and $T = 0.1\,s$. For the calculation of microscopic number density ρ_i, as given in Eqn. (6.8), we use $s_i = 0.6\,m$. A fixed time step size of $0.01\,s$ is used for the explicit time integration. The rational behaviour model is considered with and without repulsive force and eikonal force term. The social force models are considered with an eikonal force term. Fig. 6.4 shows a sample plot of the particles obtained from the model with repulsive social force term.

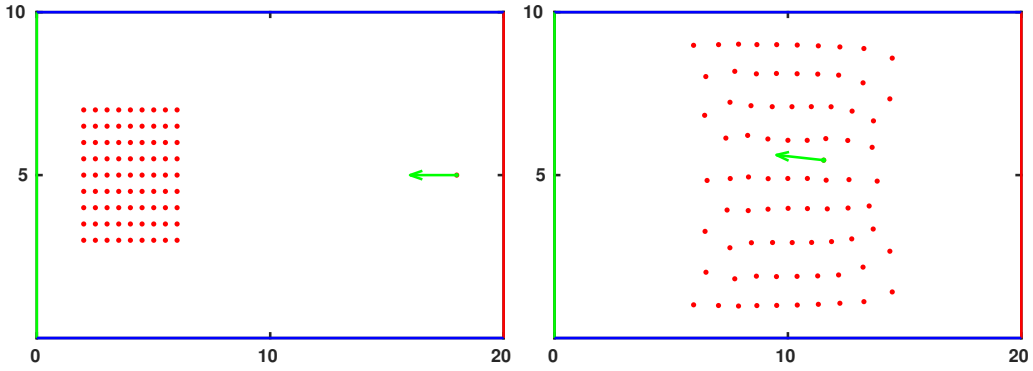

Figure 6.4 – Interaction of a group of pedestrians with a single pedestrian - plots at $t = 0\,s$ (left) and $t = 8.1\,s$ (right) .

The velocity-time graphs in Fig. 6.5 of the particle heading towards the left boundary reveal that the single pedestrian avoids collision with the oncoming group by both path and speed adjustment. There is always a forward movement (i.e. the velocity does not become positive at any time), while there is also a gradual change in speed (by changes in x-velocity) and direction (by y-velocity changes) to avoid collisions particle by particle.

We observe that the collision avoidance model with and without repulsive force E_g leads to an

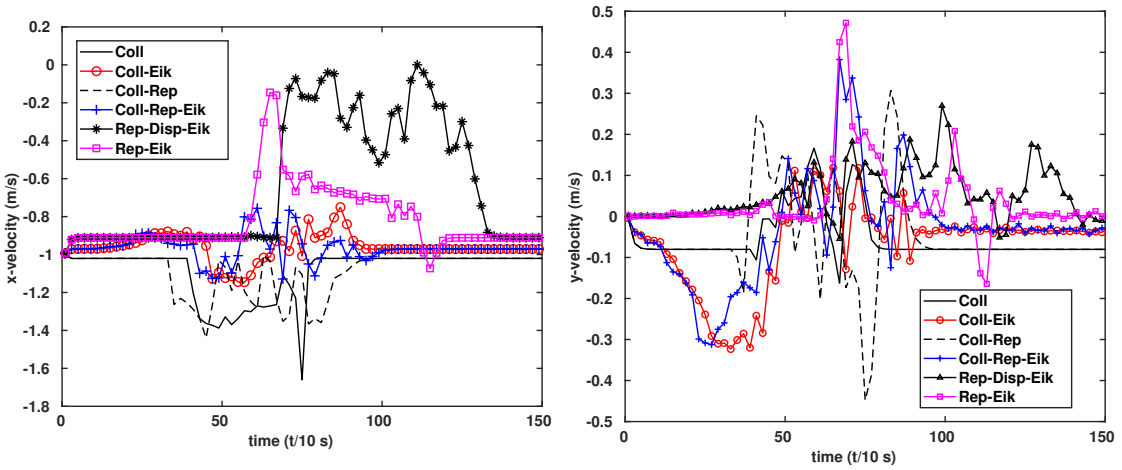

Figure 6.5 – Velocity-time graphs - x-velocity (left), y-velocity (right) - of the pedestrian moving towards left from $t = 0\,s$ to $t = 15\,s$. Color of the plots denote the various interaction forces - pure repulsion, repulsion-dissipation and collision avoidance/rational behaviour - used in the model.

accelerated movement of the particle (indicated by larger negative x-velocity) with small direction changes (indicated by changes in y-velocity). This acceleration is reduced for the case of the rational behaviour model, including the eikonal force. In this case, the pedestrian velocities remain near the maximum speed of $1\,m/s$. This is expected as the eikonal term is a relaxation towards the desired velocity.

When pure social forces are considered, a repulsion-dissipation force $E_g + E_\mu$, coupled with an eikonal force, leads to strong deceleration as the pedestrian approaches the group, followed by continuous speed and direction adjustments. On the other hand, using the pure repulsive force E_g coupled with an eikonal force leads to a less pronounced deceleration of particles along with direction changes during the collision avoidance phase, followed by an acceleration to the maximum velocity (magenta plots). Moreover, the collisions seem to be resolved more quickly, and velocity remains more bounded after the initial collision avoidance, which happens between $t = 6\,s$ and $t = 7\,s$.

Thus, using either a rational behaviour force and a repulsion or a pure repulsion together with an eikonal force gives physically reasonable results in these scenarios. We remark that although the collision-avoidance potential Φ with an additional repulsive force term E_g also produces favourable results, the parameters are very sensitive to any change in geometry or density of pedestrians or even the starting positions and velocities of the particles considered.

6.3.6 Collision avoidance - one group of particles navigating a stationary obstacle and walls

Now, we consider a corridor of length $100\,m$ and width $50\,m$ and a group of pedestrians consisting of 231 pedestrians described by the microscopic equations moving to the right with an initial velocity $v_i^{(0)} = (1,0)\,m/s$ initially uniformly distributed in a rectangular region near the left boundary, see

Figs. 6.6 for the initial setup. The target velocity $v_i^\star$ is here chosen via Eqn. (6.24) using $T^\star = 0.1\,s$. The top and bottom are boundary walls, and there is a stationary obstacle, which the group of pedestrians has to avoid. Further parameters are given in Table 6.2. For the eikonal term G_i, we use $V = V_{max}(1 - \frac{\rho}{\rho_{max}})$ with $V_{max} = 2\,m/s$, $\rho_{max} = 10\,ped/m^2$ and $T = 0.1\,s$. Note that even higher maximal densities have been measured in emergency situations, see [7]. A fixed time step of $0.001\,s$ is used for explicit time integration.

Interaction Force	Parameters
Rep., $E = E_g$ with g from (6.28)	$C_r = 4\frac{m^2}{s^2}$, $l_r = 0.5m$
Collision Avoidance $F = -\nabla_v \Phi_S$	$k = 2\frac{1}{sm^4}$, $\tilde{k} = 1\frac{s}{m^2}$, $L = 3m$, $R = 0.4m$
Rep.-Dissip., $E = E_g + E_\mu$ with g from (6.29)	$k_n = 100\frac{1}{s^2}$, $R_r = 0.42m$, $\mu_n = 50\frac{1}{s}$, $\mu_t = 10\frac{1}{s}$
Collision Avoidance + Rep., $F + E_g$ with g from (6.27)	$k = 2\frac{1}{sm^4}$, $\tilde{k} = 1\frac{s}{m^2}$, $L = 3m$, $R = 0.4m$, $D_r = 10\frac{m^3}{s^2}$, $s_r = 1m$

Table 6.2 – Parameter list for the different interaction force terms for Sections 6.3.6 to 6.3.9. Parameters not listed are set to zero.

In this case, the focus is not only to avoid collisions with other pedestrians but also to keep a minimum distance between the pedestrians in order to avoid overcrowding. A simple collision avoidance force given by Φ, as in Eqn. (6.2), is, in this case, not enough to guarantee this unless the coefficients are tuned to provide a high repulsion effect, which is impractical. An additional repulsive force E_g, which acts as a distance keeping term for the particles within the group, is more efficient in this scenario and more adaptable to density changes.

We note that in [15], for scenarios involving boundaries, the interactions of pedestrians with boundary walls are dealt with by additional distance keeping or frictional terms particular to wall interactions. Here, we include the information on the boundaries via the forcing term G and, in particular, via the boundary conditions for the eikonal equation Eqn. (6.21).

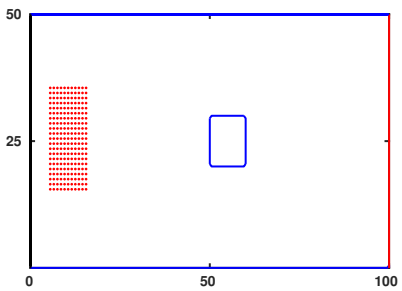

Figure 6.6 – Initial positions of 231 pedestrians for a geometry with a fixed obstacle.

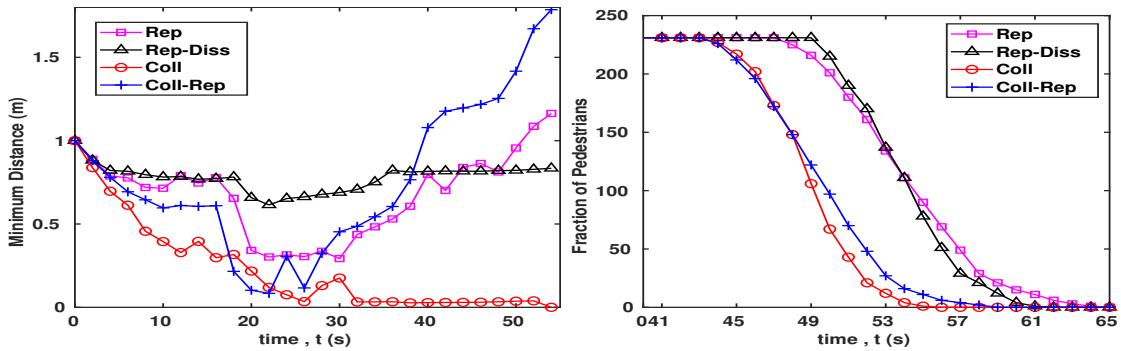

Figure 6.7 – Variation of minimum pair-wise distance between particles with time (left). Fraction of pedestrians vs. time graph showing the evacuation times (right)

In this scenario, the main point of concern is whether the pedestrians maintain their distance while navigating around the obstacle since there is a tendency to crowd near the edges of the obstacle. We analyse the overall minimum distance amongst all possible pairs of pedestrians at a particular time instant. The plot in Fig. 6.7 (left) shows the minimum distance for various possible interaction forces. We observe that using the collision avoidance potential Φ and no social force term leads to a lot of crowding. The minimal distance is near zero in this case. Hence Φ needs to be always paired with a distance keeping term E_g to maintain a minimal distance between pedestrians in the group. Meanwhile, a simple repulsive force or dissipative forces, like E_g or $E_g + E_\mu$, are also enough to guarantee distance keeping. At the same time, the non-local eikonal force guarantees the navigation around the large obstacle while moving towards the target direction and maintaining the target speed.

Fig. 6.7 (right) shows the evacuation times for the various interaction forces. We see that collision avoidance Φ with or without additional repulsive force leads to shorter evacuation times, as compared to the pure social force type models. This is because pedestrians maintain higher velocities closer to the maximum velocity in the collision avoidance models, as we observed in the cases in Section 6.3.3 and Section 6.3.5 for the chosen parameters. The social forces slow down the pedestrians significantly while navigating the obstacles.

6.3.7 Group of pedestrians navigating a stationary obstacle: hydrodynamic simulations

For the hydrodynamic simulations, we consider a corridor of length $100\,m$ and width $50\,m$ with a static obstacle in the domain. The top and bottom boundaries are rigid walls. A group of particles with an initial density of $\rho_0 = 1\,ped/m^2$ start near the left boundary and are moving towards the right boundary.

We consider the hydrodynamic model, Eqn. (6.17) and Eqn. (6.22) with force terms given by the models mentioned previously. They are, in all cases, combined with the eikonal term. We keep the parameters in the eikonal force term uniform across all simulations with parameter values as in the previous microscopic simulation in Section 6.3.6. The time step used in this case is again $0.001\,s$. Time snapshots at $t = 10\,s$ and $t = 20\,s$ of the densities in the domain for the different cases are

shown in Figs. 6.8 and 6.9. The density plots show that higher densities are observed around the edges of the obstacle. We observe that, as in the microscopic case, the highest densities are observed for the model with collision avoidance Φ without any repulsion term in comparison to the other models. Moreover, we see that the addition of a repulsive term, E_g ensures more diffusion and hence reduces overcrowded states considerably. The corresponding density plots at different vertical strips of the domain are shown in Fig. 6.10.

We conclude that when the interaction forces are used in combination with an eikonal force, which is essential to have a robust model capable of handling geometry changes easily, the qualitative results are not highly sensitive to the local pairwise interaction or collision avoidance forces between pedestrians. However, the pure rational behaviour model tends as before to unphysical overcrowding.

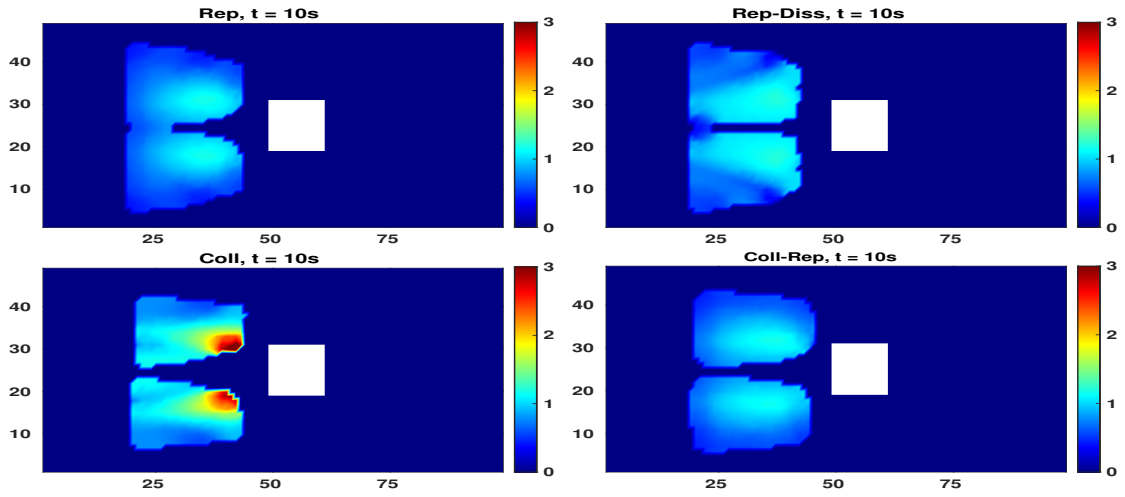

Figure 6.8 – Density (color denotes number of pedestrians/m^2) plots for the different interaction forces - pure repulsion,collision avoidance, repulsion-dissipation and collision avoidance with repulsion. Snaphot at $t = 10$ s.

6.3.8 Comparison of microscopic and macroscopic model

For the comparison of a microscopic and a macroscopic model considered in Section 6.3.6 and Section 6.3.7, respectively, we consider the numerical setup in the corresponding sections using 720 pedestrians initially separated by a distance of $1\,m$. Correspondingly, we consider a grid of 720 macroscopic particles and assign them an initial density of $1\,ped/m^2$ in each $1\,m^2$ cell corresponding to the pedestrian positions considered in the domain. We restrict ourselves to the repulsion-dissipation interaction model. The other models show similar behaviour. We numerically solve the microscopic and macroscopic models with parameter values as in Table 6.2. For the eikonal term G_i, we use $V = V_{max}(1 - \frac{\rho}{\rho_{max}})$, with $V_{max} = 2\,m/s$, $\rho_{max} = 10\,ped/m^2$ and $T = 0.1\,s$. Fig. 6.11 compares the microscopic simulation (location of pedestrians) with the macroscopic density at time $t = 20\,s$. For a more detailed comparison of microscopic and macroscopic models, we refer to [60] and [111]. In particular, in [111], a discussion and numerical comparison of the

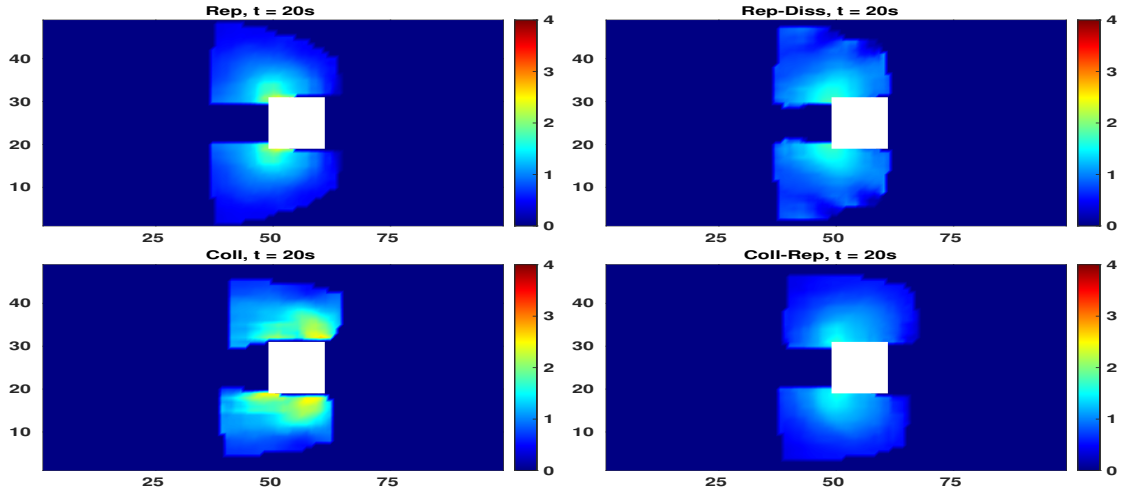

Figure 6.9 – Density (color denotes number of pedestrians/m^2) plots for the different interaction forces - pure repulsion,collision avoidance, repulsion-dissipation and collision avoidance with repulsion. Snapshot at $t = 20\,s$.

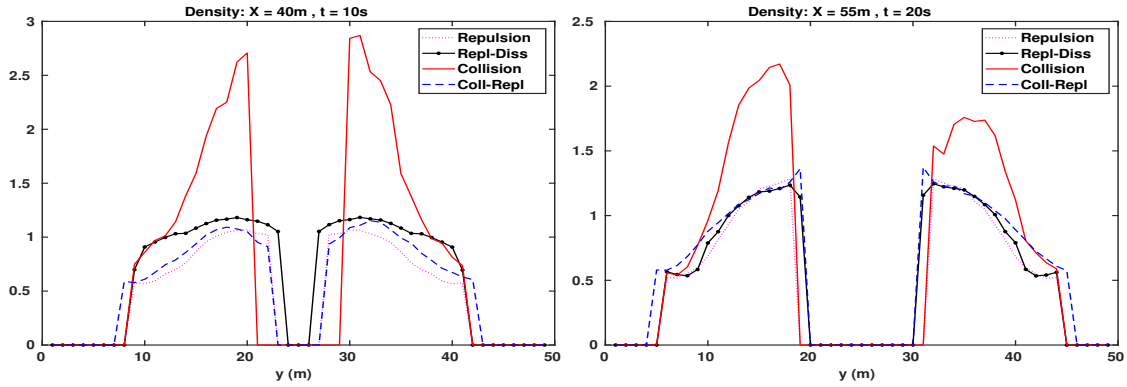

Figure 6.10 – Density plots at different vertical strips of the domain at different time instances for the stationary obstacle.

computation times for microscopic and macroscopic models is given. There, it is shown that a major gain in computation time can be obtained by using the macroscopic model as long as the number of involved pedestrians is large and a suitable discretization method is used for the macroscopic equations.

6.3.9 Effect of changing relaxation time T

In order to understand the effect of the value of the relaxation time T, we consider the hydrodynamic model considered in Section 6.3.7 with two different interaction forces, i.e. repulsion-dissipation and rational behaviour with repulsion. The numerical setup is the same as above, with a static obstacle in a rectangular corridor. The parameters for the interaction forces are chosen as given in Table 6.2, and the parameters for the eikonal force term G are as in Section 6.3.7. We vary the relaxation time T in the eikonal forcing term in Eqn. (6.23). Three values of T are considered in

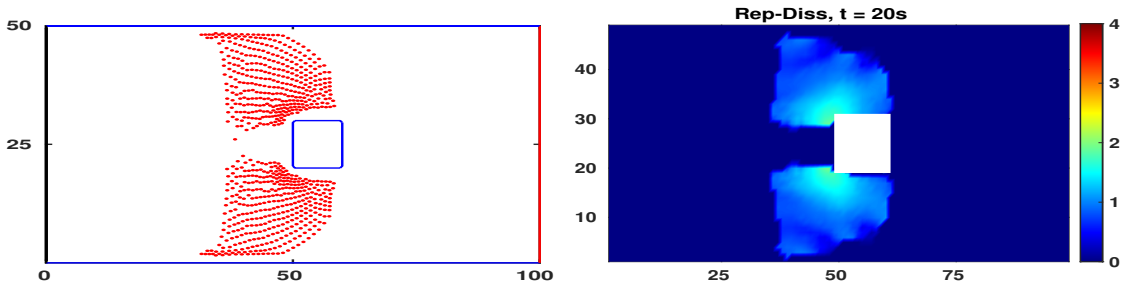

Figure 6.11 – Microscopic (left) and macroscopic (right) simulation with a fixed obstacle - snapshots at $t = 20$ s with repulsion-dissipation force E_g and eikonal term G.

Fig. 6.12. Firstly, we have set the relaxation time to $T = 0.001\,s$ which is equal to the time step for numerical integration. This ensures immediate acceleration of the particles to the desired velocity. Using this value of T implies giving a high weight to the eikonal force term. We compare these results against the ones for $T = 0.1\,s$ and $T = 0.5\,s$. We observe that increasing T leads to more diffusion and hence lower densities (compared to the case of $T = 0.001\,s$).

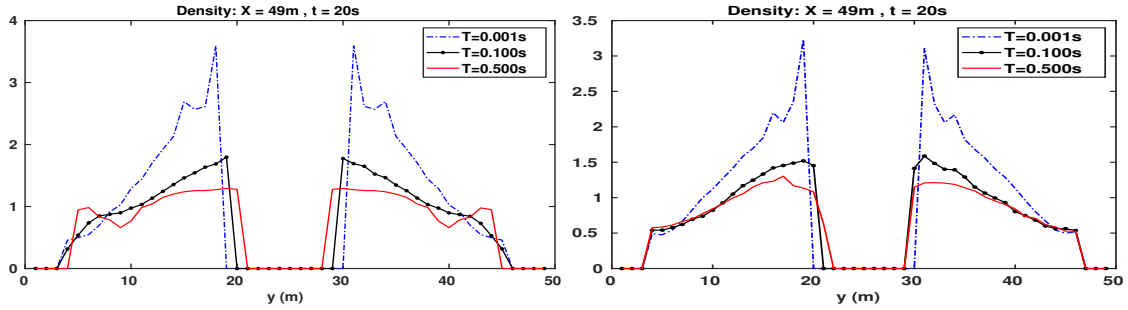

Figure 6.12 – Comparison of the density for different relaxation times $T = 0.001$ s, 0.1 s, 0.5 s for the interaction forces - repulsion-dissipation (left) and rational behaviour with repulsion (right). The data is plotted for a vertical strip at $x = 49m$ of the domain at $t = 20$ s for a stationary obstacle.

6.3.10 Pedestrian interaction with moving obstacles

Finally, we have performed numerical simulations of the collision avoidance model, with a repulsive term, under the influence of a moving obstacle, i.e. we consider Eqns. (6.17), (6.22) and (6.26). We consider, as before, a domain which is 100 m long and 50 m wide. The top and bottom boundaries are rigid walls without any entry or exit. The right boundary is the exit for pedestrians, and the left boundary is the exit for the obstacle. The initial pedestrians are concentrated in a rectangular region in the domain. The obstacle considered is rectangular in shape, 8 m long and 4 m wide. The initial density of the pedestrians is taken as $\rho_0 = 1\,ped/m^2$. The motion of the obstacle is described by Eqn. (6.26) with $V^O = V^O_{max}(1 - \frac{\rho}{\rho_{max}})$, where $V^O_{max} = 3\,m/s$.

Further computational details are given in Table 6.3. We initialize the pedestrians with a distance of $1\,m$. Explicit time integration with a fixed time step size of $0.001\,s$ is used in our simulation. The densities at various time instances t are shown in Fig. 6.13. We observe that the model involving

repulsion along with collision avoidance also gives physically reasonable results in such a moving obstacle scenario.

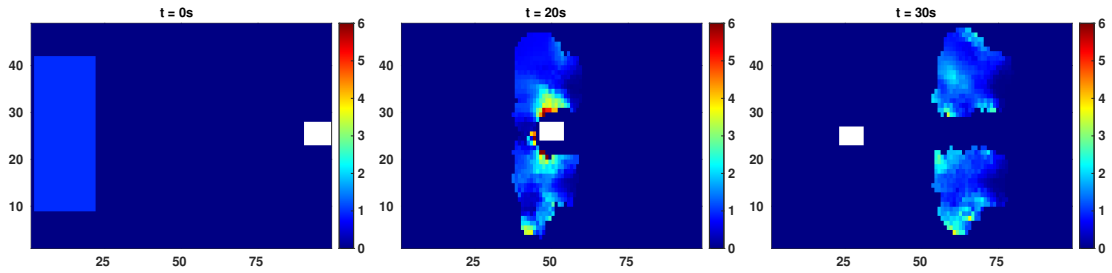

Figure 6.13 – Density (color denotes number of pedestrians/m^2) plots at different time instances - $t = 0\,s$ (left), $t = 20\,s$ (middle), $t = 30\,s$ (right) - for a moving obstacle scenario

Force terms	Parameters
Coll. avoidance, F	$R = 0.5\ m$, $L = 2\ m$, $k = 2\ \frac{1}{sm^4}$, $\tilde{k} = 1\ \frac{s}{m^2}$
Repulsive force, E_g	$D_r = 1\ \frac{m^3}{s^2}$, $s_r = 0.1$ m
Eikonal, G	T = 0.001 s, $V_{max} = 2\ \frac{m}{s}$, $\rho_{max} = 10\,ped/m^2$

Table 6.3 – Computational Details for the moving obstacle simulation

6.4 Conclusion

In the present chapter, we give a numerical investigation of a hierarchy of models to describe pedestrian flow starting from an agent based model following the work in [49] and [15]. While in [49], the authors considered an agent based model with constant speed as formulated in [129], we refer in the present chapter to the improved and more elaborate rational behaviour model with variable speeds developed in [15]. This makes the model more practically suitable for higher density scenarios and scenarios with obstacles compared to that described in [129]. A mean field kinetic model and its hydrodynamic approximation via a moment closure method using a monokinetic closure follows readily from the time continuous microscopic definitions.

Moreover, a numerical comparison has been made to highlight the similarities and differences between the current approach of using a cost potential for the velocity update and that of using explicitly defined interaction potential/force terms as in social force models. The limitations of the pure social force models is brought out by the consideration of the head-on collision scenario of Section 6.3.3. On the other hand the limitations of the pure collision avoidance approach in dealing with higher density cases is reflected in the scenarios considered in Section 6.3.5 and 6.3.6. In particular, this is shown by the fact that minimal distances are not maintained in dense situations. This requires adding additional social force type terms to the collision avoidance model as already done in [15].

To deal with walls or boundaries, [15] suggest incorporating local terms based on repulsion in the collision avoidance model. The same can be achieved in a more natural and robust way using the non-local eikonal term G_i as given by Eqn. (6.19). It is to be noted that the addition of the eikonal term implies that there are three non-local force terms in the model equations, one based on pedestrian-pedestrian collision avoidance in a vision cone, the second one on the environmental coercion terms and the last one based on the eikonal term which is responsible for avoiding boundaries and obstacles and dense regions of pedestrians.

As we see from the numerical results, in low density situation, the advantage of the pure collision avoidance approach is clearly observed. It leads to physically consistent trajectories in contrast to the social force models. However, in denser density scenarios, the addition of a social force type term is required due to the tendency of overcrowding as has been already observed in [15]. In the macroscopic simulations all models compare well qualitatively and quantitatively as long as a repulsive term is included in the collision avoidance model.

In conclusion, we have investigated microscopic and macroscopic pedestrian models based on the heuristics defined in [15]. We presented a detailed numerical investigation of these models and compared them to pure social force type models. Moreover, a preliminary comparison with a simple experiment is given. Further comparisons with experimental data can be made in future work. Also, the parameters need to be estimated to build more concrete conclusive remarks from such comparisons. The work also demonstrates the extension of the model to implement (moving) obstacle instances. This necessitates further studies to reveal the correlations between velocities or shape of obstacles and the dynamics of pedestrians.

IV Conclusion

7 Conclusion

The field of crowd dynamics is diverse and heterogeneous, composed of several subdomains of research areas. We have, through our work, contributed to two particular areas - pedestrian-moving obstacle interactions and disease contagion in crowds.

A primary objective that the work in this thesis has achieved is to develop a modelling framework and the associated numerical framework, which allows us to investigate moving pedestrian crowds in a variety of geometrical and environmental scenarios. The framework allows us to conduct numerical studies in diverse domain configurations involving boundaries and obstacles, both stationary and dynamic. Moreover, various flow conditions, uni- and bi-directional flows, low- and high-density flows and more are analysed. To the best of current knowledge, such a simplistic framework to easily cater to an array of interaction scenarios will prove to be a remarkable addition to the existing literature.

We are aware that the pedestrians by themselves are heterogeneous, varying by physical factors like age, height and weight and social factors like ethnicity and cultural differences. However, most pedestrian models, including the one in this thesis, consider a homogeneous population and the model parameters are chosen by considering their average behaviour observed in empirical studies and the real world. We remark that the parameter values should be reflective of the chosen scenario. For example, the interaction radius for the repulsive forces between pedestrians should be chosen smaller for a scenario in an Asian country than in a European country, the reason being that Asian population is more used to crowds and hence would have a higher tolerance for inter-personal distances. A more efficient model in future should try to incorporate the heterogeneity as much as necessary.

The modelling framework provides a useful tool for analysing efficient design of various pedestrian facilities and public spaces with the goal of preventing adverse conditions and providing effective evacuation strategies. For example, the model can be used to analyse how an ambulance or emergency vehicle can efficiently navigate a crowded stadium in an emergency scenario. Through numerical results, we can visualise the evolution of the pedestrian densities and movement trajectories along with their interactions within any given domain, which will be useful for the evaluation of the design and the identification of critical locations that require special attention.

The question of the well-posedness of the model is innate and needs to be answered in the context of coupling a hydrodynamic model to the Eikonal equation. In the context of coupling a macroscopic model with the microscopic kinetic equations for obstacles, we can argue that the Lagrangian formulation of the hydrodynamic model for numerics allows for an easy coupling. But the same needs to be studied for stability and well-definedness. We also remark that multiscale models can

provide efficient modelling frameworks for dealing with complex problems.
The FPM is highly efficient and robust in dealing with a variety of physical problems, including those in fluid dynamics, interacting particle systems like swarms and granular media and here crowds. In this thesis, we have demonstrated how FPM is used in handling coupled models and complex geometries. We note that the extension to multiple moving obstacles may sometimes require solving multiple eikonal equations. This can significantly increase the computational time unless the eikonal fast marching algorithm is highly efficient. This is where heap sorting becomes imperative. Moreover, the advantages of using meshfree methods overpowers that of using mesh based methods in such interacting particle systems, especially its robustness in complex geometries.
It is common knowledge that for any mathematical model, calibration of parameters from empirical studies or from real-world data is a basic requirement. There are numerous experimental studies that have been conducted to analyse specific flow patterns amongst pedestrians. A comprehensive list and review is provided in [77]. While the experiments cater to specific scenarios (like intersecting flows or bottlenecks) or to analyse specific parameters (fundamental diagrams), it is not possible to conduct experiments for a general model calibration. Further, processing real world data is still a huge computational task. Moreover, access to real data from highly crowded situations, especially of crowd disasters, from where valuable information can be extracted, is limited. Hence there is still a huge gap between models and the real world, chiefly for high-density situations.
It is quite an irony that modelling a physical system can never reach the level to satisfy the curiosity of any applied mathematician. There is always some simplification or hypothesis that one might feel the need to change or discard; that is, there is always room for improvement. Particularly in the case of complex systems, additional work is almost always essential for developing mathematical frameworks to capture, reproduce and analyse the myriad patterns and complexities that are inherent to the system.

Bibliography

[1] P. S. Abdul Salam, W. Bock, A. Klar, **and** S. Tiwari *Coupling pedestrian flow and disease contagion models* **in** In Crowd Dynamics (Vol. 4), Springer.

[2] P. S. Abdul Salam, W. Bock, A. Klar, **and** S. Tiwari. *Disease contagion models coupled to crowd motion and mesh-free simulation*. *Mathematical Models and Methods in Applied Sciences*, 31: 1277–1295, 2021. doi: 10.1142/S0218202521400066

[3] P. S. Abdul Salam, S. Tiwari, **and** A. Klar. *Modeling and Simulation of Pedestrian Interaction with Moving Obstacles Using Particle Method*. **in***Progress in Industrial Mathematics at ECMI 2021*. **byeditor**M. Ehrhardt **and** M. Günther Cham: Springer International Publishing, 2022. 337–342 doi: 10.1007/978-3-031-11818-0_44

[4] P. S. Abdul Salam, S. Tiwari, A. Klar, **and** S. Sundar. *A numerical investigation of pedestrian dynamics based on rational behaviour in different density scenarios*. *Physica A: Statistical Mechanics and its Applications*, 624: 128933, 2023. doi: 10.1016/j.physa.2023.128933

[5] P. S. Abdul Salam, S. Tiwari, A. Klar, **and** S. Sundar *Particle Method for Macroscopic Model of Coupled Pedestrian and Vehicular Traffic Flow* **in** Traffic and Granular Flow 2022 : Springer Conference Proceedings.

[6] R. Abgrall. *Numerical discretization of the first-order Hamilton-Jacobi equation on triangular meshes*. *Communications on Pure and Applied Mathematics*, 49: 1339–1373, 1996. doi: 10.1002/(sici)1097-0312(199612)49:12<1339::aid-cpa5>3.0.co;2-b (see p. 24)

[7] J. Adrian, M. Boltes, S. Holl, A. Sieben, **and** A. Seyfried. *Crowding and Queuing in Entrance Scenarios: Influence of Corridor Width in Front of Bottlenecks*. *Collective Dynamics*, 5: 189–196, 2020. doi: 10.17815/CD.2020.50 (see p. 85)

[8] J. P. Agnelli, F. Colasuonno, **and** D. Knopoff. *A kinetic theory approach to the dynamics of crowd evacuation from bounded domains*. *Mathematical Models and Methods in Applied Sciences*, 25: 109–129, 2015. doi: 10.1142/S0218202515500049 (see p. 17)

[9] J. P. Agnelli, B. Buffa, D. Knopoff, **and** G. Torres. *A Spatial Kinetic Model of Crowd Evacuation Dynamics with Infectious Disease Contagion*. *Bulletin of Mathematical Biology*, 85: 23, 2023. doi: 10.1007/s11538-023-01127-6 (see p. 52)

[10] G. Albi, N. Bellomo, L. Fermo, S.-Y. Ha, J. Kim, L. Pareschi, D. Poyato, **and** J. Soler. *Vehicular traffic, crowds, and swarms: From kinetic theory and multiscale methods to applications and research perspectives*. *Mathematical Models and Methods in Applied Sciences*, 29: 1901–2005, 2019. DOI: 10.1142/S0218202519500374 (see p. 19)

[11] B. Anvari, M. G. Bell, A. Sivakumar, **and** W. Y. Ochieng. *Modelling shared space users via rule-based social force model*. *Transportation Research Part C: Emerging Technologies*, 51: 83–103, 2015. DOI: 10.1016/j.trc.2014.10.012 (see p. 43)

[12] V. Aristov. *Biological systems as nonequilibrium structures described by kinetic methods*. *Results in Physics*, 13: 102232, 2019. DOI: 10.1016/j.rinp.2019.102232 (see p. 17)

[13] A. Aw, A. Klar, T. Materne, **and** M. Rascle. *Derivation of Continuum Traffic Flow Models from Microscopic Follow-the-Leader Models*. *SIAM Journal on Applied Mathematics*, 63: 259–278, 2002. DOI: 10.1137/s0036139900380955 (see p. 43)

[14] A. Aw **and** M. Rascle. *Resurrection of "Second Order" Models of Traffic Flow*. *SIAM Journal on Applied Mathematics*, 60: 916–938, 2000. DOI: 10.1137/S0036139997332099 (see p. 43)

[15] R. Bailo, J. A. Carrillo, **and** P. Degond. **in**: *Crowd Dynamics, Volume 1: Theory, Models, and Safety Problems*. **chapter** Pedestrian Models Based on Rational Behaviour, 259–292. Birkhäuser, Cham: Springer International Publishing, 2018. DOI: 10.1007/978-3-030-05129-7_9 (see pp. 6, 55, 69, 71, 72, 80, 85, 90, 91)

[16] M Bando, K Hasebe, A Nakayama, A Shibata, **and** Y Sugiyama. *Dynamical model of traffic congestion and numerical simulation*. *Physical review. E, Statistical physics, plasmas, fluids, and related interdisciplinary topics*, 51: 1035—1042, 1995. DOI: 10.1103/physreve.51.1035 (see p. 43)

[17] T. J. Barth **and** J. A. Sethian. *Numerical Schemes for the Hamilton–Jacobi and Level Set Equations on Triangulated Domains*. *Journal of Computational Physics*, 145: 1–40, 1998. DOI: 10.1006/jcph.1998.6007 (see p. 24)

[18] N. Bellomo, A. Bellouquid, L. Gibelli, **and** N. Outada. *A Quest Towards a Mathematical Theory of Living Systems*. Birkhäuser Cham, 2017. DOI: 10.1007/978-3-319-57436-3 (see p. 17)

[19] N. Bellomo, A. Bellouquid, **and** D. Knopoff. *From the Microscale to Collective Crowd Dynamics*. *Multiscale Modeling and Simulation*, 11: 943–963, 2013. DOI: 10.1137/130904569 (see p. 17)

[20] N. Bellomo, R. Bingham, M. A. J. Chaplain, G. Dosi, G. Forni, D. A. Knopoff, J. Lowengrub, R. Twarock, **and** M. E. Virgillito. *A multiscale model of virus pandemic: Heterogeneous interactive entities in a globally connected world*. *Mathematical Models and Methods in Applied Sciences*, 30: 1591–1651, 2020. DOI: 10.1142/S0218202520500323 (see p. 52)

[21] N. BELLOMO, P. DEGOND, **and** E. TADMOR. *Active Particles, Volume 1: Advances in Theory, Models, and Applications*. Birkhäuser Cham, 2017. DOI: 10.1007/978-3-319-49996-3 (see p. 17)

[22] N. BELLOMO **and** C. DOGBÉ. *On the Modeling of Traffic and Crowds: A Survey of Models, Speculations, and Perspectives*. *SIAM Review*, 53: 409–463, 2011. DOI: 10.1137/090746677 (see p. 19)

[23] N. BELLOMO **and** C. DOGBÉ. *ON THE MODELLING CROWD DYNAMICS FROM SCALING TO HYPERBOLIC MACROSCOPIC MODELS*. *Mathematical Models and Methods in Applied Sciences*, 18: 1317–1345, 2008. DOI: 10.1142/S0218202508003054 (see p. 18)

[24] N. BELLOMO, L. GIBELLI, **and** N. OUTADA. *On the interplay between behavioral dynamics and social interactions in human crowds*. *Kinetic and Related Models*, 12: 397–409, 2019. DOI: 10.3934/krm.2019017 (see pp. 17, 54)

[25] E. BEN-JACOB. *From snowflake formation to growth of bacterial colonies II: Cooperative formation of complex colonial patterns*. *Contemporary Physics*, 38: 205–241, 1997. DOI: 10.1080/001075197182405 (see p. 15)

[26] L. BIAN. *A Conceptual Framework for an Individual-Based Spatially Explicit Epidemiological Model*. *Environment and Planning B: Planning and Design*, 31: 381–395, 2004. DOI: 10.1068/b2833 (see p. 51)

[27] V. BLUE, M. EMBRECHTS, **and** J. ADLER. *Cellular automata modeling of pedestrian movements*. **in***1997 IEEE International Conference on Systems, Man, and Cybernetics. Computational Cybernetics and Simulation*. **volume** 3 1997. 2320–2323 vol.3 DOI: 10.1109/ICSMC.1997.635272 (see p. 15)

[28] W. BOCK, T. FATTLER, I. RODIAH, **and** O. TSE. *An analytic method for agent-based modeling of spatially inhomogeneous disease dynamics*. **in***Structure, Function and Dynamics from NM to Gm*. **volume** 1871 AIP Conference Proceedings American Institute of Physics, 2017. 020008, 020008 DOI: 10.1063/1.4996518 (see pp. 51, 54, 55)

[29] L. BOLTZMANN. *Weitere Studien über das Wärmegleichgewicht unter Gasmolekülen*. *Kinetische Theorie II: Irreversible Prozesse Einführung und Originaltexte*, 115–225, 1970. DOI: 10.1007/978-3-322-84986-1_3 (see p. 19)

[30] I. BONZANI **and** L. MUSSONE. *From experiments to hydrodynamic traffic flow models: I—modelling and parameter identification*. *Mathematical and Computer Modelling*, 37: 1435–1442, 2003. DOI: 10.1016/s0895-7177(03)90051-3 (see p. 27)

[31] R. BORSCHE **and** A. MEURER. *Microscopic and macroscopic models for coupled car traffic and pedestrian flow*. *Journal of Computational and Applied Mathematics*, 348: 356–382, 2019. DOI: 10.1016/j.cam.2018.08.037 (see p. 44)

[32] M. BRACKSTONE **and** M. MCDONALD. *Car-following: a historical review*. *Transportation Research Part F: Traffic Psychology and Behaviour*, 2: 181–196, 1999. DOI: 10.1016/s1369-8478(00)00005-x (see p. 43)

[33] F. BRAUER. **in**: *Mathematical Epidemiology*. **chapter** Compartmental Models in Epidemiology, 19–79. Berlin, Heidelberg: Springer Berlin Heidelberg, 2008. DOI: 10.1007/978-3-540-78911-6_2 (see p. 51)

[34] S. BUCHMUELLER **and** U. WEIDMANN. *Parameters of pedestrians, pedestrian traffic and walking facilities*. *Schriftenreihe des IVT*, 132: 2006. DOI: 10.3929/ethz-b-000047950 (see p. 30)

[35] J. BUISSON, S. GALLAND, N. GAUD, M. GONÇALVES, **and** A. KOUKAM. *Real-time Collision Avoidance for Pedestrian and Bicyclist Simulation: A Smooth and Predictive Approach*. *Procedia Computer Science*, 19: The 4th International Conference on Ambient Systems, Networks and Technologies (ANT 2013), the 3rd International Conference on Sustainable Energy Information Technology (SEIT-2013), 815–820, 2013. DOI: 10.1016/j.procs.2013.06.108 (see p. 29)

[36] C. BURSTEDDE, K. KLAUCK, A. SCHADSCHNEIDER, **and** J. ZITTARTZ. *Simulation of pedestrian dynamics using a two-dimensional cellular automaton*. *Physica A: Stat. Mech. Appl.*, 295: 507–525, 2001. DOI: 10.1016/S0378-4371(01)00141-8 (see p. 15)

[37] P CHAKROBORTY, S. AGRAWAL, **and** K VASISHTHA. *Microscopic modeling of driver behavior in uninterrupted traffic flow*. *Journal of Transportation Engineering*, 130: 438–451, 2004. DOI: 10.1061/(asce)0733-947x(2004)130:4(438) (see p. 43)

[38] R. E. CHANDLER, R. HERMAN, **and** E. W. MONTROLL. *Traffic Dynamics: Studies in Car Following*. *Operations Research*, 6: 165–184, 1958. DOI: 10.1287/opre.6.2.165 (see p. 43)

[39] S. CHAPMAN **and** J. LARMOR. *The kinetic theory of simple and composite monatomic gases : viscosity, thermal conduction, and diffusion*. *Proceedings of the Royal Society of London. Series A, Containing Papers of a Mathematical and Physical Character*, 93: 1–20, 1916. DOI: 10.1098/rspa.1916.0046 (see p. 20)

[40] X. CHEN, M. TREIBER, V. KANAGARAJ, **and** H. LI. *Social force models for pedestrian traffic – state of the art*. *Transport Reviews*, 38: 625–653, 2018. DOI: 10.1080/01441647.2017.1396265 (see p. 17)

[41] R. CHOWDHURY, K. HENG, M. S. R. SHAWON, G. GOH, D. OKONOFUA, C. OCHOA-ROSALES, V. GONZALEZ-JARAMILLO, A. BHUIYA, D. REIDPATH, S. PRATHAPAN, S. SHAHZAD, C. L. ALTHAUS, N. GONZALEZ-JARAMILLO, **and** O. H. FRANCO. *Dynamic interventions to control COVID-19 pandemic: a multivariate prediction modelling study comparing 16 worldwide countries*. *European Journal of Epidemiology*, 35: 389–399, 2020. DOI: 10.1007/s10654-020-00649-w (see p. 51)

[42] C. CONTARDO **and** L. COSTA. *On the optimal layout of a dining room in the era of COVID-19 using mathematical optimization*. *International Transactions in Operational Research*, 29: 3294–3315, 2022. DOI: 10.1111/itor.13139 (see p. 52)

[43] V. COSCIA **and** C. CANAVESIO. *FIRST-ORDER MACROSCOPIC MODELLING OF HUMAN CROWD DYNAMICS*. *Mathematical Models and Methods in Applied Sciences*, 18: 1217–1247, 2008. DOI: 10.1142/S0218202508003017 (see p. 18)

[44] M. G. CRANDALL **and** P.-L. LIONS. *Viscosity Solutions of Hamilton-Jacobi Equations*. *Transactions of the American Mathematical Society*, 277: 1–42, 1983. DOI: 10.1090/S0002-9947-1983-0690039-8 (see p. 24)

[45] Z. CUI, M. CAI, Y. XIAO, Z. ZHU, **and** G. CHEN. *Influences of obstacle factors on the transmission trends of respiratory infectious diseases in indoor public places*. *Journal of Building Engineering*, 64: 105706, 2023. DOI: 10.1016/j.jobe.2022.105706 (see p. 52)

[46] S. CURTIS **and** D. MANOCHA. *Pedestrian Simulation Using Geometric Reasoning in Velocity Space*. **in***Pedestrian and Evacuation Dynamics 2012*. **byeditor**U. WEIDMANN, U. KIRSCH, **and** M. SCHRECKENBERG Cham: Springer International Publishing, 2014. 875–890 DOI: 10.1007/978-3-319-02447-9_73 (see p. 29)

[47] J. E. CUTTING, P. M. VISHTON, **and** P. A. BRAREN. *How we avoid collisions with stationary and moving objects. Psychological Review*, 102: 627–651, 1995. DOI: 10.1037/0033-295x.102.4.627 (see p. 29)

[48] C. F. DAGANZO. *Requiem for second-order fluid approximations of traffic flow*. *Transportation Research Part B: Methodological*, 29: 277–286, 1995. DOI: 10.1016/0191-2615(95)00007-z (see pp. 43, 44)

[49] P. DEGOND, C. APPERT-ROLLAND, M. MOUSSAID, J. PETTRÉ, **and** G. THERAULAZ. *A hierarchy of heuristic-based models of crowd dynamics*. *Journal of Statistical Physics*, 152: 1033–1068, 2013. DOI: 10.1007/s10955-013-0805-x (see pp. 20, 49, 55, 69, 71–73, 76, 90)

[50] P. DEGOND, C. APPERT-ROLLAND, J. PETTRÉ, **and** G. THERAULAZ. *Vision-based macroscopic pedestrian models*. *Kinetic and Related Models*, 6: 809–839, 2013. DOI: 10.3934/krm.2013.6.809 (see p. 20)

[51] M. DELITALA **and** A. TOSIN. *MATHEMATICAL MODELING OF VEHICULAR TRAFFIC: A DISCRETE KINETIC THEORY APPROACH*. *Mathematical Models and Methods in Applied Sciences*, 17: 901–932, 2007. DOI: 10.1142/S0218202507002157 (see p. 44)

[52] M. DI FRANCESCO, P. A. MARKOWICH, J.-F. PIETSCHMANN, **and** M.-T. WOLFRAM. *On the Hughes' model for pedestrian flow: The one-dimensional case*. *Journal of Differential Equations*, 250: 1334–1362, 2011. DOI: 10.1016/j.jde.2010.10.015 (see pp. 18, 77)

[53] D. DIXON *Fishergate Shared Space, Preston, Lancashire, England* [Photograph] 14 January 2015 URL: https://www.geograph.org.uk/photo/4313459 (see p. 5)

[54] C. DOGBÉ. *On the numerical solutions of second order macroscopic models of pedestrian flows*. *Computers & Mathematics with Applications*, 56: 1884–1898, 2008. DOI: 10.1016/j.camwa.2008.04.028 (see p. 18)

[55] C. DRUMM, S. TIWARI, J. KUHNERT, **and** H.-J. BART. *Finite pointset method for simulation of the liquid–liquid flow field in an extractor*. *Computers & Chemical Engineering*, 32: 2946–2957, 2008. DOI: 10.1016/j.compchemeng.2008.03.009 (see p. 9)

[56] N. Z. EL AZMI, M. I. P. HIDAYAT, **and** A. D. PRAMATA. *Numerical simulation of effects of number of beds and presence of aerosol flow from sanitation machine to air circulation in hospital isolation room of COVID-19 patients*. *Materials Research Communications*, 2: 13–19, 2021. DOI: 10.12962/j2746279x.v2i1.9918 (see p. 52)

[57] D. ENSKOG. *Kinetische theorie der Vorgänge in mässig verdünnten Gasen. I. Allgemeiner Teil*. *Uppsala: Almquist & Wiksells Boktryckeri*, 1917. (see p. 20)

[58] ERAUCH *Nederlands Woonerf (Dan Burden)* [Photograph] 15 November 2004 URL: https://commons.wikimedia.org/wiki/File:Dutch_woonerf.jpg (see p. 5)

[59] R. ESCOBAR **and** A. DE LA ROSA. *Architectural Design for the Survival Optimization of Panicking Fleeing Victims*. **in***Advances in Artificial Life. ECAL 2003*. **byeditor**W. BANZHAF, J. ZIEGLER, T. CHRISTALLER, P. DITTRICH, **and** J. T. KIM Berlin, Heidelberg: Springer Berlin Heidelberg, 2003. 97–106 DOI: 10.1007/978-3-540-39432-7_11 (see p. 4)

[60] R. ETIKYALA, S. GÖTTLICH, A. KLAR, **and** S. TIWARI. *Particle methods for pedestrian flow models: From microscopic to nonlocal continuum models*. *Mathematical Models and Methods in Applied Sciences*, 24: 2503–2523, 2014. DOI: 10.1142/S0218202514500274 (see pp. 19, 20, 29–31, 49, 72, 76, 77, 79, 80, 87)

[61] B. R. FAJEN **and** W. H. WARREN. *Behavioral dynamics of steering, obstacle avoidance, and route selection*. *Journal of experimental psychology. Human perception and performance*, 29: 343–362, 2003. DOI: 10.1037/0096-1523.29.2.343 (see p. 69)

[62] N. M. FERGUSON, D. LAYDON, G. NEDJATI-GILANI, N. IMAI, K. AINSLIE, M. BAGUELIN, S. BHATIA, A. BOONYASIRI, Z. CUCUNUBÁ, G. CUOMO-DANNENBURG, **andothers** *Impact of non-pharmaceutical interventions (NPIs) to reduce COVID-19 mortality and healthcare demand. Imperial College COVID-19 Response Team* techreport 20 Imperial College COVID-19 Response Team, 2020, 77482 URL: https://www.imperial.ac.uk/mrc-global-infectious-disease-analysis/covid-19/report-9-impact-of-npis-on-covid-19/ (see p. 51)

[63] L. Fermo **and** A. Tosin. *A Fully-Discrete-State Kinetic Theory Approach to Modeling Vehicular Traffic*. *SIAM Journal on Applied Mathematics*, 73: 1533–1556, 2013. DOI: 10.1137/120897110 (see p. 44)

[64] P. Fiorini **and** Z. Shiller. *Motion Planning in Dynamic Environments Using Velocity Obstacles*. *The International Journal of Robotics Research*, 17: 760–772, 1998. DOI: 10.1177/027836499801700706 (see p. 29)

[65] A. Flor, C. Han, T. Xue, **and** M. Aanjaneya. *Interactive Simulation of Disease Contagion in Dynamic Crowds*. **in***Proceedings of the 14th ACM SIGGRAPH Conference on Motion, Interaction and Games*. MIG '21 Virtual Event, Switzerland: Association for Computing Machinery, 2021. 1–11 DOI: 10.1145/3487983.3488298 (see p. 52)

[66] H.-T. Fritzsche. *A model for traffic simulation*. *Traffic engineering & control*, 35: 317–321, 1994. (see p. 43)

[67] M. Fukui **and** Y. Ishibashi. *Self-organized phase transitions in cellular automaton models for pedestrians*. *Journal of the physical society of Japan*, 68: 2861–2863, 1999. DOI: 10.1143/jpsj.68.2861 (see p. 15)

[68] Y. Gao, T. Chen, P. B. Luh, **and** H. Zhang. *Experimental study on pedestrians' collision avoidance*. **in***Proceeding of the 11th World Congress on Intelligent Control and Automation*. IEEE, 2014. 2659–2663 DOI: 10.1109/WCICA.2014.7053145 (see p. 39)

[69] H. Gayathri, P. Aparna, **and** A. Verma. *A review of studies on understanding crowd dynamics in the context of crowd safety in mass religious gatherings*. *International Journal of Disaster Risk Reduction*, 25: 82–91, 2017. DOI: 10.1016/j.ijdrr.2017.07.017 (see p. 5)

[70] D. C. Gazis, R. Herman, **and** R. W. Rothery. *Nonlinear Follow-the-Leader Models of Traffic Flow*. *Operations Research*, 9: 545–567, 1961. DOI: 10.1287/opre.9.4.545 (see p. 43)

[71] J. J. Gibson. *The ecological approach to visual perception.* Houghton, Mifflin **and** Company, 1979. DOI: 10.4324/9780203767764 (see p. 69)

[72] L. Goscé, D. A. W. Barton, **and** A. Johansson. *Analytical Modelling of the Spread of Disease in Confined and Crowded Spaces*. *Scientific Reports*, 4: 4856, 2014. DOI: 10.1038/srep04856 (see p. 51)

[73] H Grad. *Asymptotic theory of the Boltzmann equation. II, 1963 Rarefied Gas Dynamics*. *Pros. 3rd Internat. Sympos., Palais de l'UNESCO, Paris, 1962*, 1: 26–59, 1962. (see p. 20)

[74] H. Greenberg. *An Analysis of Traffic Flow*. *Operations Research*, 7: 79–85, 1959. DOI: 10.1287/opre.7.1.79 (see p. 27)

[75] B. Greenshields, J. Bibbins, W. Channing, **and** H. Miller. *A study of traffic capacity*. *Highway Research Board proceedings*, 1935: 1935. (see p. 27)

[76] A. GUTTENBERG. *The Woonerf-a social invention in urban structure*. *ITE JOURNAL-INSTITUTE OF TRANSPORTATION ENGINEERS*, 51: 17–22, 1981. (see p. 5)

[77] M. HAGHANI. *Empirical methods in pedestrian, crowd and evacuation dynamics: Part II. Field methods and controversial topics*. *Safety Science*, 129: 104760, 2020. DOI: 10.1016/j.ssci.2020.104760 (see p. 96)

[78] L. HANF *Kumbh Mela in Allahabad (Indien)* [Photograph] 6April 2019 URL: https://www.larsreisen.de/2019/04/06/besuch-der-kumbh-mela-in-allahabad-indien-das-groesste-pilgertreffen-der-welt/ (see p. 4)

[79] D. HELBING, L. BUZNA, A. JOHANSSON, **and** T. WERNER. *Self-Organized Pedestrian Crowd Dynamics: Experiments, Simulations, and Design Solutions*. *Transportation Science*, 39: 1–24, 2005. DOI: 10.1287/trsc.1040.0108 (see p. 4)

[80] D. HELBING, I. FARKAS, **and** T. VICSEK. *Simulating dynamical features of escape panic*. *Nature*, 407: 487–490, 2000. DOI: 10.1038/35035023 (see p. 17)

[81] D. HELBING **and** A. JOHANSSON. **in**: *Encyclopedia of Complexity and Systems Science*. **chapter** Pedestrian, Crowd and Evacuation Dynamics, 6476–6495. New York, NY: Springer New York, 2009. DOI: 10.1007/978-0-387-30440-3_382 (see pp. 17, 19)

[82] D. HELBING **and** P. MOLNÁR. *Social force model for pedestrian dynamics*. *Physical Review E*, 51: 4282–4286, 1995. DOI: 10.1103/PhysRevE.51.4282 (see pp. 6, 16, 29, 69, 71)

[83] L. HENDERSON. *On the fluid mechanics of human crowd motion*. *Transportation Research*, 8: 509–515, 1974. DOI: 10.1016/0041-1647(74)90027-6 (see p. 18)

[84] R. HERMAN **and** K. GARDELS. *Vehicular Traffic Flow*. *Scientific American*, 209: 00368733, 35–43, 1963. DOI: http://www.jstor.org/stable/24935962 (see p. 43)

[85] H. W. HETHCOTE. *The Mathematics of Infectious Diseases*. *SIAM Review*, 42: 599–653, 2000. DOI: 10.1137/S0036144500371907 (see p. 51)

[86] D. HILBERT. *Begründung der kinetischen Gastheorie*. *Mathematische Annalen*, 72: 562–577, 1912. DOI: 10.1007/BF01456676 (see p. 20)

[87] S. HOOGENDOORN **and** P. H.L. BOVY. *Simulation of pedestrian flows by optimal control and differential games*. *Optimal Control Applications and Methods*, 24: 153–172, 2003. DOI: 10.1002/oca.727 (see p. 69)

[88] S. P. HOOGENDOORN, P. H. L. BOVY, **and** W. DAAMEN. *Walking infrastructure design assessment by continuous space dynamic assignment modeling*. *Journal of Advanced Transportation*, 38: 69–92, 2004. DOI: 10.1002/atr.5670380106 (see p. 7)

[89] S. P. HOOGENDOORN **and** P. H. BOVY. *Dynamic user-optimal assignment in continuous time and space*. *Transportation Research Part B: Methodological*, 38: 571–592, 2004. DOI: 10.1016/j.trb.2002.12.001 (see p. 7)

[90] S. P. HOOGENDOORN, F. L. VAN WAGENINGEN-KESSELS, W. DAAMEN, **and** D. C. DUIVES. *Continuum modelling of pedestrian flows: From microscopic principles to self-organised macroscopic phenomena*. *Physica A: Statistical Mechanics and its Applications*, 416: 684–694, 2014. DOI: 10.1016/j.physa.2014.07.050 (see p. 18)

[91] S. HOOGENDOORN **and** P. BOVY. *Pedestrian route-choice and activity scheduling theory and models*. *Transportation Research Part B: Methodological*, 38: 169–190, 2004. DOI: 10.1016/s0191-2615(03)00007-9 (see p. 7)

[92] L. HUANG, S. WONG, M. ZHANG, C.-W. SHU, **and** W. H. LAM. *Revisiting Hughes' dynamic continuum model for pedestrian flow and the development of an efficient solution algorithm*. *Transportation Research Part B: Methodological*, 43: 127–141, 2009. DOI: 10.1016/j.trb.2008.06.003 (see pp. 8, 18, 19)

[93] M. HUBER, Y.-H. SU, M. KRÜGER, K. FASCHIAN, S. GLASAUER, **and** J. HERMSDÖRFER. *Adjustments of Speed and Path when Avoiding Collisions with Another Pedestrian*. *PLOS ONE*, 9: 1–13, 2014. DOI: 10.1371/journal.pone.0089589 (see p. 39)

[94] R. L. HUGHES. *A continuum theory for the flow of pedestrians*. *Transp. Res. B: Methodol.*, 36: 507–535, 2002. DOI: 10.1016/S0191-2615(01)00015-7 (see pp. 8, 18, 29, 77)

[95] R. L. HUGHES. *THE FLOW OF HUMAN CROWDS*. *Annual Review of Fluid Mechanics*, 35: 169–182, 2003. DOI: 10.1146/annurev.fluid.35.101101.161136 (see pp. 18, 77)

[96] F. T. ILLIYAS, S. K. MANI, A. PRADEEPKUMAR, **and** K. MOHAN. *Human stampedes during religious festivals: A comparative review of mass gathering emergencies in India*. *International Journal of Disaster Risk Reduction*, 5: 10–18, 2013. DOI: 10.1016/j.ijdrr.2013.09.003 (see p. 3)

[97] J. JACOBS. *The Death and Life of Great American Cities*. New York : Vintage, 1961. (see p. 5)

[98] KAI NAGEL **and** MICHAEL SCHRECKENBERG. *A cellular automaton model for freeway traffic*. *Journal de Physique I*, 2: 2221–2229, 1992. DOI: 10.1051/jp1:1992277 (see p. 43)

[99] D. P. KENNEDY, J. GLÄSCHER, J. M. TYSZKA, **and** R. ADOLPHS. *Personal space regulation by the human amygdala*. *Nature Neuroscience*, 12: 1226–1227, 2009. DOI: 10.1038/nn.2381 (see p. 54)

[100] W. O. KERMACK **and** A. G. MCKENDRICK. *A contribution to the mathematical theory of epidemics*. *Proceedings of the royal society of london. Series A, Containing papers of a mathematical and physical character*, 115: 700–721, 1927. (see p. 51)

[101] Z. H. KHAN, T. A. GULLIVER, W. IMRAN, K. S. KHATTAK, A. B. ALTAMIMI, **and** A. QAZI. *A macroscopic traffic model based on relaxation time*. *Alexandria Engineering Journal*, 61: 585–596, 2022. DOI: 10.1016/j.aej.2021.06.042 (see p. 43)

[102] D. KIM **and** A. QUAINI. *A kinetic theory approach to model pedestrian dynamics in bounded domains with obstacles*. *Kinetic and Related Models*, 12: 1273–1296, 2019. DOI: 10.3934/krm.2019049 (see p. 17)

[103] D. KIM **and** A. QUAINI. *Coupling kinetic theory approaches for pedestrian dynamics and disease contagion in a confined environment*. *Mathematical Models and Methods in Applied Sciences*, 30: 1893–1915, 2020. DOI: 10.1142/S0218202520400126 (see pp. 52, 54, 60)

[104] D. KIM **and** A. QUAINI. **in**: *Crowd Dynamics, Volume 3: Modeling and Social Applications in the Time of COVID-19*. **chapter** A Kinetic Theory Approach to Model Crowd Dynamics with Disease Contagion, 157–183. Cham: Springer International Publishing, 2021. DOI: 10.1007/978-3-030-91646-6_7 (see p. 52)

[105] D. KIM **and** A. QUAINI. **in**: *Predicting Pandemics in a Globally Connected World, Volume 1: Toward a Multiscale, Multidisciplinary Framework through Modeling and Simulation*. **chapter** A 2D Kinetic Model for Crowd Dynamics with Disease Contagion, 265–284. Cham: Springer International Publishing, 2022. DOI: 10.1007/978-3-030-96562-4_9 (see p. 52)

[106] S. KIM **and** R. COOK. *3-D traveltime computation using second-order ENO scheme*. *Geophysics*, 64: 1867–1876, 1999. DOI: 10.1190/1.1444693 (see p. 20)

[107] A. KIRCHNER **and** A. SCHADSCHNEIDER. *Simulation of evacuation processes using a bionics-inspired cellular automaton model for pedestrian dynamics*. *Physica A: Statistical Mechanics and its Applications*, 312: 260–276, 2002. DOI: 10.1016/s0378-4371(02)00857-9 (see p. 15)

[108] K. KITAZAWA **and** T. FUJIYAMA. *Pedestrian Vision and Collision Avoidance Behavior: Investigation of the Information Process Space of Pedestrians Using an Eye Tracker*. **in***Pedestrian and Evacuation Dynamics 2008*. **byeditor**W. W. F. KLINGSCH, C. ROGSCH, A. SCHADSCHNEIDER, **and** M. SCHRECKENBERG Berlin, Heidelberg: Springer Berlin Heidelberg, 2010. 95–108 DOI: 10.1007/978-3-642-04504-2_7 (see p. 29)

[109] A. KLAR **and** R. WEGENER. *Enskog-like kinetic models for vehicular traffic*. *Journal of Statistical Physics*, 87: 91–114, 1997. DOI: 10.1007/BF02181481 (see p. 44)

[110] A. KLAR, R. D. KÜHNE, **and** R. WEGENER "Mathematical Models for Vehicular Traffic" 1995 URL: https://kluedo.ub.rptu.de/frontdoor/index/index/docId/591 (see p. 27)

[111] A. KLAR **and** S. TIWARI. *A Multiscale Particle Method for Mean Field Equations: The General Case*. *Multiscale Modeling and Simulation*, 17: 233–259, 2019. DOI: 10.1137/17M112957X (see pp. 49, 69, 79, 87)

[112] KONEVI *Mecca Saudi Arabia* [Photograph] 19 September 2019 URL: https://pxhere.com/en/photo/1596771 (see p. 4)

[113] A. KOROBEINIKOV. *Lyapunov functions and global properties for SEIR and SEIS epidemic models*. *Mathematical Medicine and Biology: A Journal of the IMA*, 21: 75–83, 2004. DOI: 10.1093/imammb/21.2.75 (see p. 51)

[114] T. KRÜGER, H. KUSUMAATMAJA, A. KUZMIN, O. SHARDT, G. SILVA, **and** E. M. VIGGEN. *The lattice Boltzmann method*. Springer Cham, 2017. DOI: 10.1007/978-3-319-44649-3 (see p. 6)

[115] R. KÜHNE **and** M. RÖDIGER. *Macroscopic simulation model for freeway traffic with jams and stop-start waves*. **in***1991 Winter Simulation Conference Proceedings*. Los Alamitos, CA, USA: IEEE Computer Society, 1991. 762,763,764,765,766,767,768,769,770 DOI: 10.1109/WSC.1991.185683 (see p. 27)

[116] W. H. LAM, J. F. MORRALL, **and** H. HO. *Pedestrian flow characteristics in Hong Kong*. *Transportation research record*, 1487: 56–62, 1995. (see p. 28)

[117] K. LEWIN. *Field theory in social science: selected theoretical papers (Edited by Dorwin Cartwright.)* Oxford, England: Harpers, 1951. (see p. 16)

[118] M. J. LIGHTHILL **and** G. B. WHITHAM. *On kinematic waves II. A theory of traffic flow on long crowded roads*. *Proceedings of the Royal Society of London. Series A. Mathematical and Physical Sciences*, 229: 317–345, 1955. DOI: 10.1098/rspa.1955.0089 (see pp. 19, 43)

[119] G. LIU. *Mesh Free Methods: Moving Beyond the Finite Element Method*. CRC Press, 2002. DOI: 10.1201/9781420040586 (see p. 21)

[120] K. LYNCH. *The image of the city*. Cambridge : MIT press, 1960. (see p. 5)

[121] N. MAHATO, A KLAR, **and** S TIWARI. *A meshfree particle method for a vision-based macroscopic pedestrian model*. *International Journal of Advances in Engineering Sciences and Applied Mathematics*, 10: 41–53, 2018. DOI: 10.1007/s12572-018-0204-2 (see p. 55)

[122] N. MAHATO, A. KLAR, **and** S. TIWARI. *Particle methods for multi-group pedestrian flow*. *Applied Mathematical Modelling*, 53: 447–461, 2018. DOI: 10.1016/j.apm.2017.08.024 (see p. 56)

[123] B. MAURY **and** S. FAURE. *Crowds in Equations-An introduction to the microscopic modeling of crowds*. Hackensack, NJ: WORLD SCIENTIFIC (EUROPE), 2018. DOI: 10.1142/q0163 (see p. 77)

[124] J. C. MAXWELL. *IV. On the dynamical theory of gases*. *Philosophical Transactions of the Royal Society of London*, 157: 49–88, 1867. DOI: 10.1098/rstl.1867.0004 (see p. 19)

[125] M. MEKAWY **and** M. A. GABR. *Against a workplace contagion: a digital approach to support hygiene-conscious office space planning*. *Open House International*, 46: 391–400, 2021. DOI: 10.1108/OHI-02-2021-0029 (see p. 52)

[126] D. Y. Melesse **and** A. B. Gumel. *Global asymptotic properties of an SEIRS model with multiple infectious stages*. *Journal of Mathematical Analysis and Applications*, 366: 202–217, 2010. DOI: 10.1016/j.jmaa.2009.12.041 (see p. 51)

[127] I Michel, S. Bathaeian, J Kuhnert, D Kolymbas, C.-H. Chen, I Polymerou, C Vrettos, **and** A Becker. *Meshfree generalized finite difference methods in soil mechanics—part II: numerical results*. *GEM-International Journal on Geomathematics*, 8: 191–217, 2017. DOI: 10.1007/s13137-017-0096-5 (see p. 9)

[128] M. Moussaïd, D. Helbing, S. Garnier, A. Johansson, M. Combe, **and** G. Theraulaz. *Experimental study of the behavioural mechanisms underlying self-organization in human crowds*. *Proceedings of the Royal Society B: Biological Sciences*, 276: 2755–2762, 2009. DOI: 10.1098/rspb.2009.0405 (see pp. 82, 83)

[129] M. Moussaïd, D. Helbing, **and** G. Theraulaz. *How simple rules determine pedestrian behavior and crowd disasters*. *Proceedings of the National Academy of Sciences*, 108: 6884–6888, 2011. DOI: 10.1073/pnas.1016507108 (see pp. 6, 17, 69, 90)

[130] M. Muramatsu **and** T. Nagatani. *Jamming transition in two-dimensional pedestrian traffic*. *Physica A: Statistical Mechanics and its Applications*, 275: 281–291, 2000. DOI: 10.1016/s0378-4371(99)00447-1 (see p. 15)

[131] A. Müseler *Entry and exit ramp of the Loveparade 2010* [Photograph] 24 July 2010 URL: https://commons.wikimedia.org/wiki/File:Loveparade_2010_duisburg_tunnel_ramp.jpg (see p. 4)

[132] A. Nakayama, K. Hasebe, **and** Y. b. u. Sugiyama. *Instability of pedestrian flow and phase structure in a two-dimensional optimal velocity model*. *Phys. Rev. E*, 71: 036121, 2005. DOI: 10.1103/PhysRevE.71.036121 (see p. 17)

[133] P. Nelson. *A kinetic model of vehicular traffic and its associated bimodal equilibrium solutions*. *Transport Theory and Statistical Physics*, 24: 383–409, 1995. DOI: 10.1080/00411459508205136 (see p. 44)

[134] K. Nishinari, A. Kirchner, A. Namazi, **and** A. Schadschneider. *Extended floor field CA model for evacuation dynamics*. *IEICE Transactions on information and systems*, 87: 726–732, 2004. DOI: 10.48550/arXiv.cond-mat/0306262 (see p. 15)

[135] S. Okazaki **and** S. Matsushita. *A study of simulation model for pedestrian movement with evacuation and queuing*. **in***Engineering for crowd safety : proceedings of the International Conference on Engineering for Crowd Safety*. **volume** 271 Elsevier, 1993. (see p. 17)

[136] J. Ondřej, J. Pettré, A.-H. Olivier, **and** S. Donikian. *A Synthetic-Vision Based Steering Approach for Crowd Simulation*. *ACM Transactions on Graphics*, 29: 1–9, 2010. DOI: 10.1145/1778765.1778860 (see p. 69)

[137] S. Osher **and** J. A. Sethian. *Fronts propagating with curvature-dependent speed: Algorithms based on Hamilton-Jacobi formulations*. *Journal of Computational Physics*, 79: 12–49, 1988. DOI: 10.1016/0021-9991(88)90002-2 (see p. 24)

[138] S. Osher **and** C.-W. Shu. *High-Order Essentially Nonoscillatory Schemes for Hamilton–Jacobi Equations*. *SIAM Journal on Numerical Analysis*, 28: 907–922, 1991. DOI: 10.1137/0728049 (see p. 24)

[139] S. Paveri-Fontana. *On Boltzmann-like treatments for traffic flow: A critical review of the basic model and an alternative proposal for dilute traffic analysis*. *Transportation Research*, 9: 225–235, 1975. DOI: 10.1016/0041-1647(75)90063-5 (see p. 44)

[140] H. Payne. *Mathematical models of public systems*. **in***Simul. Counc. Proc. Ser.* **volume** 1 1971. 51–61 (see p. 43)

[141] C. S. Peskin. *Flow patterns around heart valves: A numerical method*. *Journal of Computational Physics*, 10: 252–271, 1972. DOI: 10.1016/0021-9991(72)90065-4 (see p. 9)

[142] B. Piccoli **and** A. Tosin. **in**: *Mathematics of Complexity and Dynamical Systems*. **chapter** Vehicular Traffic: A Review of Continuum Mathematical Models, 1748–1770. New York, NY: Springer New York, 2011. DOI: 10.1007/978-1-4614-1806-1_112 (see p. 44)

[143] B. Piccoli **and** A. Tosin. *Pedestrian flows in bounded domains with obstacles*. *Continuum Mechanics and Thermodynamics*, 21: 85–107, 2009. DOI: 10.1007/s00161-009-0100-x (see p. 19)

[144] L. A. Pipes. *An Operational Analysis of Traffic Dynamics*. *Journal of Applied Physics*, 24: 274–281, 1953. DOI: 10.1063/1.1721265 (see p. 43)

[145] . Plot Digitizer Accessed: 16 January 2023 URL: https://plotdigitizer.com/app (see p. 83)

[146] I. Prigogine. *A Boltzmann-like approach to the statistical theory of traffic flow*. *Theory of traffic flow*, 1961. (see p. 44)

[147] J. Qian, Y. Zhang, **and** H. Zhao. *Fast Sweeping Methods for Eikonal Equations on Triangular Meshes*. *SIAM Journal on Numerical Analysis*, 45: 83–107, 2007. DOI: 10.1137/050627083 (see p. 79)

[148] F. Qin, Y. Luo, K. B. Olsen, W. Cai, **and** G. T. Schuster. *Finite-difference solution of the eikonal equation along expanding wavefronts*. *Geophysics*, 57: 478–487, 1992. DOI: 10.1190/1.1443263 (see p. 20)

[149] K. Rathinakumar **and** A. Quaini. *A microscopic approach to study the onset of a highly infectious disease spreading*. *Mathematical Biosciences*, 329: 108475, 2020. DOI: 10.1016/j.mbs.2020.108475 (see p. 52)

[150] P. I. RICHARDS. *Shock Waves on the Highway*. *Operations Research*, 4: 42–51, 1956. DOI: 10.1287/opre.4.1.42 (see p. 43)

[151] A. SCHADSCHNEIDER, W. KLINGSCH, H. KLÜPFEL, T. KRETZ, C. ROGSCH, **and** A. SEYFRIED. **in**: *Encyclopedia of Complexity and Systems Science*. **chapter** Evacuation Dynamics: Empirical Results, Modeling and Applications, 3142–3176. New York, NY: Springer New York, 2009. DOI: 10.1007/978-0-387-30440-3_187 (see p. 27)

[152] M. J. SEITZ **and** G. KÖSTER. *Natural discretization of pedestrian movement in continuous space*. *Physical Review E*, 86: 046108, 2012. DOI: 10.1103/PhysRevE.86.046108 (see p. 80)

[153] J. A. SETHIAN. *A fast marching level set method for monotonically advancing fronts*. *Proceedings of the National Academy of Sciences*, 93: 1591–1595, 1996. DOI: 10.1073/pnas.93.4.1591 (see p. 25)

[154] J. A. SETHIAN. *Fast Marching Methods*. *SIAM Review*, 41: 199–235, 1999. DOI: 10.1137/S0036144598347059 (see pp. 33, 79)

[155] J. A. SETHIAN. *Level set methods and fast marching methods: evolving interfaces in computational geometry, fluid mechanics, computer vision, and materials science*. **volume** 3 Cambridge university press, 1999. (see p. 25)

[156] N. SHIWAKOTI, X. SHI, **and** Z. YE. *A review on the performance of an obstacle near an exit on pedestrian crowd evacuation*. *Safety Science*, 113: 54–67, 2019. DOI: 10.1016/j.ssci.2018.11.016 (see p. 29)

[157] C. I. SIETTOS **and** L. RUSSO. *Mathematical modeling of infectious disease dynamics*. *Virulence*, 4: PMID: 23552814, 295–306, 2013. DOI: 10.4161/viru.24041 (see p. 51)

[158] P. SUCHDE **and** J. KUHNERT. *A fully Lagrangian meshfree framework for PDEs on evolving surfaces*. *Journal of Computational Physics*, 395: 38–59, 2019. DOI: 10.1016/j.jcp.2019.06.031 (see p. 24)

[159] P. SUCHDE, J. KUHNERT, **and** S. TIWARI. *On meshfree GFDM solvers for the incompressible Navier–Stokes equations*. *Computers & Fluids*, 165: 1–12, 2018. DOI: 10.1016/j.compfluid.2018.01.008 (see p. 24)

[160] H. TAKANASHI, T. KAWAI, T. TAMURA, **and** N. OTA. *Prediction of Pedestrian's Walking Route for Moving Obstacles*. **in***Proceedings of the 5th International Symposium on Future Active Safety Technology toward Zero Accidents*. 2019. (see p. 39)

[161] L. TANG, Y. ZHOU, L. WANG, S. PURKAYASTHA, L. ZHANG, J. HE, F. WANG, **and** P. X.-K. SONG. *A Review of Multi-Compartment Infectious Disease Models*. *International Statistical Review*, 88: 462–513, 2020. DOI: 10.1111/insr.12402 (see p. 51)

[162] P. A. THOMPSON **and** E. W. MARCHANT. *A computer model for the evacuation of large building populations*. *Fire Safety Journal*, 24: 131–148, 1995. DOI: 10.1016/0379-7112(95)00019-p (see p. 17)

[163] S. TIWARI **and** J. KUHNERT. *A Meshfree Method For Incompressible Fluid Flows with Incorporated Surface Tension*. *Revue Européenne des Éléments Finis*, 11: 965–987, 2002. DOI: 10.3166/reef.11.965-987 (see p. 9)

[164] S. TIWARI **and** J. KUHNERT. *Finite Pointset Method Based on the Projection Method for Simulations of the Incompressible Navier-Stokes Equations*. **in***Meshfree Methods for Partial Differential Equations*: **byeditor**M. GRIEBEL **and** M. A. SCHWEITZER. Berlin, Heidelberg: Springer Berlin Heidelberg, 2003. 373–387 DOI: 10.1007/978-3-642-56103-0$_$26 (see pp. 9, 24, 32, 69)

[165] S. TIWARI **and** J. KUHNERT. *Modeling of two-phase flows with surface tension by finite pointset method (FPM)*. *Journal of Computational and Applied Mathematics*, 203: 376–386, 2007. DOI: 10.1016/j.cam.2006.04.048 (see p. 9)

[166] A. TREUILLE, S. COOPER, **and** Z. POPOVIĆ. *Continuum Crowds*. *ACM Trans. Graph.*, 25: 1160–1168, 2006. DOI: 10.1145/1141911.1142008 (see p. 29)

[167] M. R. VIRKLER **and** S. ELAYADATH. *Pedestrian speed-flow-density relationships*. *Transportation research record*, 1438: 51–58, 1994. URL: https://onlinepubs.trb.org/Onlinepubs/trr/1994/1438/1438-007.pdf(see p. 28)

[168] P. G. T. WALKER, C. WHITTAKER, O. J. WATSON, M. BAGUELIN, P. WINSKILL, A. HAMLET, B. A. DJAFAARA, Z. CUCUNUBÁ, D. O. MESA, W. GREEN, H. THOMPSON, S. NAYAGAM, K. E. C. AINSLIE, S. BHATIA, S. BHATT, A. BOONYASIRI, O. BOYD, N. F. BRAZEAU, L. CATTARINO, G. CUOMO-DANNENBURG, A. DIGHE, C. A. DONNELLY, I. DORIGATTI, S. L. VAN ELSLAND, R. FITZJOHN, H. FU, K. A. M. GAYTHORPE, L. GEIDELBERG, N. GRASSLY, D. HAW, S. HAYES, W. HINSLEY, N. IMAI, D. JORGENSEN, E. KNOCK, D. LAYDON, S. MISHRA, G. NEDJATI-GILANI, L. C. OKELL, H. J. UNWIN, R. VERITY, M. VOLLMER, C. E. WALTERS, H. WANG, Y. WANG, X. XI, D. G. LALLOO, N. M. FERGUSON, **and** A. C. GHANI. *The impact of COVID-19 and strategies for mitigation and suppression in low- and middle-income countries*. *Science*, 369: 413–422, 2020. DOI: 10.1126/science.abc0035 (see p. 51)

[169] Z. WAN, C. JIANG, M. FAHAD, Z. NI, Y. GUO, **and** H. HE. *Robot-Assisted Pedestrian Regulation Based on Deep Reinforcement Learning*. *IEEE Transactions on Cybernetics*, 50: 1669–1682, 2020. DOI: 10.1109/TCYB.2018.2878977 (see p. 29)

[170] W. H. WARREN. *Chapter 14 Action Modes and Laws of Control for the Visual Guidance Of Action*. **in***Complex Movement Behaviour*: **byeditor**O. G. MEIJER **and** K. ROTH. **volume** 50 Advances in Psychology Elsevier, 1988. 339–379 DOI: 10.1016/S0166-4115(08)62564-9 (see p. 69)

[171] G. WHITHAM. *Linear and nonlinear waves*. John Wiley & Sons, 1974. DOI: 10.1002/9781118032954 (see p. 43)

[172] M. J. WIERBOS, V. L. KNOOP, F. S. HÄNSELER, **and** S. P. HOOGENDOORN. *A macroscopic flow model for mixed bicycle–car traffic*. *Transportmetrica A: Transport Science*, 17: 340–355, 2021. DOI: 10.1080/23249935.2019.1708512 (see p. 43)

[173] T. XIAO, T. MU, S. SHEN, Y. SONG, S. YANG, **and** J. HE. *A dynamic physical-distancing model to evaluate spatial measures for prevention of Covid-19 spread*. *Physica A: Statistical Mechanics and its Applications*, 592: 126734, 2022. DOI: 10.1016/j.physa.2021.126734 (see p. 5)

[174] H. XU, J. ZHANG, W. SONG, Y. HU, X. LI, X. REN, L. YANG, H. YU, **and** K. JIANG. *The effect of moving obstacle on regulation of pedestrian flow in a single exit room*. *Journal of Statistical Mechanics: Theory and Experiment*, 2022: 023407, 2022. DOI: 10.1088/1742-5468/ac4c3f (see p. 29)

[175] K. YAMAMOTO **and** M. OKADA. *Continuum model of crossing pedestrian flows and swarm control based on temporal/spatial frequency*. **in***2011 IEEE International Conference on Robotics and Automation*. IEEE, 2011. 3352–3357 DOI: 10.1109/ICRA.2011.5980444 (see p. 29)

[176] R. YANO. *Effect of form of obstacle on speed of crowd evacuation*. *Phys. Rev. E*, 97: 032319, 2018. DOI: 10.1103/PhysRevE.97.032319 (see p. 4)

[177] Q. YIN, L. CHEN, **and** S. GÖTTLICH. *The mean field kinetic equation for interacting particle systems with non-Lipschitz force*. *Mathematical Methods in the Applied Sciences*, 43: 1901–1914, 2020. DOI: 10.1002/mma.6013 (see p. 20)

[178] Y.-T. ZHANG, H.-K. ZHAO, **and** J. QIAN. *High Order Fast Sweeping Methods for Static Hamilton–Jacobi Equations*. *Journal of Scientific Computing*, 29: 25–56, 2006. DOI: 10.1007/s10915-005-9014-3 (see p. 24)

[179] H. ZHAO. *A fast sweeping method for Eikonal equations*. *Mathematics of Computation*, 74: 603–627, 2005. DOI: 10.1090/s0025-5718-04-01678-3 (see p. 24)

List of Figures

List of Tables

Akademischer Lebenslauf

April 2021	Annahme als Doktorand von Prof. Dr. Axel Klar am Fachbereich Mathematik an der RPTU Kaiserslautern (unter dem DAAD Bi-national betreute Promotionen Programm).
Juli 2017	Annahme als Doktorand von Prof. Dr. Subbiah Sundar am Fachbereich Mathematik an dem IIT Madras (Chennai, Indien).
Juli 2016	Master-Abschluss in Mathematik am Fachbereich Mathematik an dem IIT Madras (Chennai, Indien). Thema der Master-Arbeit: Reaktions - Diffusions - Gleichungen.
Juni 2013	Bachelor-Abschluss in Mathematik am Fachbereich Mathematik an der Government Victoria College Palakkad (Kerala, Indien).

April 2022 - September 2022	Wissenschaftliche Hilfskraft an der Fraunhofer ITWM, Kaiserslautern.
Juli 2018 - Juli 2019	Studentische Hilfskraft an der IIT Madras (Chennai, Indien).
August 2016 - Juli 2017	Wissenschaftlicher Mitarbeiter an der Institut des Mathematische Wissenschaften (Chennai, Indien).

Academic curriculum vitae

April 2021	Registration as a Doctoral Student of Prof. Dr. Axel Klar in the Department of Mathematics at RPTU Kaiserslautern-Landau (under the DAAD Bi-nationally Supervised Doctoral Degree Programme).
July 2017	Registration as a Doctoral Student of Prof. Dr. Subbiah Sundar in the Department of Mathematics at IIT Madras (Chennai, India).
July 2016	M.Sc Mathematics from the Department of Mathematics at IIT Madras (Chennai, India). Title of Master-Dissertation : Reaction-Diffusion Equations.
June 2013	B.Sc Mathematics from the Department of Mathematics at Government Victoria College Palakkad (Kerala, India).

April 2022 - September 2022	Student Research Assistant at the Fraunhofer ITWM, Kaiserslautern.
July 2018 - July 2019	Student Teaching Assistant at the IIT Madras.
August 2016 - July 2017	Research Project Assistant at the Institute of Mathematical Sciences (Chennai, India).